Modelling of a Passive Hydraulic Steering for Locomotives

by

Torsten Peter Löwe

Submitted in partial fulfilment of the requirements for the degree

Master of Engineering

in the Faculty of

Engineering, Built Environment and Information Technology (EBIT)

University of Pretoria, Pretoria

October 2014

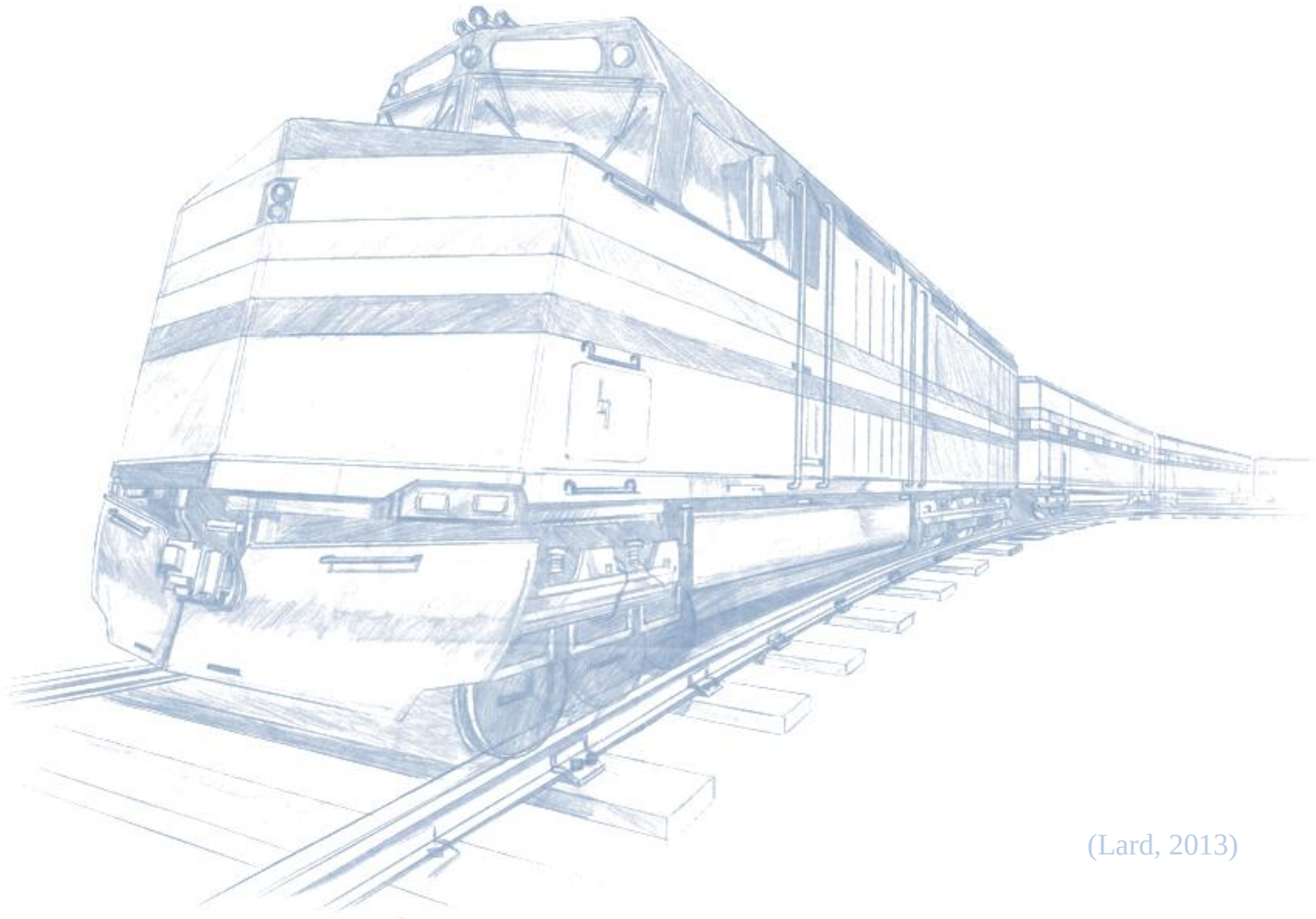

(Lard, 2013)

Modelling of a Passive Hydraulic Steering for Locomotives.

Candidate: Torsten Peter Löwe
Supervisor: Prof P.S. Els
Co-Supervisor: Dr C. Kat
Department: Mechanical and Aeronautical Engineering
Degree: Master of Engineering

Abstract

During the past few decades, substantial improvements were made to rail infrastructure worldwide. This was necessary to accommodate the ever increasing transportation demand and requirements. Nowadays, trains are required to transport heavier loads and to travel at higher speeds.

One of the major improvements was achieved by the development of the off-flange curving bogie designs to reduce wheel and rail wear. Off-flange designs include passive steering and actively controlled steering. The development and implementation of self-steering bogies on locomotives was promoted in the early 1980's by two major locomotive manufacturers. Up to date, thousands of these locomotives, with built-in self-steering bogies, have been manufactured and taken into service (Swenson, 1999).

Most self-steering bogies have mechanical linkage systems to steer the wheel sets. As an alternative to the mechanical linkage system, the DCD Group (a South African manufacturer of rail and mining equipment) initiated the development of a Passive Hydraulic Steering (PHS) system.

First PHS prototype systems, developed by DCD, have proven that huge wear reduction possibilities exist on both, rails and wheels. In addition the prototype systems also significantly decreased noise and vibration levels when negotiating tight corners (Swenson & Scott, 1996 and DCD Rolling Stock, 2012). However, existing prototype solutions require further improvements and development for optimisation. To be able to identify and implement improvements, the need exists to perform modelling and testing of the systems to obtain a better understanding of the operation and suitability of a complete unit.

The aim of this research project is thus, to mathematically model an existing prototype PHS system and validate the model with data from experiments and tests. This model can then be used in order to improve and optimise performance, cost and reliability of the system, before mass production is considered.

A literature survey was conducted, focusing on general wheel and rail wear mechanisms, techniques to improve wheel and rail life and on existing techniques for modelling the hydraulics and multi-body dynamics of locomotive systems.

The literature survey was followed by extensive laboratory tests on component basis, a quarter PHS system and on the full PHS system. From these tests all parameters needed for the characterisation of the PHS and the mathematical model were determined. These tests also provided data for the validation of the PHS model.

Finally, a mathematical model of the PHS system was successfully generated and validated. This model can now be used in a multi-body dynamic locomotive simulation to evaluate its effectiveness.

The results and findings of the literature survey, experiments and modelling are reported on and discussed in this report.

Acknowledgements

I wish to thank my study leader, Prof P.S. Els, co-supervisor Dr C. Kat, my family and friends for their continued guidance, support and contribution to making this project possible. Furthermore, I would like to thank Mr P. Smith and Mr A. Pieterse from DCD, Mr S. Maartens from Transnet, Mr C. Cassel from HYTEC and Mr C. Becker from the University of Pretoria for the valuable information, help and opportunities provided.

This project allowed the student to gain valuable knowledge and experience in engineering design, especially in the field of rail infrastructure and systems. Contacts have been made, which may be very useful for the student's future career as an engineer.

Also, a big thank you goes to the DCD Group and the National Research Foundation for providing funds for this project.

The financial assistance of the National Research Foundation (NRF) towards this research is hereby acknowledged. Opinions expressed and conclusions arrived at, are those of the author and are not necessarily to be attributed to the NRF.

Table of Contents

List of Figures

List of Tables

List of Symbols

English Letters and Symbols

A = Area [m^2]

A_0 = Benedict Webb Rubin (BWR) constant [$(m^3/kg)^3.(N/m^2)$]

$A_{accum.}$ = Accumulator area [m^2]

a = BWR constant [$(m^3/kg)^3.(N/m^2)$]

B_0 = BWR constant [m^3/kg]

b = BWR constant [$(m^3/kg)^3$]

C_0 = BWR constant [$(m^3/kg)^3.K^2.(N/m^2)$]

C_v = Real gas specific heat capacity [J/(kg.K)]

C_{vo} = Ideal gas specific heat capacity [J/(kg.K)]

c = Damping constant [N/(m/s)] or BWR constant [$(m^3/kg)^3.K^2.(N/m^2)$] (Context dependent)

D = Diameter [m]

d = Displacement [m]

F = Force [N]

$F_{accum.}$ = Accumulator force [N]

F_{spring} = Spring force [N]

F_{damper} = Damping force [N]

k_s = Spring constant [N/m]

m = Mass [kg]

N_1 *to* N_9 = Specific heat constants

n = Polytropic constant

P = Pressure [Pa]

P = Probability

$P_{accum.}$ = Accumulator pressure [Pa]

P_c = Critical pressure [Pa]

P_r = Reduced pressure [Pa]

q = Volumetric flow rate [m^3/s]

q_A = Volumetric flow rate in and out of an accumulator [m^3/s]

R = Universal gas constant [J/(kg.K)]

T = Temperature [K]

T_c = Critical temperature [K]

T_g = Gas temperature [K]

T_r = Reduced temperature [K]

T_s = Atmospheric temperature [K]

$\dot{T}_g$ = Time derivative of the gas temperature

t = Time [s]

V = Total fluid volume of the PHS at atmospheric pressure [m^3]

V_A = Accumulator volume [m^3]

V_F = Fluid volume in the accumulator [m^3]

v = Piston velocity [m/s]

$\dot{v}$ = Time derivative of the gas specific mass

x = Displacement [m]

$\dot{x}$ = Velocity [m/s]

Z = Compressibility factor

Greek Letters and Symbols

α = BWR constant [$(m^3/kg)^3$]

β = Bulk modulus [Pa]

τ = Thermal time constant [s]

γ = Adiabatic index or BWR constant [$(m^3/kg)^2$] (Context dependent)

Δ = Change

Abbreviations

AAR	Association of American Railroads
BWR	Benedict Webb Rubin
DCD	DCD Group South Africa
EE	Energy Equation
EMD	Electro-Motive Division
GE	General Electric
GPS	Global Positioning System
HYTEC	Hydraulic Equipment and Components Distributor
IG	Ideal Gas
ISO	International Organization for Standardization
MSC ADAMS	Multi-body Dynamic Software Package
$m\%RE^m$	Mean percentage relative error
$m\%RE^s$	Mean percentage relative error below a specified percentage error
NRSR	National Railway Safety Regulator
NUCARS	Multi-body Dynamic Software Package
PHS	Passive Hydraulic Steering
PRASA	Passenger Rail Agency of South Africa
SANS	South African National Standards
SABS	South African Bureau of Standards
SIMPACK	Multi-body Dynamic Software Package
TFR	Transnet Freight Rail
UM Loco	Multi-body Dynamic Software Package
VDG	Vehicle Dynamics Group

1. Introduction

In South Africa, as in most other countries, the transport infrastructure forms the backbone of economic growth and development. A limited or overloaded transport system hampers development, economic growth and foreign investment. The South African transport infrastructure is overloaded due to ageing rail and road transport facilities and the ever increasing demand for transport. The road network in most areas of South Africa cannot accommodate the drastically increasing number of vehicles and is causing a bottle neck for growth (SABS Design Institute, 2005). This is not acceptable for the country, as it needs economic growth to be able to raise the standard of living of its rapidly increasing population. Figure 1-1 is a humoristic example of how transport mechanisms are used to their limits.

Figure 1-1. Limited and overloaded transport infrastructure in Africa (Freespirit, 2013).

The high demand for transport, which exponentially increases every year, must to a large extent be met by an improved and expanded rail transport system that is operated as efficiently as possible with low maintenance costs. Unfortunately, the railway infrastructure (including rails, locomotives and coaches) in most areas of South Africa is old and insufficient.

According to the Department of Transport (2013), the Passenger Rail Agency of South Africa (PRASA) transported about 250 million passengers and Transnet Freight Rail about 200 million tons of cargo in the year 2012 (Transnet Freight Rail, 2012). As these volumes will increase considerably, a rapid improvement and expansion of the rail transport system is essential.

It is pleasing to be able to report that large capital investments have been approved to upgrade the rail system as soon as possible. The aim of these investments is to develop systems and components with reduced running costs, improved reliability and to increase the transportation capacity in order to improve customer service (Dept. of Transport, 2013).

Over the past years, damage or wear to the train wheel flanges and tracks was identified to be one of the major problems contributing to high running costs. It was also identified that the wear was considerably more in curves than in straight stretches (Olofsson & Lewis, 2006). One option of reducing this wear on wheels and tracks is the use of an off-flange curving bogie design, such as the Passive Hydraulic Steering (PHS) system developed by the DCD group.

Passive Hydraulic Steering systems exist in concept and existing prototypes have proven that considerable wear reduction possibilities exist. The prototype systems also significantly decreased noise and vibration when negotiating tight corners (Swenson & Scott, 1996 and DCD Rolling Stock, 2012). However, the existing prototype solutions (based on hand calculations) are not optimal yet and improvements are necessary. To be able to identify and implement improvements, the need exists to perform modelling of the systems to obtain a better understanding of the system as a whole.

Therefore, the purpose of this research project is to mathematically model an existing prototype PHS system, validate the model using experimental tests and use the model to improve and optimise performance, cost and reliability of the system, before mass production begins.

The experimental tests are aimed at the testing of an existing prototype PHS system and the testing of the individual components (cylinder, accumulators and piping) in a laboratory.

This research forms part of the development of a novel self-steering system that can be applied to the locomotives that will be acquired in the next 5 years. As this new technology promises to significantly reduce wear on wheels and rails and thus extending the service life of these components, the transportation via rail could be more efficient, lucrative and environmentally friendly.

2. Literature Survey

2.1. Known Major Problems of Rail Systems

In many countries, such as South Africa, the rail infrastructure is old and this leads to regular breakdowns, which again result in high running costs (Department of Transport, 2013). Further, the transportation capacity is often pushed to its limits, resulting in overloading of the available infrastructure. There are also many other issues, such as theft of cables, reckless usage of the trains, obstacles on the tracks (such as livestock) and lack of maintenance.

The list of known problems is very long and can be grouped into either age related deterioration or traffic related deterioration (Enblom, 2009). However, for this research project only a few problems are discussed in more detail, being those mainly due to traffic related deterioration.

2.1.1. Wheel and Rail Wear

According to Swenson and Scott (1996), the Illinois Institute of Technology researchers have identified the following parameters to have the highest influence on wheel-rail contact wear (in the order of importance):

1. Metallurgy (Wheel and rail materials used).
2. Angle of Attack (Wheel direction vs. Rail direction).
3. Adhesion coefficients (Important for braking and accelerating).
4. Axle load.

Further, Olofsson and Lewis (2006) state that different wear mechanisms can occur between contacting bodies, each of them producing different wear rates. They propose a simple wear classification that is used to group the wear in “mild” and “severe” wear. The “mild” wear classification is used for wear that results in a smooth surface and is characterised by the removal of materials in very small fragments. This type of wear can be favourable but can worsen the form of the contact surface between the wheel and rail and thus result in other problems. The “mild” wear group also includes oxidative wear, where the contact temperature and asperity level influence the wear rate. (Olofsson and Lewis, 2006)

The “severe” wear classification is often associated with seizure and the wear results in a rough surface. This abrasive wear on the wheels and the rail is mostly caused by hard particles between the wheel-rail contact surfaces. Olofsson and Lewis (2006) also conclude that the transfer from mild acceptable wear to severe wear depends strongly on the surface topography.

The wear on wheels can be separated into wheel flange wear and tread wear (Enblom, 2009). The flange wear is a result of the angle of attack of the wheel with respect to the rail. This can be explained by the fact that the flange of the leading outer wheel of conventional bogies can be continually running against the rail as a result of the angle of attack. Thus, the flange wear mainly occurs when the train is driving through curves, where bigger angles of attack are present, which result in a contact force and relative slip between the flange and rail surfaces. It must also be noted that for these scenarios, not only the wear of the wheel flange is accelerated, but also the wear on the gauge face of the rail. (Swenson & Scott, 1996)

Tread wear is generally always present during normal operation of a train. However, it is more severe in cases where high slippage between the wheel and rail is present. According to Swenson & Scott (1996) all of the wheels with an angle of attack continually slip laterally across the top of the rail. Therefore, for a train negotiating a curve, the wear of the wheel tread surface (of the slipping wheel) is accelerated. This also results in an accelerated wear of the top of the rail.

Generally, the train wheels are made of softer materials than used for the rail track. This is to ensure that the wear occurs on the wheels rather than on the rails, as the repair or replacement of the rails is much more expensive. Further, a damaged track could also result in downtime of a whole rail route, which is much more critical than the downtime of a single train, which can be replaced by another train fairly quickly. However, wear on the rail tracks is not eliminated, as briefly discussed above.

Very often, general wear on tracks results in corrugation of tracks. Corrugation is wave-like wear on the top of the rail, resulting in the destruction of the rail and the trains. Corrugations can have a long (mostly observed on rails that are used by trains with high annual tonnage and axle loading) or short (which frequently occur on mass transit lines and are also known as “roaring rail”) wavelength.

Effects on train safety of short wavelength corrugations are not as severe as long wavelength corrugations on rails. Therefore, long wavelength corrugations can be very hazardous and the damaged rails require regular repair or replacement. (Liu, Zhang & Zhou, 2003)

Further, according to Olofsson & Lewis (2006), the wear rate is not only influenced by the contact pressure and the size of the sliding component, but also by natural and applied lubrication.

In conclusion, excessive wear on the wheels and rail can result in alterations of the shape of the wheel and rail profiles. This again can result in inadequate performance (i.e. unacceptable adhesion during braking or pulling away), high noise and vibration levels during normal operation (Swenson & Scott, 1996 and DCD Rolling Stock, 2012). In extreme cases, excessive wear can even result in derailing damages. Hence the importance to find further measures to reduce the wear rate of the wheels and rails, especially when the train is negotiating curves.

2.1.2. Wheel and Rail Fatigue

Another possible deterioration of rails and wheels can be due to rolling contact fatigue, which results in cracks in the material. The fatigue damages can be classified into two groups, namely subsurface-initiated (mostly caused by metallurgical defects) and surface-initiated (seem to be the result of traffic intensity and axle load) (Olofsson & Lewis, 2006).

However, the total damage to wheels and rails due to fatigue is only a very small portion in comparison to the total damage due to wear. Therefore, for this research project, the effects of fatigue are not considered in more detail.

2.1.3. Wheel-Rail Friction Conditions

According to Olofsson & Lewis (2006), friction plays an important role in the wheel-rail interface processes, such as for adhesion, rolling contact fatigue and wear. Therefore effective control of friction levels is advantageous. By maintaining friction levels, one can optimise the friction in the wheel flange-rail gauge contact and the intermediate friction between wheel tread–rail top contacts.

This means that an optimum friction condition balance has to be found (i.e. enough friction to have adequate adhesion, but also as low as possible to have a lower wear rate). Therefore, for this research project, the effect of friction has to be considered.

2.2. Measures to Improve Wheel and Rail Life

Over the last hundred years many improvements have been made to railway systems to accommodate the ever increasing loads and user requirements. Wheels and rail infrastructure were improved drastically by metallurgical means, such as surface coatings, heat treatment and using improved material alloys. However, deterioration cannot be eliminated, only reduced.

Mr Smit, from DCD Group, explained that the main aim of improving the wheel and rail design relationship is to achieve an ideal high speed stability and ideal curving ability. This is achieved by designing for high inter-axle shear stiffness and a low inter-axle bending stiffness.

Further, as rails are more expensive and difficult to maintain, the train wheels are designed to wear in preference to the rails. The wheels are designed to have “extra” wear material, which makes it possible to refurbish wheels by truing (re-profiling) (DCD Rolling Stock, 2012). The amount of material removed and thus the number of possible wheel refurbishments, depends highly on the application of the wheel (i.e. the working environment, bogie design and operating conditions).

Another measure to reduce the wear on the wheels (especially on the flanges) is by lubricating the wheel flange (Meier & Schrader, 2001). During lubrication, care has to be taken with respect to the amount and placement of lubrication, to ensure that adhesion is not lost when needed. Further, the wear rate of the wheel flanges can also be reduced by improving rail routes, i.e. increase the radius of very small curves or prevent small radii curves. This, however, is seldom possible on most routes.

The literature survey highlighted one very important fact and that is that bogie design can have a profound effect on traffic related rail and roadbed damage. This is due to the fact that the bogie design dictates how the wheel interacts with the rail.

If one considers the scenario where the train drives around a corner, firstly the inner and outer wheels of each wheel set must travel different distances to negotiate the curve and secondly, the wheels now also have an angle of attack that has to be overcome. However, the axles are rigid and are prevented to rotate horizontally in conventional bogies (DCD, 2012). Thus during curving, the slipping of wheels can only partially be reduced by having the bogie rotating underneath the train and by the wheel rolling radius differences of the tapered tread profiles. The rest of the slipping is not prevented, which results in an accelerated wear rate that is not ideal.

Major train manufacturing companies have identified this and started improving their bogie designs. First attempts of improving the bogies, were to exchange rubber elements in the one sided links (which align the wheel sets longitudinally) using rubber of a softer stiffness. This enabled a partial radial alignment of the wheel sets, but only resulted in small improvements (Meier & Schrader, 2001).

This is when the research in off-flange curving designs, such as passive steering and actively controlled steering, was initiated. This is discussed in more detail in the following section of the report, focusing on the bogies used for locomotives.

2.3. Off-Flange Curving Designs

The off-flange curving designs can be divided into the forced-steering group and the passive/self-steering group. According to Swenson and Scott (1996), forced steering, also known as active steering, requires perfectly maintained forcing mechanisms that are currently very expensive to implement and not yet fully robust. Therefore, once active control can be implemented to be robust, fail-safe and affordable, such solutions may be very attractive.

On the other hand, Swenson and Scott (1996) also note that the passive steering/self-steering is more tolerant of imperfections from wear or manufacturing tolerances. Therefore, at this point in time passive steering designs are a very attractive option.

In South Africa, the development of self-steering started in the late 1960's by Dr H. Scheffel. The first application of the self-steering bogies in South Africa was on the newly built Sishen-Saldana line. After successful implementation and test runs, the self-steering bogies were also implemented on passenger and locomotive bogies used in South Africa. (DCD, 2012)

Further, the development of self-steering bogies on locomotives was promoted in the early 1980's by two major locomotive manufactures, i.e. General Electric (GE) and Electro-Motive Division (EMD) of General Motors Corporation. Up to date, both companies together have manufactured thousands of locomotives with built-in self-steering bogies (Swenson, 1999).

Other companies such as Bombardier, Adtranz and DCD Group also developed self-steering bogies for locomotives. To provide a better overview of the different concepts developed, some of the self-steering designs are discussed in more detail in the following subsections.

2.3.1. EMD Radial Steering Bogie

The EMD radial steering bogie was introduced in 1993 on both DC and AC traction locomotives by the General Motors Corporation. In Figure 2-1, the development process followed by the EMD is shown. It shows that the self-steering was first designed and implemented on a two-axle bogie (known as the Bo-Bo bogie) and after successful implementation also on the three-axle bogie (known as the Co-Co bogie). The implementation of the radial steering on both bogie configurations is almost the same. (Swenson, 1999)

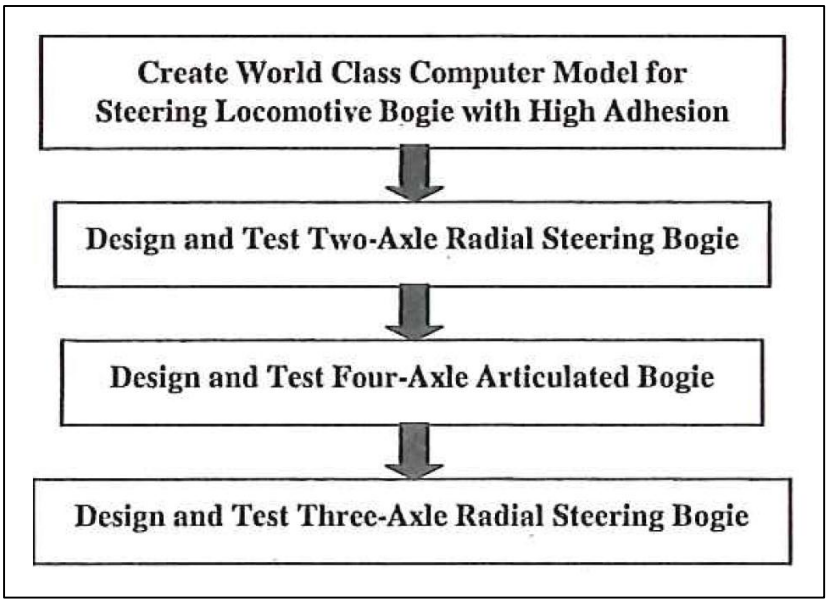

Figure 2-1. EMD Radial Steering Bogie Development (Swenson, 1999).

In Figure 2-2, a conventional co-co bogie is compared with the EMD radial steering co-co bogie. As can be seen on the figure, the radial steering bogie allows the varying longitudinal wheel forces in a curve to steer the leading and trailing axles within the bogie frame. This allows better wheel alignment on the rails and minimises the angle of attack.

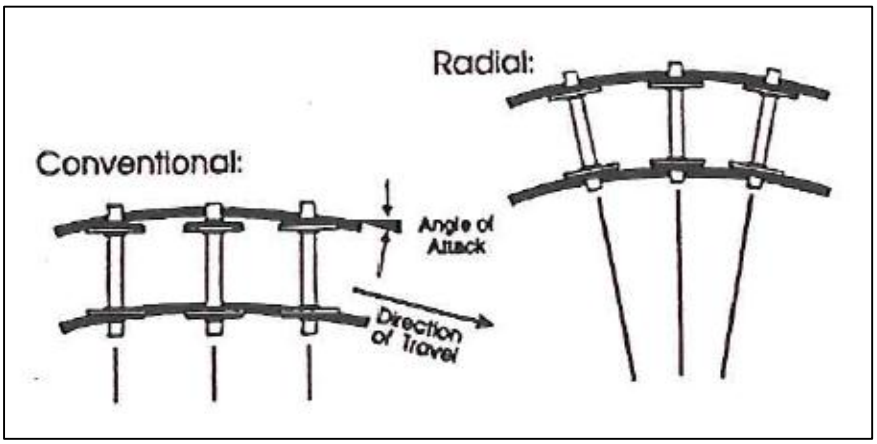

Figure 2-2. Conventional and Radial Bogie Concept (Swenson & Scott, 1996).

The differential longitudinal force is a result of longitudinal differential slip between wheels of the same axle, which is again a result of the rolling radius difference when driving around a curve (as discussed in Section 2.2). On the EMD radial steering bogie, the differential longitudinal force experienced is transmitted through the traction rods to the steering beam (shown in Figure 2-3) to achieve optimum steering of the axles. (Swenson & Scott, 1996)

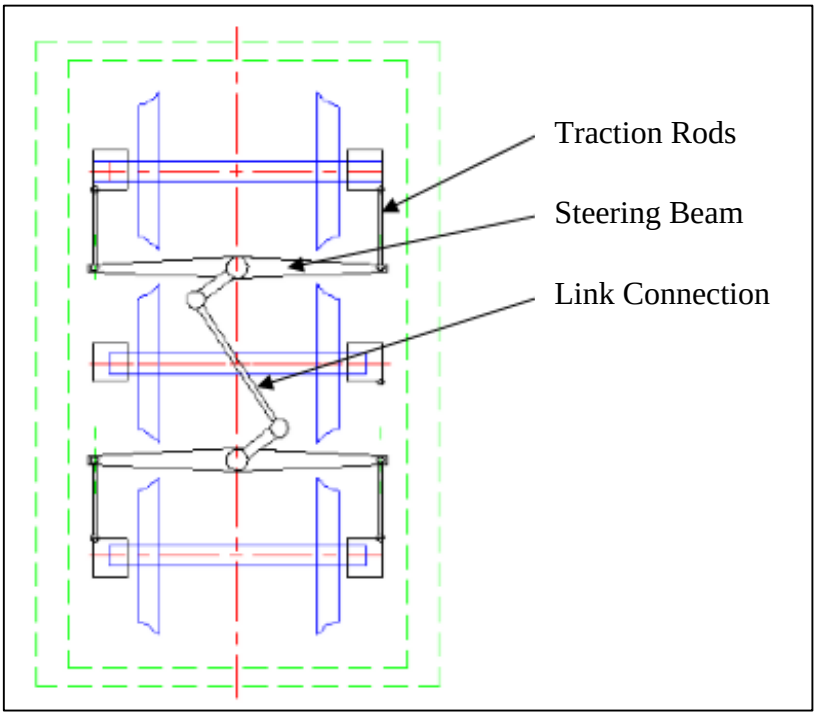

Figure 2-3. Schematic of the EMD Radial Steering Bogie (DCD Rolling Stock, 2012).

From Figure 2-3, it can be observed that for the co-co bogie the middle axle is restricted to turn radially (i.e. only lateral axle movement is allowed) and that the leading and trailing axles are connected by a steering linkage to ensure opposite sense yaw. (DCD Rolling Stock, 2012)

Since the deployment of the first EMD radial steering bogies, extensive experiments and research showed the following:

1. The radial steering bogie exhibited reduced angles of attack. On average they were less than one third of that measured on conventional bogies (Swenson, 1999).
2. The wheel flange wear is almost eliminated, due to reduced curving forces (Swenson, 1999).
3. According to tests and research performed by EMD and AAR (Association of American Railroads), adhesion in curves was improved to adhesion levels of about 45 % for starting heavy trains and to 35 % and higher for normal train operation, thereby reducing the use of sand for improving adhesion. Wheel tread wear was also not increased in spite of dramatic adhesion increases. (Swenson & Scott, 1996)
4. The amount of wheel material lost during wheel re-profiling was reduced (averaging 1.3 mm on the tread in a wheel wear study on a railroad with a very curvy track) due to less wear on the wheel flange (Swenson and Wagner, 1994). This improvement is visualised in Figure 2-4, where general wheel re-profiling results for a conventional and the radial bogie are compared.

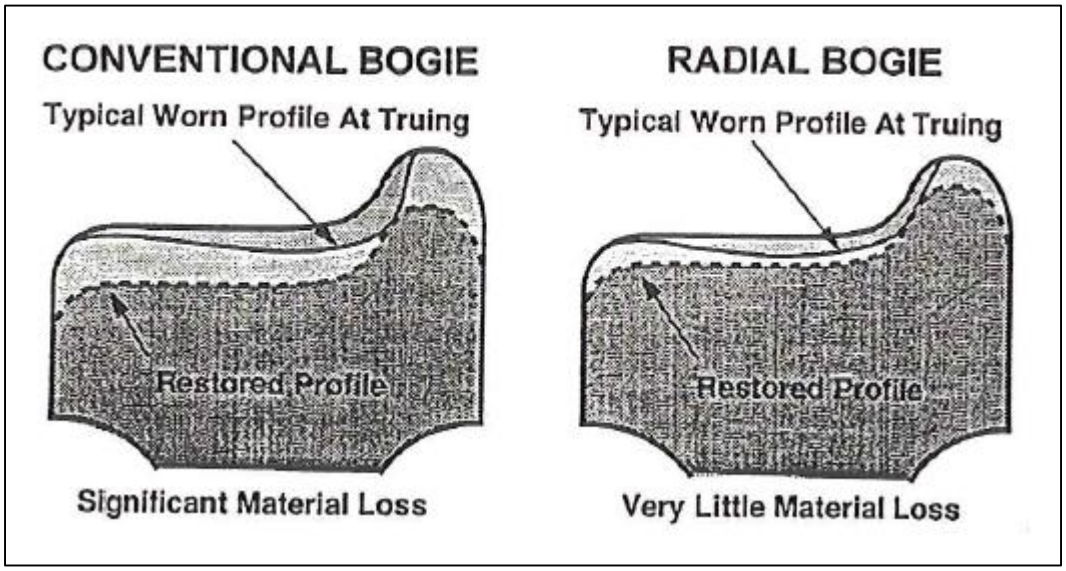

Figure 2-4. Wheel Re-profiling Results (Swenson, 1999).

5. Reduced wheel-rail contact fatigue is achieved during curving and normal operation (Swenson, 1999).
6. During curving, optimised balancing of wheel loads is observed (Swenson, 1999).
7. The passive steering is still effective in the presence of high tractive and braking forces. (Swenson & Scott, 1996)

The above mentioned improvements have several benefits including improved safety, increased loading capacity, etc. However, the economic benefits have to be highlighted, as immense cost savings can be made. The economic benefits are achieved by the extended bogie overhaul cycles, general energy savings, reduced derailment damage and the reduction of wheel and rail wear costs (Swenson, 1999).

2.3.2. General Electric Three-Axle Steerable Truck/bogie

The GE Three-Axle Steerable Bogie was developed by the General Electric Company in America. It works on the same principles as discussed for the EMD radial steering bogie in Section 2.3.1. The only difference is the construction and layout of the steering mechanism, as can be seen in Figure 2-5 below.

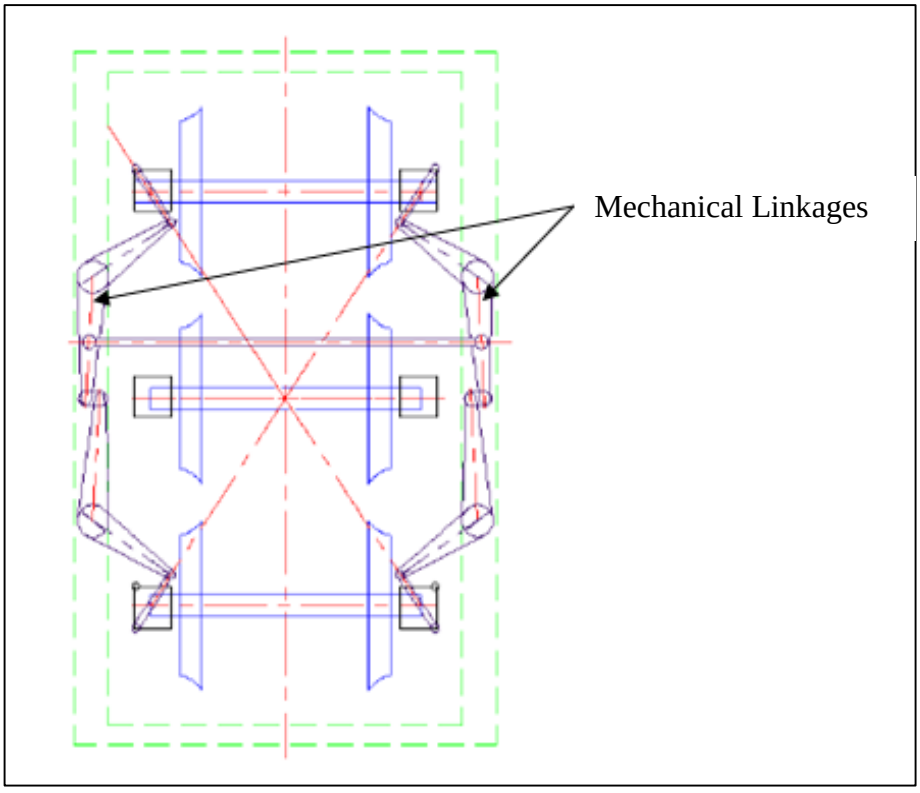

Figure 2-5. Coupling shaft mechanism for radial alignment (DCD, 2012).

This self-steering design also provides similar improvements, as discussed for the EMD radial bogies, also resulting in very attractive economic benefits. (General Electric Corporation, 1997)

2.3.3. Adtranz Shifting Axle Drive

The Shifting Axle Drive was developed by Adtranz and is in successful operation on various locomotives since 1987. Adtranz also implemented mechanical linkages to allow radial axle movement. However, there is one major difference of the shifting axle drive design compared to the two designs discussed in Sections 2.3.1 and 2.3.2. For the distribution of the tractive forces, a laterally displaceable nose suspended drive (shifting axle drive) is used (Meier & Schrader, 2001). A schematic of the design is shown in Figure 2-6 below.

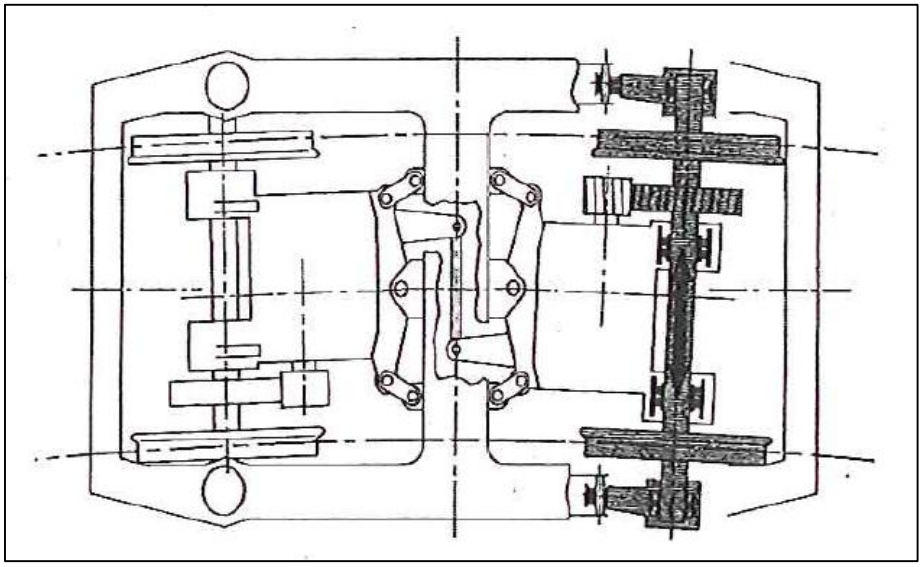

Figure 2-6. Concept of shifting axle drive (Meier & Schrader, 2001).

Similar improvements, as discussed for the EMD radial bogies, were obtained during the implementation of the shifting axle drive and thus this shifting axle concept has proven to also have very attractive economic benefits (Meier & Schrader, 2001).

The shifting axle drive was also adapted to the co-co bogie configuration. This is shown in Figure 2-7.

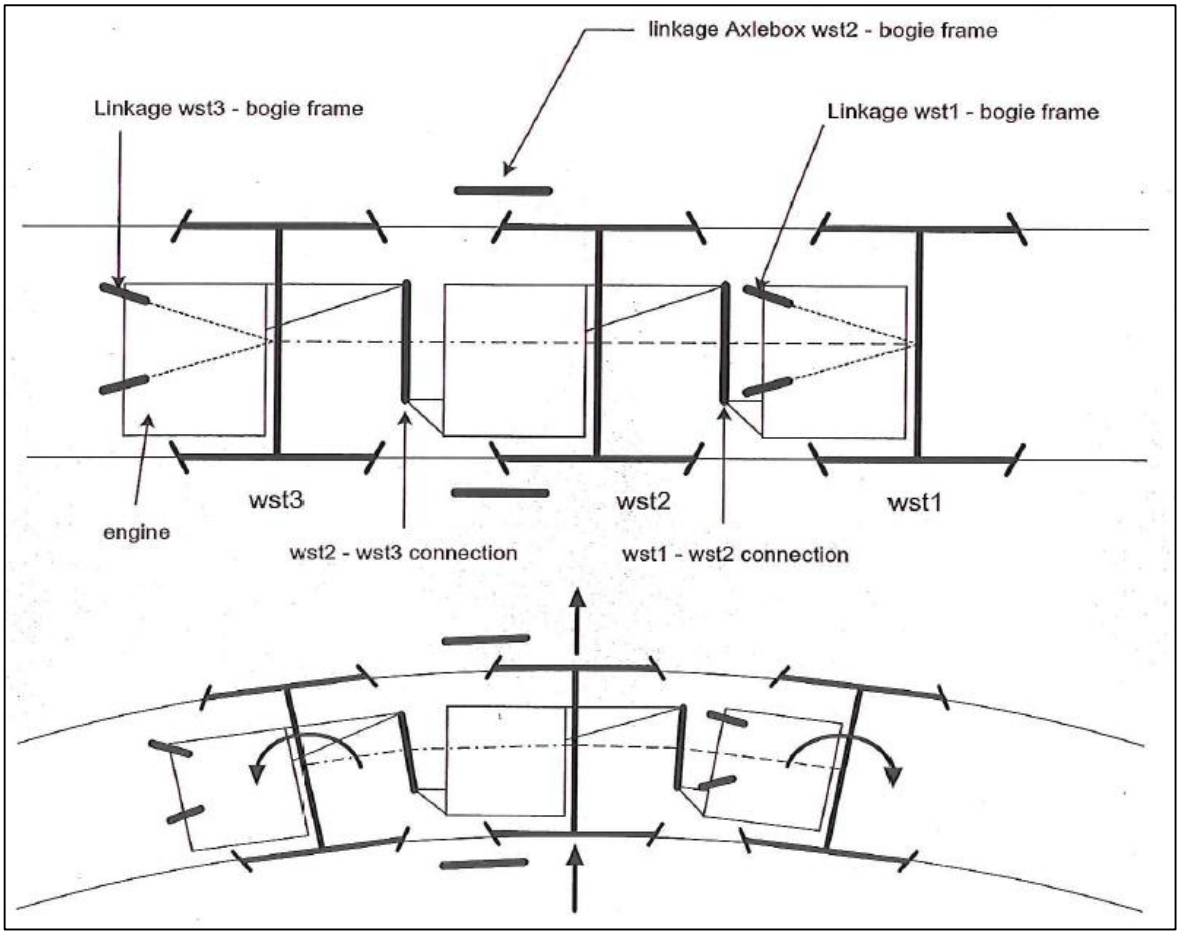

Figure 2-7. Adaption of the shifting axle drive system to a 3-axle bogie concept (Meier & Schrader, 2001).

2.3.4. DCD Passive Hydraulic Steering (PHS)

The Passive Hydraulic Steering for locomotive bogies was developed by the DCD Group as an alternative to the mechanical linkage systems (i.e. the EMD radial bogie, GE steerable truck, the Adtranz shifting axle drive, etc.). As this research project is aimed to evaluate the PHS system, a detailed explanation and discussion of this design concept is given in the following section (i.e. section 2.4 and sub-sections).

2.4. The Passive Hydraulic Steering (PHS) System Concept

As briefly discussed in Section 2.3.4, the PHS has been developed by the Research and Development Department of DCD Rolling Stock as a further improvement in overall efficiency over and above the improvements achieved with mechanically activated bogie steering systems. The following subsections describe the components and functioning of the PHS system in more detail.

2.4.1. The PHS Components

The main components of the PHS system are the hydraulic cylinders, accumulators, reservoirs, pipelines and external dampers. A drawing of the assembly of the PHS system, without the bogie, is shown in Figure 2-8. Each PHS component is discussed on its own in this section. The first component under consideration is the hydraulic cylinder.

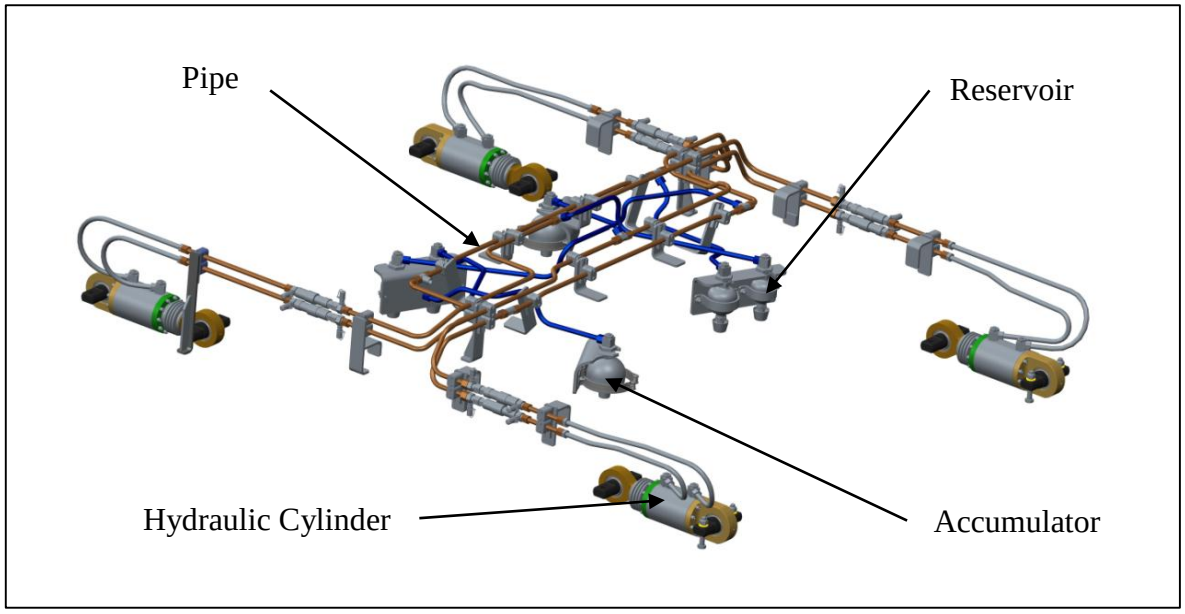

Figure 2-8. PHS Assembly (DCD, 2014).

2.4.1.1. The Hydraulic Cylinder

DCD outsourced the design of a maintenance free hydraulic cylinder, which is required to have an absolute reliability during its service cycle. This cylinder was developed by the Vehicle Dynamics Research Group (VDG) at the University of Pretoria and was designed to be very robust (i.e. designed for a normal load smaller than 30 kN and a maximum working load of 60 kN) and compact. After some tests, DCD made design improvements to the cylinders to ease manufacturing and reduce weight even more.

The overall static distance between the centres of the connecting rings of the hydraulic cylinder is 400 mm and the stroke is 60 mm (i.e. the distance between the centres of the connecting rings is maximum 430 mm and minimum 370 mm). The internal cylinder diameter is 100 mm and the diameter of the cylinder rod is 32 mm. In Fig. 2-9, a disassembled cylinder (which was used for the experimental lab tests) is shown.

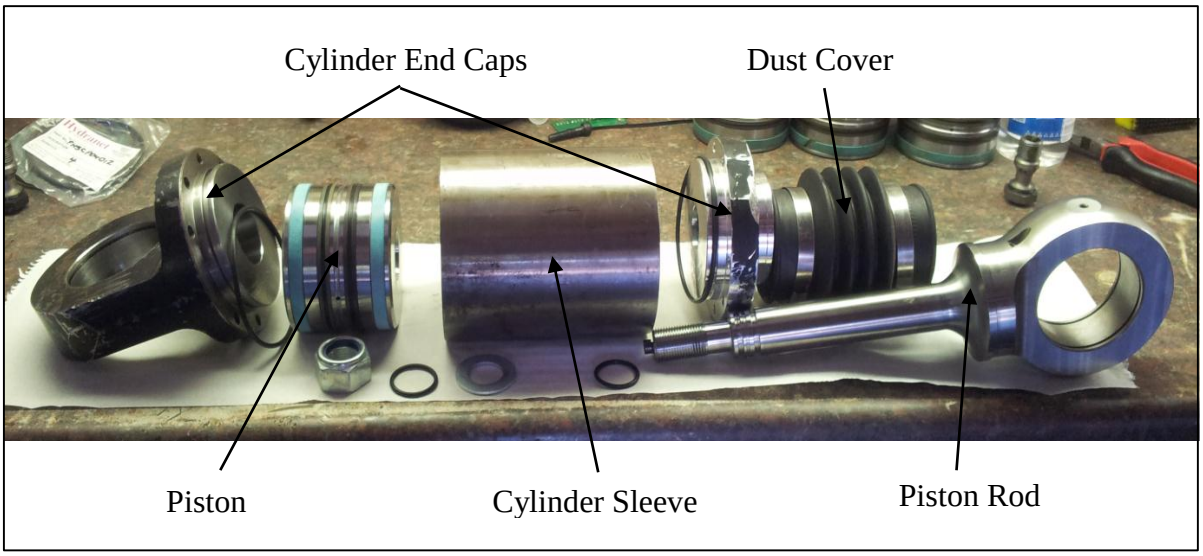

Figure 2-9. Disassembled PHS Cylinder

2.4.1.2. The Accumulators and Reservoirs

Accumulators are installed on the PHS as reservoirs and to limit the operating oil pressure to 15 MPa. The accumulators used on the PHS are Rexroth diaphragm accumulators, which were sourced from HYTEC, South Africa. Accumulators and reservoirs used on the prototype locomotives are shown in Figure 2-10.

The accumulators used to limit the PHS oil pressure have a gas volume of 0.75 litres and a gas pre-charge pressure of 15 MPa. The gas used is nitrogen. The accumulators used as reservoirs have a gas volume of 0.32 litres and no gas pre-charge. Further, the reservoir accumulators are installed unconventionally, i.e. the oil is filled into the gas side and a breather is installed on the oil side inlet. The aim of the reservoirs on the hydraulic line is to prevent cavitation of the hydraulic fluid by providing extra hydraulic fluid during vacuum scenarios.

The effects of the accumulators and reservoirs on the PHS are very critical and thus further investigation of the suitability of the selected accumulators and installation is required.

Figure 2-10. Accumulators and Reservoirs used on the PHS system.

2.4.1.3. The Hydraulic Pipe System and Oil

The pipe system connects the PHS hydraulic components and is made up of quick couplings (to ease manufacture and assembly), steel pipes, couplings and flexible hydraulic pipes. The figure below shows some of the piping currently installed on a prototype bogie for the PHS.

Figure 2-11. Pipelines installed on a Bo-Bo bogie for the PHS.

For optimal performance of the hydraulic cylinders, DCD decided to use a hydraulic oil with an ISO viscosity grade of 68. The hydraulic oil was also supplied by HYTEC.

2.4.1.4. The External Dampers

After first prototype testing, DCD decided to use external dampers to assist the damping on the PHS system. However, investigations on the implementation of external dampers are still in progress and are not part of this project.

2.4.2. The PHS Working Principle

The aim of the PHS is to allow the varying longitudinal wheel forces in a curve to steer the leading and trailing axles within the bogie frame, i.e. allow movement in the bending mode only. To achieve this, the PHS couples the wheel sets to ensure opposite sense yaw and to prevent the wheel sets to move in the shear, braking/tractive and longitudinal anti-phase mode (vibrational mode). For clarity sake, the different modes are visualised in Figure 2-12.

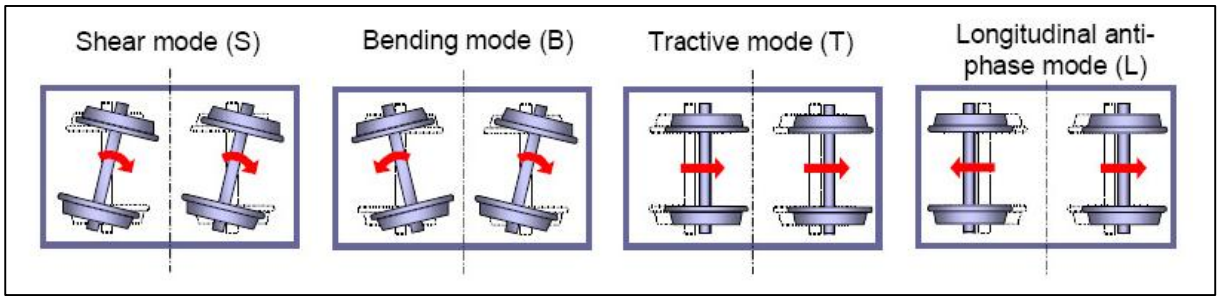

Figure 2-12. Possible train axle movement (DCD, 2012).

Figure 2-13 shows a schematic of the newly developed PHS system. The blue lines indicate the pipelines (L1 to 4), the green circles the reservoirs (R1 to 4) and the orange circles the accumulators (A1 and A2). Also, from the schematic, it can be noted that the PHS is symmetric about two axes (i.e. when looking at each cylinder and its connections)

In Figure 2-14, the forces and moments acting on the PHS system are illustrated. The coupling of the wheel sets (mentioned above) is achieved by mounting each PHS cylinder to one of the wheel axle ends, i.e. axle bearing housing. This allows the leading axle to transfer the forces (i.e. F_{x1} and F_{x2} in Fig. 2-14) experienced to the PHS system, which again transfers the force (i.e. R_{x3} and R_{x4} in Fig. 2-14) to the trailing axle. The forces in the PHS system are transferred by means of hydraulic oil flow (due to pressure differences) between the interlinked cylinders. The resulting moments of the axles are also indicated on Fig. 2-14 by M_{z1} and M_{z2}.

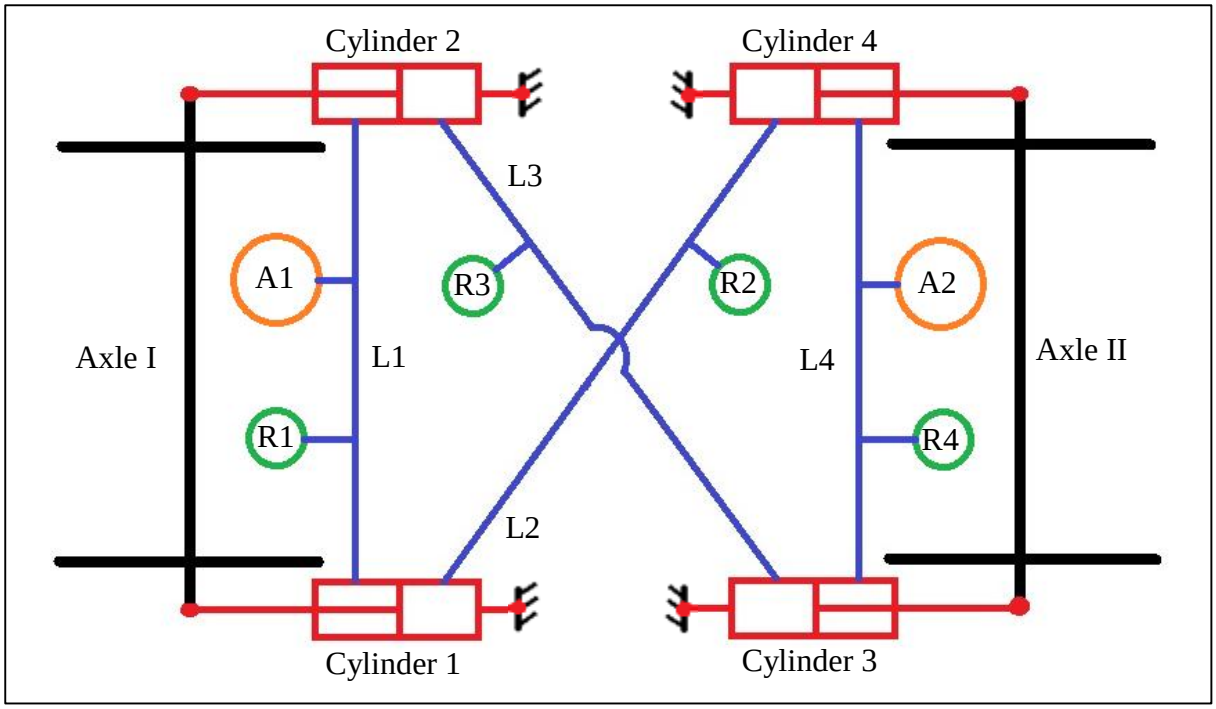

Figure 2-13. Schematic of the PHS system (A – Accumulator, R – Reservoir).

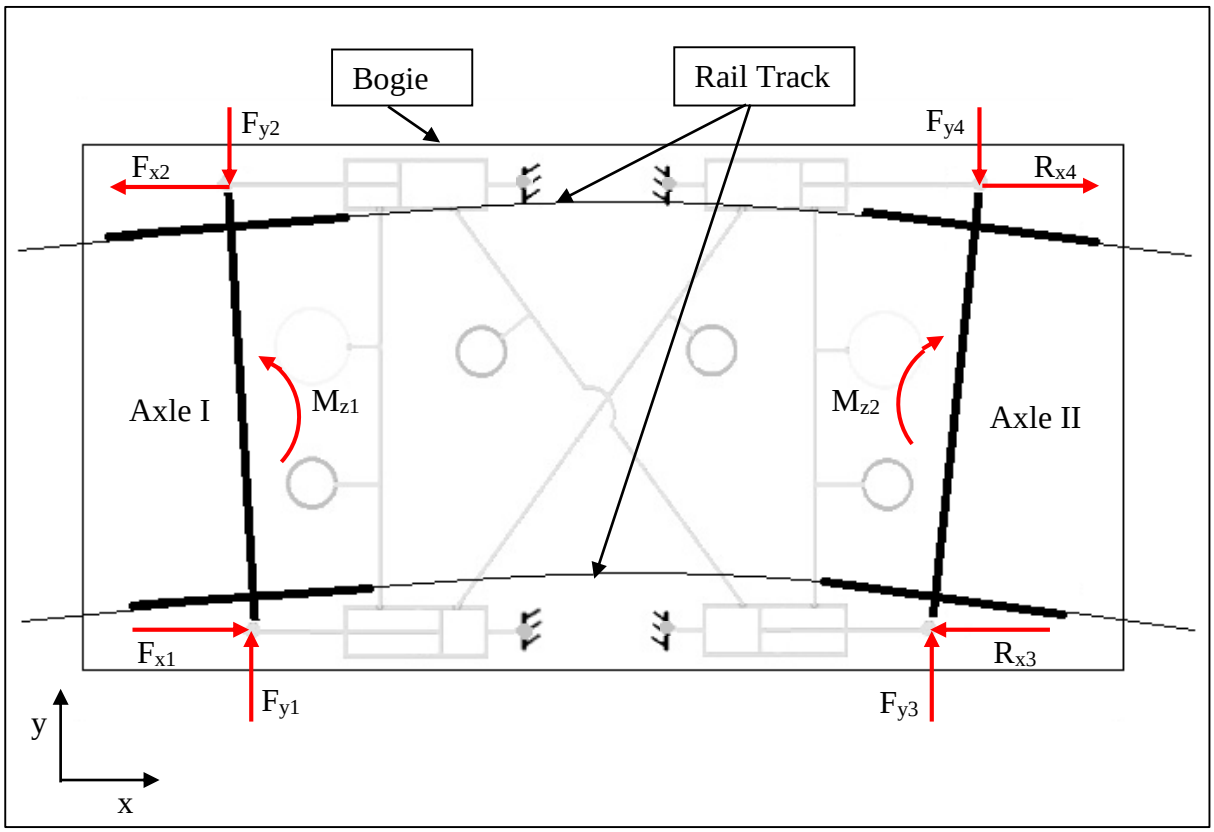

Figure 2-14. Force and Moment Diagram of the PHS.

2.4.3. PHS for Bo-Bo and Co-Co Bogie Configurations

DCD planned to implement the PHS on two and three axle bogies. The implementation of the PHS on both bogie configurations is conceptually the same. However, there are differences in the positioning of the PHS cylinders.

The first PHS prototype was installed on a 19E-Locomotive (as shown in Figure 2-15) in 2010. The 19E-Locomotives have Bo-Bo bogies installed. Up to date, different test 19E-Locomotives were fitted with PHS and were operating daily under normal working conditions on the Ermelo-Richards Bay line.

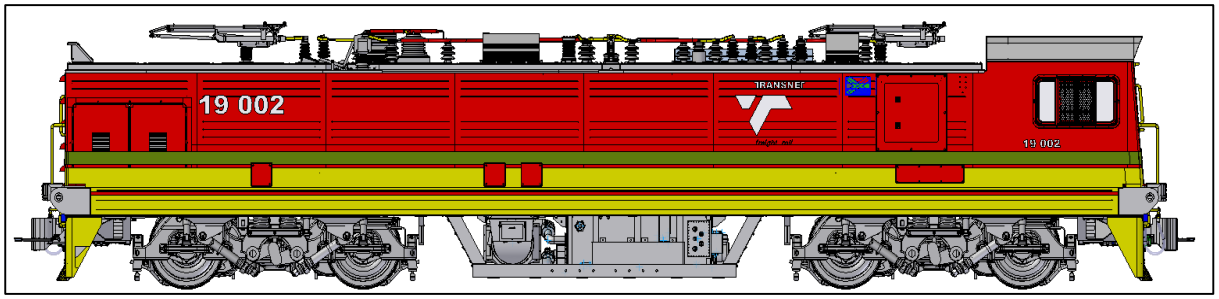

Figure 2-15. 19E-Locomotive (TFR Technology Management, 2010).

Further, the PHS was designed to be implemented on older Bo-Bo bogies, without rebuilding/redesigning the whole bogie. This is achieved by installing the hydraulic cylinders in place of the rigid axle locating linkages, which prevent longitudinal and radial movement of the axle within the bogie. Also, the hydraulic pipes are mounted on the outside/bottom of the bogie to ease access. A drawing of a Bo-Bo bogie, with the PHS implemented, is shown in Figure 2-16. The bogie is shown from the bottom.

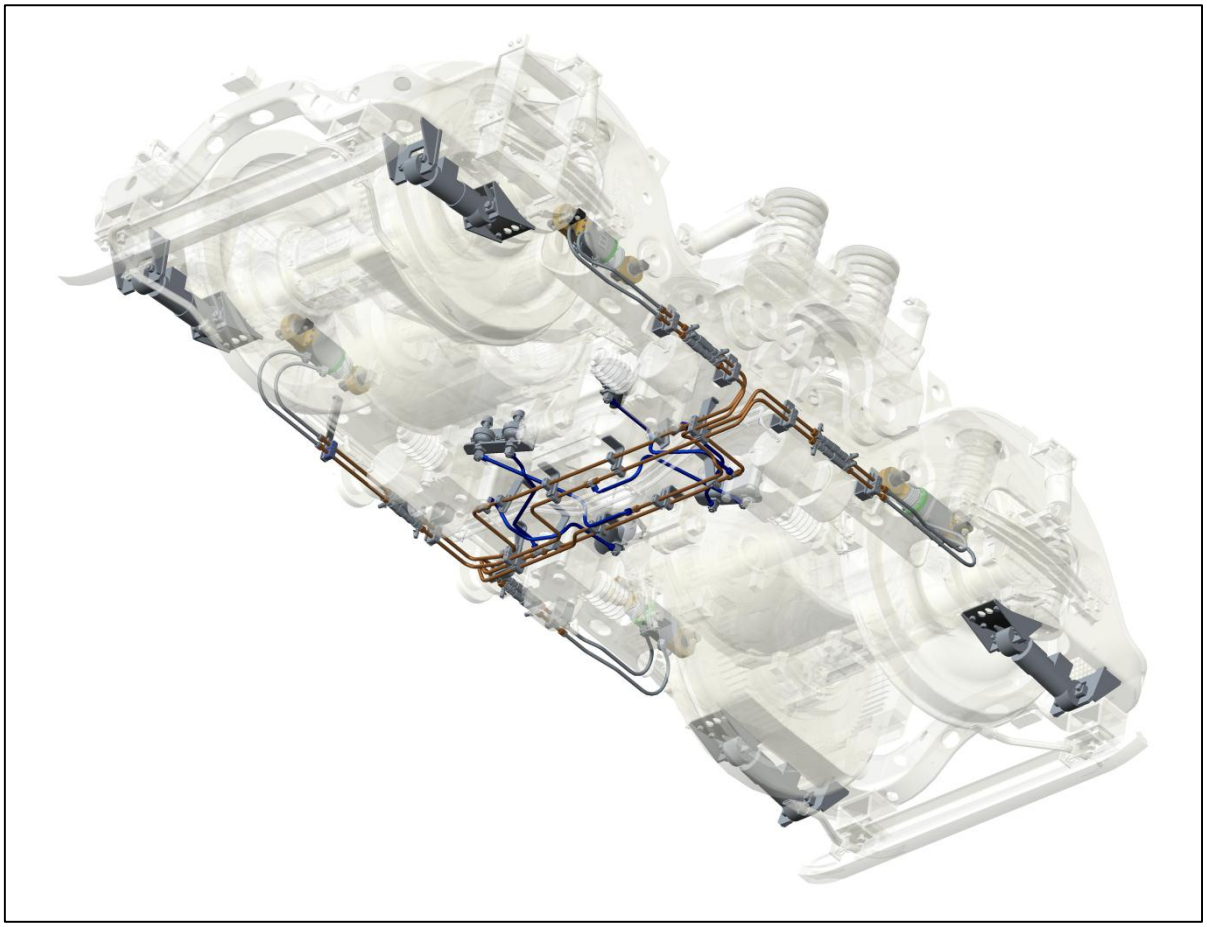

Figure 2-16. PHS fitted on a Bo-Bo bogie (DCD, 2014).

The design of the PHS on the Co-Co three axle bogie configuration has been completed. However, the first Co-Co test bogie is only planned to be assembled as soon as the PHS is implemented successfully on the Bo-Bo bogies.

As discussed before, the implementation on the Co-Co bogie is very similar to the implementation on the Bo-Bo bogie. On the Co-Co configuration, the leading and trailing wheel sets are also coupled by the PHS to ensure opposite sense yaw. The centre axle mounting design is not changed, as the original implemented bogie design allows lateral axle movement.

Another difference on the Co-Co bogie implementation is that the hydraulic cylinders of the PHS are mounted at an angle to provide shear stiffness. Mr Smit from DCD explained that if the PHS cylinders are positioned fully diagonally, the steering forces do not disturb the frame and this would be ideal. A schematic of the implementation of the PHS on the Co-Co bogie is shown in Figure 2-17.

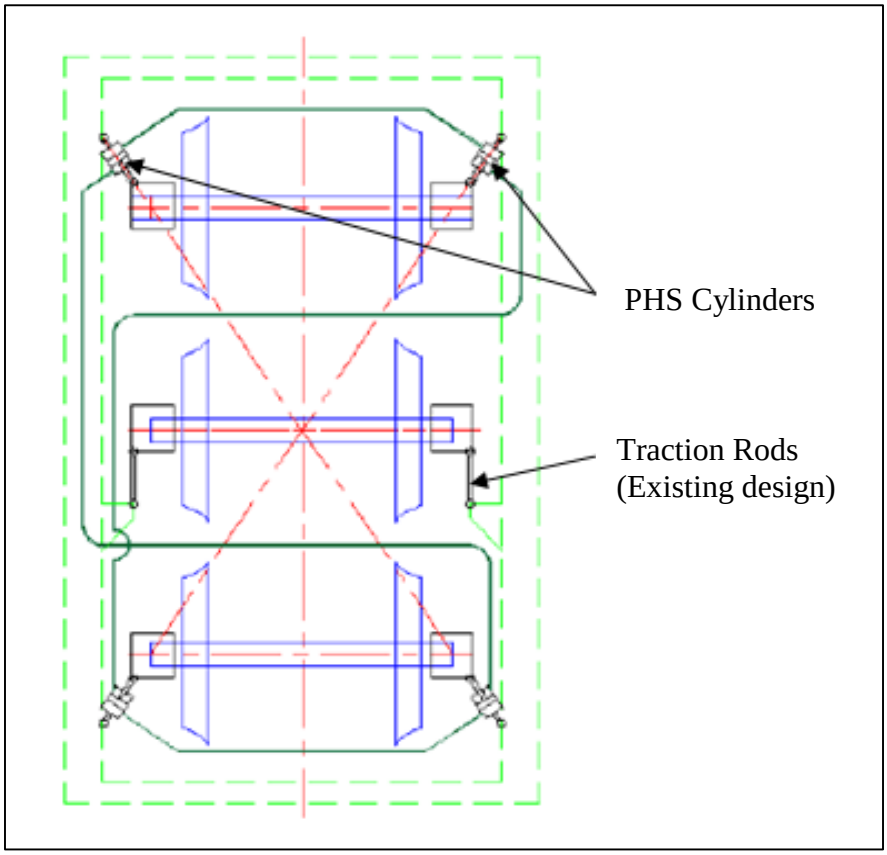

Figure 2-17. PHS fitted on a Co-Co bogie (DCD Rolling Stock, 2012).

2.4.4. Previous Simulations and Experimental Tests of the PHS

According to DCD Rolling Stock (2012), initial MSC.Adams/Rail simulations showed high improvements on the wear index (almost a factor of 7) when comparing a bogie with the PHS and a production bogie (without the PHS). They explain that this trend is mainly due to the low angle of attack of the wheels on the bogie fitted with the PHS. However, it must be noted that the PHS system was simply modelled by changing the stiffness of the traction rods (linking arms between the axles and the bogie) and needed to be validated.

To verify the simulations, initial experimental tests were performed on the PHS prototype in 2010 on the Ermelo-Richards Bay line by TFR and DCD Research Department. Second tests were performed on the Sishen-Saldana line in August 2011 and January 2012. From the tests it was concluded that a great improvement on wear reduction was observed when using the PHS, but initial simulations could not be validated. Also, problems such as oil leaks and air in the hydraulic lines were observed (Transnet Freight Rail (TFR) Technology Management, 2010 and DCD Rolling Stock, 2012).

After improving the initial PHS designs, further tests were performed in 2013 and the beginning of 2014 on the Ermelo-Richards Bay line. The tests were again aimed to evaluate how the PHS performs under normal operating conditions and to validate simulations. Similar results were obtained as mentioned for the previous tests. One of the three test locomotives, connected to a reference locomotive (without the PHS), is shown in Figure 2-18.

Figure 2-18. Test Locomotives, E 19 109 (fitted with the PHS system) and E 19 063 (Reference Locomotive).

2.4.5. Possible Advantages and Disadvantages of the PHS

The DCD Group predicts that the PHS offers similar improvements, as discussed for the EMD radial bogie in Section 2.3.1, which has very attractive economic benefits.

Further, according to Mr Smit, the PHS bogie has the following advantages compared to other mechanically activated bogie steering systems:

1. The hydraulic connections use less space than the bulky mechanical linkages.
2. The PHS is less susceptible to ageing and wear of the steering mechanism.
3. The mass of the PHS is lower and thus provides a mass advantage.

However, the implementation of the PHS has shown some disadvantages that have to be addressed. These include problems during manufacture and installation, such as the difficulty of removing air from the hydraulic system and the prevention of oil leaks.

2.5. Standards & Safety for Rail systems

In South Africa, standards and safety regulations for railway systems are stipulated in the National Railway Safety Regulator Act (NRSR Act) of 2002. The main aim of the act is to provide and establish safety standards and regulatory practice for the protection of persons, property and the environment; and to provide for matters connected therewith.

For the purpose of this research project, chapter five (part two) of the NRSR Act has the highest relevance. However, it must be noted that this does not mean that the other parts of the Act are less important. Chapter five provides the regulations regarding design, construction, operation and alteration of rolling stock, infrastructure and stations.

Further, different ISO and SANS Standards are available for the design and alterations of components of rail systems. However, these are very specific and are all linked to specific railway components (SABS Design Institute, 2013).

The different Standards and Regulations were taken into consideration during the design process of the PHS system, by the product engineers at DCD. As this research project is aimed in developing and verifying a model/simulation of the PHS system (developed by the DCD Group), we assume that the system under consideration meets all the requirements of the Act and Standards.

2.6. Modelling and Simulating hydraulics and multi-body dynamics of locomotive systems

Different commercially available software packages can be utilised to model multi-body dynamics of locomotive systems, such as MSC ADAMS, SIMPACK, UM Loco and NUCARS. Each software package has advantages and disadvantages when compared to each other. As it is aimed to evaluate the PHS system, developed by DCD Rolling Stock, the software package used by DCD should be preferred. For previous projects, DCD developed several train models in MSC ADAMS/RAIL.

For simulations of hydraulic systems there are also different commercial software packages available. These include MATLAB SimHydraulics, Automation Studio, HyPneu, Fluidsim, SimulationX and MSC Easy5. Again, each software package has different features and thus different advantages and disadvantages. However, the decision on which package to use depends highly on the available resources and the simulation requirements.

Further, hydraulic systems can be modelled using first principles, i.e. by using general hydraulic equations and relationships. These also generally form the backbone of the hydraulic simulation software packages discussed before. Extensive literature on these hydraulic equations and relationships is available. For example in the thesis *Investigation of the Time- and Temperature Dependency of Hydropneumatic Suspension Systems* written by Els and Grobbelaar (1993) and the thesis *Suspension forces on a tri-axle air suspended semi-trailer* written by Kat (2009).

As the PHS system is a complex hydraulic system, in the sense that different hydraulic components are interconnected, the student decided to generate the PHS hydraulic model using first principles. The software package used for the coding is the MATLAB/Simulink package, which is available at the University of Pretoria and allows one to incorporate the generated code into any ADAMS Multi-body Dynamic Model of a locomotive (by using a co-simulation). Also, a "bottom-up" modelling methodology was followed by first modelling the individual components, then the sub-systems and then the complete system.

3. Problem Statement and Scope of Work

As discussed in the previous sections, the need exists to perform modelling of the PHS system to obtain a better understanding of the system as a whole. Therefore, this research project is aimed to mathematically model an existing prototype PHS system and to validate the model using experimental tests.

The research commenced with a literature survey that focused on railway rolling stock wheel and rail wear as well as techniques to improve wheel and rail life. Further, existing techniques for modelling the hydraulics and multi-body dynamics of locomotive systems were investigated. The detail of the survey and findings were documented in chapter 2 of this report. Also, in chapter 2 the Passive Hydraulic Steering (PHS) concept is described in detail and previous development and research on the PHS is discussed.

The literature survey was followed by experimental laboratory testing and modelling. Initial model development and test preparations are discussed in chapter 4. The first tests and modelling were performed on a single PHS cylinder, then on a quarter PHS system and finally on a complete PHS system. The results and findings are reported on in chapters 5 to 7 respectively. In these chapters the validation of the different models is also discussed.

The report ends with an overall conclusion and recommendations in chapter 8.

4. Initial Model Development and Experimental Test Preparation

From the literature survey, it is evident that there are different possibilities to model and simulate hydraulics. It was decided to model each component individually and then assemble them to create the complete PHS model. It is assumed that no leakage, internal or external, would be taking place and that all components are ideal. The friction of the system will only be considered for the complete system and not on component basis.

The following subsections give a detailed explanation and discussion on the PHS components (as discussed in Section 2.4.1) mathematical model development, possible approaches on how thermal effects on the PHS can be incorporated into the model and on initial experimental test preparations.

4.1. PHS Component Models

The modelling was started off, by deciding which input and output of the models would be required. It was decided to use the PHS piston displacements (approximating the longitudinal displacement of the locomotive axles at each wheel) as an input for the system, which should result in cylinder force outputs (approximating the effect of the input steering or reaction forces on the reacting axle). Keeping this in mind, the following PHS component models were generated:

4.1.1. Hydraulic Cylinder Model

The force and pressure acting on the hydraulic cylinder is related by the following equation:

$$F = PA \tag{1}$$

Where A is the surface area of the cylinder piston in contact with the hydraulic oil. It must be noted that the areas for the two cylinder chambers are not the same. The area on the piston rod side is smaller.

The volume flow rate (q) of the hydraulic oil in a cylinder can be approximated by

$$q = vA \tag{2}$$

Where v is the velocity of the piston and can be determined from

$$v = \frac{\Delta d}{\Delta t} \tag{3}$$

And Δd is the change in displacement over the time step Δt.

By using Equations (1) to (3), a cylinder model was generated in Matlab. The model can accept an external force or displacement or velocity or pressure input and approximates the resulting hydraulic pressure, hydraulic force, piston displacement or oil volume flow rate in each cylinder chamber.

The effect of friction will be dealt with in a separate friction model. Also, it is assumed that the inputs provided to the model will be within the design limits of the hydraulic cylinder. If this is not possible, one could include boundary conditions in the model.

4.1.2. Accumulator and Reservoir Model

The reservoirs on the hydraulic line prevent boiling of the hydraulic fluid by providing extra hydraulic fluid during vacuum scenarios and extra oil volume to obtain an ideal stiffness of the PHS. Therefore, the reservoir allows one to assume for the mathematical model that boiling will not occur and that there will be enough hydraulic fluid in the system for all different PHS working scenarios (i.e. will provide continuous oil flow).

The reservoirs are accumulators (with a volume of 0.32 litres) and are filled with nitrogen at atmospheric pressure. Also, on the two cross pipe lines, i.e. the pipe connection between cylinder 1 and 2 and cylinder 3 and 4, larger accumulators (with a volume of 0.75 litres) were installed as a blow off safety vessel for pressures higher than 15 MPa. Thus, the modelling of the accumulators and reservoirs is critical.

The modelling of an accumulator can be very complex. Firstly, the accumulator acts as a spring and damper system on the hydraulic system and at very high pressures (pressures higher than the pre-charge). It also acts as an oil reservoir.

The first approach for modelling an accumulator is to approximate the accumulator as a hydraulic cylinder connected to a spring and damper. This is shown in the following schematic below (Fig. 4-1).

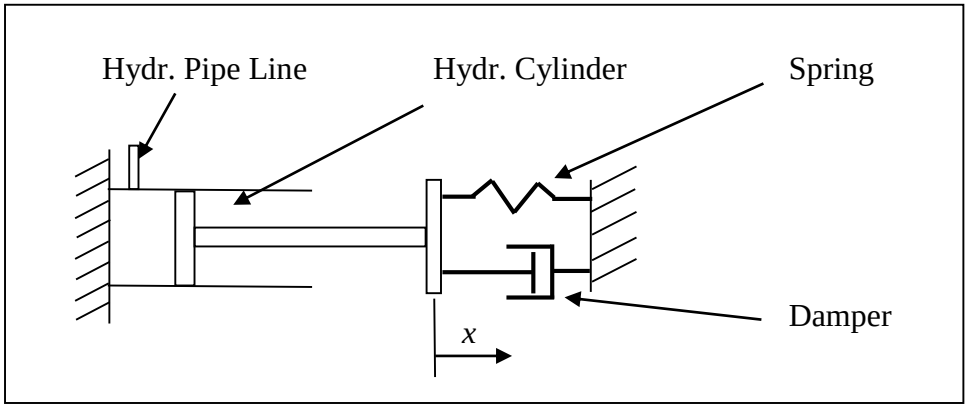

Figure 4-1. Accumulator Approximation Option 1.

The force generated by the spring and damper opposes the force produced by the pressurised hydraulic oil. Therefore, the forces in the accumulator can be approximated by

$$F_{accum.} = F_{spring} + F_{damper} \quad (4)$$

Where

$$F_{accum.} = P_{accum.}(A_{accum.}) \quad (5)$$

And

$$F_{spring} = k_s x \quad (6)$$

And

$$F_{damper} = c\dot{x} \quad (7)$$

This approximation is difficult to implement, as the displacement (x), spring constant (k) and damping constant (c) are unknowns. Also, the area is not constant in a bladder accumulator. Therefore, further assumptions are needed to simplify this model.

A second option is to make the initial accumulator model very basic. This can be achieved by assuming that the accumulator (used as a reservoir) only provides a constant oil pre-charge pressure of 2 MPa to the hydraulic line and that the bigger accumulator only acts as a blow-off valve with the reservoir (which limits the maximum hydraulic system pressure to 15 MPa). Unfortunately, initial laboratory tests have indicated that the PHS system is very sensitive and that using such a simplified accumulator model will result in severe simulation errors.

Another possibility for modelling the accumulator is to model the hydraulic fluid flow in and out of the accumulator. The fluid volumetric flow rate in or out of the accumulator is:

$$q_A = \frac{dV_F}{dt} \tag{8}$$

Where V_F is the fluid volume in the accumulator.

If one now makes the assumption that no loading on the accumulator membrane gas and oil separator (such as inertia and friction) is considered, one can approximate the pressure of the fluid in the accumulator to be the same as of the gas in the accumulator. This allows one to approximate the fluid (i.e. oil) pressure by modelling the gas side of the accumulator.

The initial volume of the gas (i.e. nitrogen for the PHS system) in the accumulators is approximated as it is a design parameter. Also, the oil volume flow rate into the accumulator can be approximated. This now makes it possible to determine how the change in gas volume can be used to predict the corresponding gas pressure.

For this approximation purpose, different gas models, based on the thermodynamics of ideal gases, are available. The modelling of accumulators with this approach is well discussed and documented by Els (2006) and Van der Westhuizen and Els (2014). They state that the accuracy of each approximation is dependent on the system modelled. Thus it was decided to generate different accumulator models and then to evaluate which model most accurately represents the accumulators used for the PHS.

The models considered are three ideal gas (IG) law variations, i.e. isothermal, adiabatic and the IG with the energy equation (EE), and a real gas approach (Benedict Webb Rubin (BWR) equation with the EE). These models are based on the assumption that the fluid in the accumulator is incompressible, but can be modified by including the bulk modulus in the volume calculations.

The ideal gas law is defined by

$$P = \frac{mRT}{V} \; or \; P = \frac{RT}{v} \tag{9}$$

Where m is the mass of the gas, R the universal gas constant, T the gas temperature, v the specific gas volume and P and V the gas pressure and volume respectively. For a closed system compressed from state 1 to state 2, Equation (9) can be re-written as

$$\frac{P_1V_1}{T_1} = \frac{P_2V_2}{T_2} \tag{10}$$

In an isothermal process the temperature remains constant and thus one can write

$$P_1V_1 = P_2V_2 \tag{11}$$

Further, for a system which is assumed to be a polytropic system, Eq. 11 can be redefined as

$$P_1V_1^n = P_2V_2^n \tag{12}$$

Where n is the polytropic constant and for an adiabatic process $n = \gamma$, where γ is the adiabatic index of the gas (for air and nitrogen $\gamma \approx 1.4$). It must be noted that n may not always be constant for a system.

The approximations previously discussed are only valid for ideal gas behaviour. A general compressibility chart (Annexure A, Fig. A-1) can be used to determine whether the ideal gas approach is valid and if not, a real gas approximation must be used. Different real gas equations are available, but only the BWR is considered. The BWR equation is based on the ideal gas law and adds corrective terms to improve accuracy. However, this makes the BWR only appropriate for systems with a specified temperature and pressure range and thus its appropriateness for the PHS model has to be validated.

The BWR equation is as follows

$$P = \frac{RT}{v} + \frac{B_0RT - A_0 - \frac{C_0}{T^2}}{v^2} + \frac{bRT - a}{v^3} + \frac{a\alpha}{v^6} + \frac{c\left(1 + \frac{\gamma}{v^2}\right)e^{\frac{-\gamma}{v^2}}}{v^3T^2} \tag{13}$$

Where B_0, A_0, C_0, a, b, c, α and γ are BWR constants and are included in Annexure A.

All the models have limitations due to the assumptions made. One limitation of the ideal gas equation and BWR equation is that no heat transfer between the gas and its surroundings is taken into account. This, however, can be changed by using the energy equation (EE), also known as the first law of thermodynamics, for a closed system. The full derivation is discussed by Els (2006) and Van der Westhuizen and Els (2014). They conclude that the IG with EE is described by

$$P = \frac{RT_g}{v} \tag{14}$$

And T_g is approximated by solving the following first order differential equation by means of the 4th order Runga Kutta method.

$$\dot{T}_g = \frac{(T_s - T_g)}{\tau} - \frac{P\dot{v}}{C_{vo}} \tag{15}$$

Where

$\dot{T}_g$ = First time derivative of the gas temperature

$\dot{v}$ = First time derivative of the gas specific mass

C_{vo} = Specific heat capacity of the gas

τ = Thermal time constant

Similarly, the BWR with EE is defined as

$$P = \frac{RT_g}{v} + \frac{B_0RT_g - A_0 - \frac{C_0}{T_g^2}}{v^2} + \frac{bRT_g - a}{v^3} + \frac{a\alpha}{v^6} + \frac{c\left(1 + \frac{\gamma}{v^2}\right)e^{\frac{-\gamma}{v^2}}}{v^3T_g^2} \tag{16}$$

Where the first order differential equation for the temperature T_g is

$$\dot{T}_g = \frac{(T_s - T_g)}{\tau} - \frac{\dot{v}}{C_v}\left[\frac{T_g R}{v}\left(1 + \frac{b}{v^2}\right) + \frac{1}{v^2}\left(T_g B_0 R + \frac{2C_0}{T_g^2}\right) - \frac{2c}{v^3 T_g^2}\left(1 + \frac{\gamma}{v^2}\right)e^{\frac{-\gamma}{v^2}}\right] \quad (17)$$

And

T_s = Atmospheric temperature

γ = BWR constant (not to be confused with the adiabatic index). Please also note that the BWR constants remain the same as given in Annexure A.

Further, the ideal gas specific heat capacity required in Eq. (15) is approximated with

$$C_{vo} = R\left(\frac{N_1}{T_g^3} + \frac{N_2}{T_g^2} + \frac{N_3}{T_g} + (N_4 - 1) + N_5 T_g + N_6 T_g^2 + N_7 T_g^3 + \frac{N_8 \frac{N_9}{T_g}^2 e^{\frac{N_9}{T_g}}}{\left(e^{\frac{N_9}{T_g}} - 1\right)^2}\right) \quad (18)$$

And the real gas specific heat capacity is approximated by

$$C_v = C_{vo} + \frac{6}{T_g^3}\left(\frac{C_0}{v} - \frac{c}{\gamma}\right) + \frac{3c}{T_g^3}\left(\frac{2}{\gamma} - \frac{1}{v^2}\right)e^{\left(-\frac{\gamma}{v^2}\right)} \quad (19)$$

All nitrogen constants are also provided in Annexure A. The equations and constants were obtained from Els (2006).

For the PHS modelling, all four models were implemented in MATLAB and the accuracy/appropriateness will be investigated at the end of this project. Please note that the modelling of the thermal effects on the PHS is discussed further in section 4.2. Also in this section, it is initially proven that the ideal gas behaviour can be assumed for the modelling of the PHS system.

4.1.3. Piping System Model

The flow in the piping system can be modelled as viscous flow in ducts. However, this approach is very complex as steady state is not achieved and properties, such as temperature, friction factors and oil properties have to be taken into account. Further, the geometry of the piping system has an effect on the flow.

Therefore, as a first approach one can simplify the fluid flow by assuming a constant friction factor, constant temperature and constant oil properties. Also, the expected oil flow will be low and the pipe diameter should be sufficient to have no significant influence on the flow. This implies that one can assume a constant pressure loss over the different pipes. As an initial approximation, it is further assumed that the pipes have in any event, a very small (approximating zero) pressure drop. The effects of the piping on the system (if any) will, however, be included in the friction model.

During initial laboratory tests, it was observed that the flexible hydraulic pipes may be expanding slightly under high pressures, but as this effect is difficult to approximate, it has initially been assumed to be negligible.

4.1.4. Hydraulic Oil Model

In general one can make the assumption that oil is incompressible. However, this is not always valid due to air trapped in a system (i.e. in the hydraulic connections, small cavities, dissolved in the oil and between seals) and the nature of the system under consideration.

During the preparation of the experimental tests, it was evident that it is very difficult to remove air trapped in the PHS system. Further, the system is required to be very stiff. Thus the compressibility of the hydraulic oil (possibly containing a small volume of air) will have an effect on the accuracy of the PHS modelling. The effect of the compressibility of the oil can be quantified by determining the bulk modulus of the oil-air mixture. The bulk modulus is defined by

$$\beta = \frac{\Delta P}{\left(\frac{\Delta V}{V}\right)} \tag{20}$$

Where

β = Bulk modulus of the fluid [Pa]

ΔP = Fluid pressure change during two conditions [Pa]

ΔV = Fluid volume change during the same two conditions [m^3]

V = Total fluid volume of the system at atmospheric pressure [m^3]

From Eq. 20, it is evident that for modelling purposes, accurate approximations of the oil volumes of the PHS components are required. These are tabulated in Table 4-1.

The oil volumes were determined with two different approaches. The calculated oil volume was obtained by using the design dimensions of the components and the measured oil volume was obtained by measuring the physical volume of oil filled into the components. The two values correspond very well.

Table 4-1. Approximate Oil Volumes of the Different PHS Components.

PHS Component	Calculated Oil Volume in m^3	Measured Oil Volume in m^3
Hydraulic Cylinder (Both chambers together)	0.000447	0.00045
Accumulator	0.00075	0.00074
Reservoir	0.00032	0.00031
Pipe per meter (12mm inside diameter on average)	0.000113	0.000115

Further, the compressibility of oil can be incorporated as a refining correction in the calculation of the gas volume in the accumulator.

It must also be noted that at the PHS cylinder equilibrium position, the oil in diagonal pipelines has a lower pre-charge (approx. 1.8 MPa) than in the cross connections (approx. 2 MPa). This is to account for the different cross-sectional areas of the cylinder chambers.

4.2. Modelling of Thermal Effects on the PHS System

In some locomotive working environments, the surrounding temperature can range from very cold to very hot and has an effect on the working temperature of the locomotive. For example on the Ermelo-Richards Bay line in winter, the temperature can range from – 12 to 28 °C on the same day. Also, the heat given off by the train cooling system affects the working temperature of the train. Thus temperature effects on the PHS have to be investigated in more detail.

The properties that can be affected by temperature (in the range of -20 and 50°C) are the oil and nitrogen gas properties. Firstly, looking at the hydraulic oil used, generally pour points of oil with an ISO viscosity grade of 68 are below -30 °C and have a flash point above 240 °C. The oil properties that are affected the most by temperature are viscosity and density. This could thus have an effect on the oil volume and flow resistance of the system. On the other hand, the system is a closed system and all components experience the same effect. Further, the working temperatures are higher than the pour point and much lower than the flash point. Thus, the assumption is made that the temperature effect on the oil is negligible for normal working conditions. This assumption will have to be validated in train tests.

According to Els (2006), thermal effects (from the surrounding environment and from a system itself) on hydro-pneumatic systems are not negligible. Therefore, to be able to include thermal effects on the PHS system, one can consider an experimentally determined thermal time constant for the modelling of the nitrogen gas behaviour in the accumulators and reservoirs (as discussed in section 4.1.2). The thermal time constant is a measure of the heat transfer coefficient between a gas in a closed container and its surroundings (Els & Grobbelaar, 1993). In general, the thermal time constant is defined in terms of temperature. However, it is extremely difficult to measure temperature changes at high speed. Thus, one possible option is to determine the thermal time constant from pressure or force measurements. This, however, is only valid if the ideal gas assumption holds (Els, 2006).

Now the question has to be answered if it is reasonable to assume ideal gas behaviour. This can be done by looking at the reduced pressure (P_r) and temperature (T_r) of the nitrogen gas. These are defined as follows:

$$P_r = \frac{P}{P_c} \tag{21}$$

$$T_r = \frac{T}{T_c} \tag{22}$$

Where

P = Pressure for a given state [Pa]

P_c = Critical pressure [Pa]

T = Temperature for the same state [K]

T_c = Critical temperature [K]

The critical pressure for nitrogen is 3.39 MPa and the critical temperature is 126.2 K (Borgnakke & Sonntag, 2009). If it is assumed that the normal operating temperature will be on average about 25 °C (298.2 K), the reduced temperature can be calculated to be approximately 2.4 (per Eq. 22). It must also be noted that the reduced temperature only changes about 8 % when changing the average temperature by 20 °C. On the other hand, the pressure in the PHS system can range in extreme scenarios from approximately 0 to 20 MPa. Therefore, the reduced pressure can range from approximately 0 to 5.9 (per Eq. 21).

These values can now be used to determine a compressibility factor (Z) from the Lee-Kessler simple fluid compressibility chart (available in Annexure A). From the chart it can be noted, that for a reduced temperature of 2.4, the factor Z can be approximated to be 1 for the range of reduced pressures calculated (highlighted on Figure A-1). A $Z \approx 1$, indicates that the ideal gas assumption is valid.

4.3. Experimental Test Preparation

The experimental laboratory tests were performed in the Sasol laboratories of the University of Pretoria. The purpose of the tests was to find parameters that can be used to improve initial mathematical models. Properties under consideration were hydraulic fluid properties (bulk modulus, viscosity), system stiffness and accumulator characteristics. Also, changes to the reservoir design were investigated.

The tests were done in two phases. For the first phase, the different sub-systems and components of the PHS system were tested and characterised. For the second phase the complete PHS system (only hydraulic components) was tested.

To prevent confusion and possible misinterpretation of data and simulations, the following sign convention was used for the tests and simulations:

1. Tension force is considered as positive.
2. Compression force is considered as negative.
3. Any extension of the PHS cylinder relative to a reference point is seen to be positive displacement and negative when under compression.
4. Extensional speed is considered as positive.

5. Compressional speed is considered as negative.
6. Oil volume flow rate into cylinder is considered as positive and flow out as negative.

Different setups were planned to characterise and parameterise the PHS components. The components required for the laboratory tests were supplied by DCD and assembled in the Sasol Laboratories. After all parameters were determined, a quarter PHS system setup and a full PHS setup was used to obtain validation data for the mathematical model. All test equipment was calibrated for the tests. The necessary safety precautions were taken in view of the high stresses and pressures in the system and to which the system elements would be subjected to.

As no valid field test data is available as yet, it was decided to generate some test scenarios. The scenarios were based on information discussed and explained by Mr Smit and Mr Maartens (from DCD and TFR). For normal operating conditions the following loads (on each wheel) can be expected:

- For Braking:
  - The force due to a brake block pressing against a wheel is approximately 30 kN.
  - The force due to braking for 0.25 adhesion and approximate wheel load of 13 ton is approximately 32.5 kN and for 0.4 adhesion about 52 kN.
  - Thus the total force due to braking is approx. 62.5 to 82 kN
- For Steering:
  - The forces are generally below 30 kN.
- For traction and electrical braking:
  - The forces can be approximated to be 32.5 kN, when assuming 0.25 adhesion and 52 kN for 0.4 adhesion.
- For unusual conditions, such as heavy shunting, derailment and overloading:
  - It is assumed that accelerations of about 5g can be expected, which gives an approximate wheel force of 175 kN.

The above mentioned forces are also summarised in Table 4-2. For validation purposes, displacement input signals are generated that result in forces as tabulated. The shapes of the different inputs are chosen to be sinusoidal, triangular wave, step and ramp inputs. Some of the results obtained for these inputs are discussed in the validation section.

Table 4-2. Approximate Wheel Forces.

Simulation Scenario	Approximate Longitudinal Forces acting on the PHS Cylinders [kN]
Braking	62.5 to 82
Steering	< 30
Traction and Electrical Braking	32.5 to 52
Unusual conditions	< 175

5. Testing, Modelling and Validating of a PHS Cylinder

The first experimental tests and modelling were performed on a single PHS cylinder. The cylinder under consideration was Cylinder 1 and is highlighted in the schematic below. While performing the tests on the cylinder, the hydraulic piping and oil used was also investigated. This was done be connecting different lengths of piping (hydraulic flexible hose and steel pipes) to the cylinder and estimating a bulk modulus of the oil. This chapter discusses how the tests were performed, which results were obtained and which modelling decisions were made during the validation process.

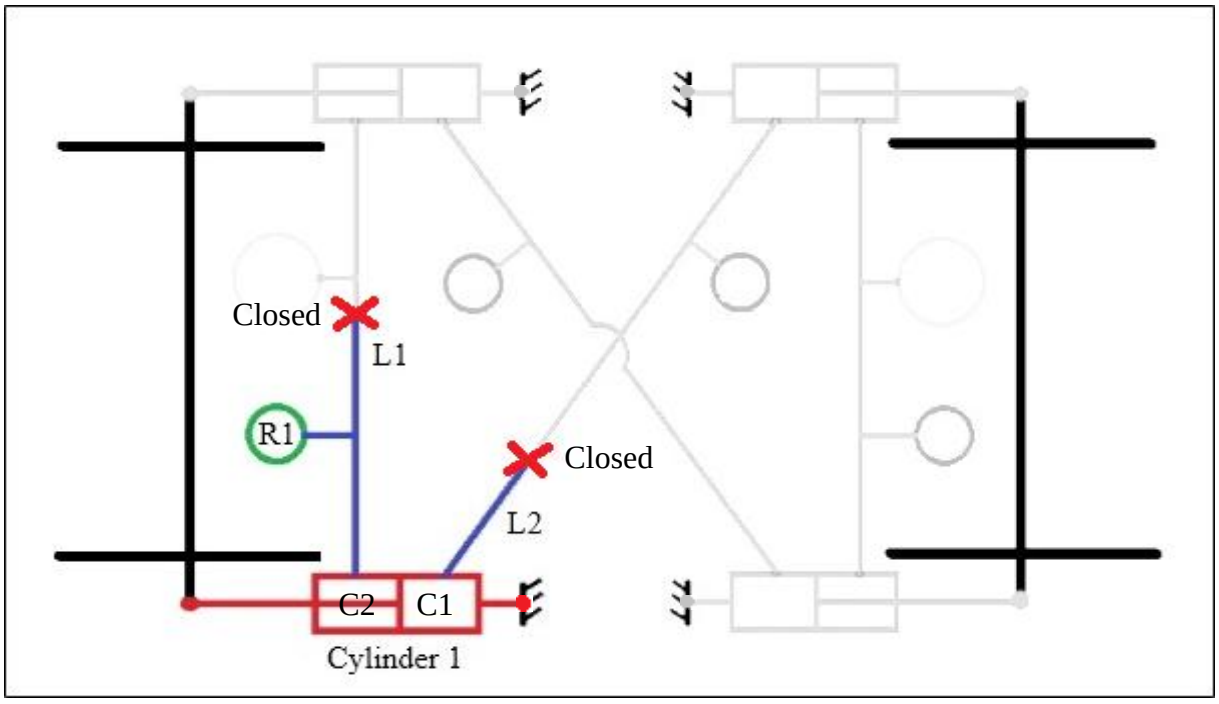

Figure 5-1. Schematic of the PHS, highlighting one hydraulic cylinder (C1 – Chamber 1, C2 – Chamber 2).

5.1. Laboratory Testing

The test setup is shown in Figure 5-2. The actuator was a 160 kN Schenck actuator and the test frame was used to hold the PHS cylinder. A laser displacement transducer was mounted to the cylinder to ensure accurate piston displacement measurements. During calibration and initial testing, it was noticed that the laser was mounted too far away from the cylinder (as shown in Figure 5-2) and needed to be mounted even closer to improve the accuracy. A Wika pressure transducer (40 MPa) was utilised to measure the oil pressure and a load cell (160 kN) to measure the force on the PHS cylinder.

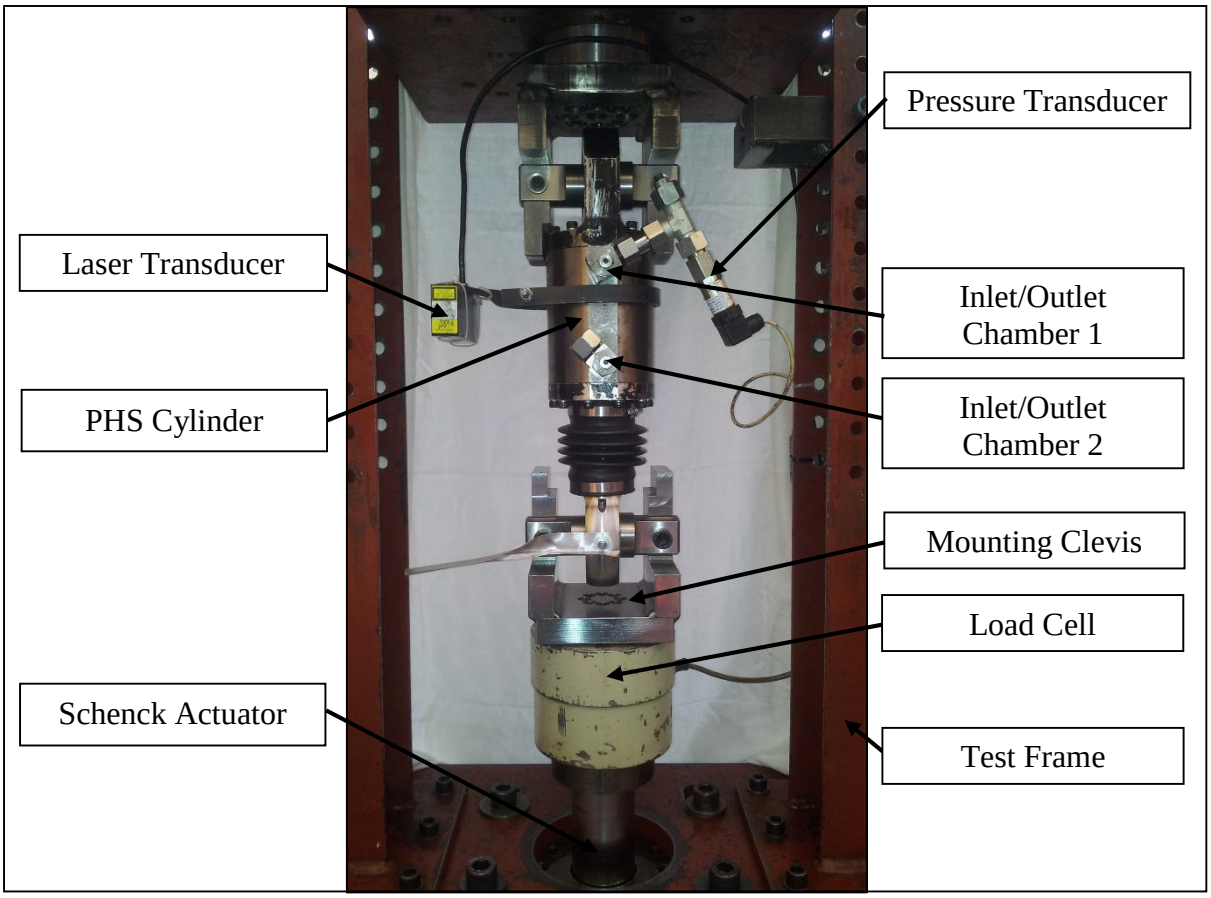

Figure 5-2. Test Setup of a single PHS Cylinder.

5.1.1. Bulk modulus Determination

The determination of the bulk modulus (β) was discussed in section 4.1.4. To determine the bulk modulus experimentally, the chamber with the smaller volume (chamber 2) was connected to an oil reservoir, to allow the oil to flow freely in and out of the piston chamber. The chamber with the bigger oil volume (chamber 1) was filled with oil and was closed. Care was taken to bleed the chamber (as thoroughly as possible) and to measure the oil filled into it accurately. The cylinder was then activated by a ramp input and the corresponding oil pressure, piston displacement and force exerted by the cylinder was measured.

The pressure measured is plotted against the normalised volume (ΔV/V) on Figure 5-3. On the graph, it can be observed that at pressures above 2 MPa, the bulk modulus can be approximated to be 1.4 GPa. The high compression of the fluid under 2 MPa is mainly due to air trapped in the oil.

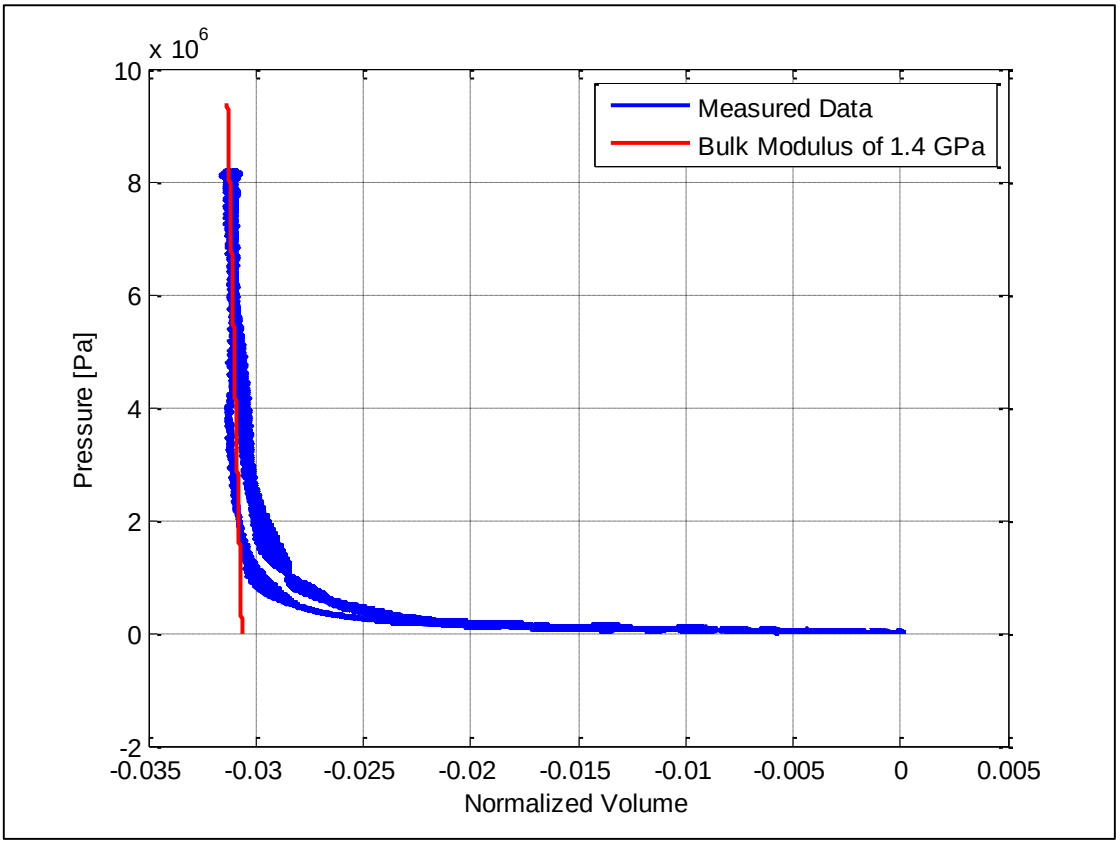

Figure 5-3. Measured Bulk Modulus for a single PHS cylinder.

For the second setup, the test oil volume was increased by connecting an 860 mm long flexible hose to chamber 1. Similar observations were made as previously discussed and, again, the bulk modulus can be approximated to be 1.4 GPa. A pressure versus normalised volume graph is given in Figure 5-4. Different length of piping (flexible rubber hose and steel) were tested and similar results were obtained. Therefore, one can assume that the expansion effects of the pipes are negligible.

According to literature, the bulk modulus for hydraulic fluids generally ranges between 1.1 and 1.9 GPa, depending on test conditions (i.e. temperature and test pressure). The bulk modulus for hydraulic fluids, tested at 22 °C and at 14 MPa, was approximated to be 1.5 GPa (Turolla, 2013). Therefore, the bulk modulus of 1.4 GPa should be a realistic approximation for the PHS system, which has a maximum working pressure of 7.7 MPa (approx. 60 kN).

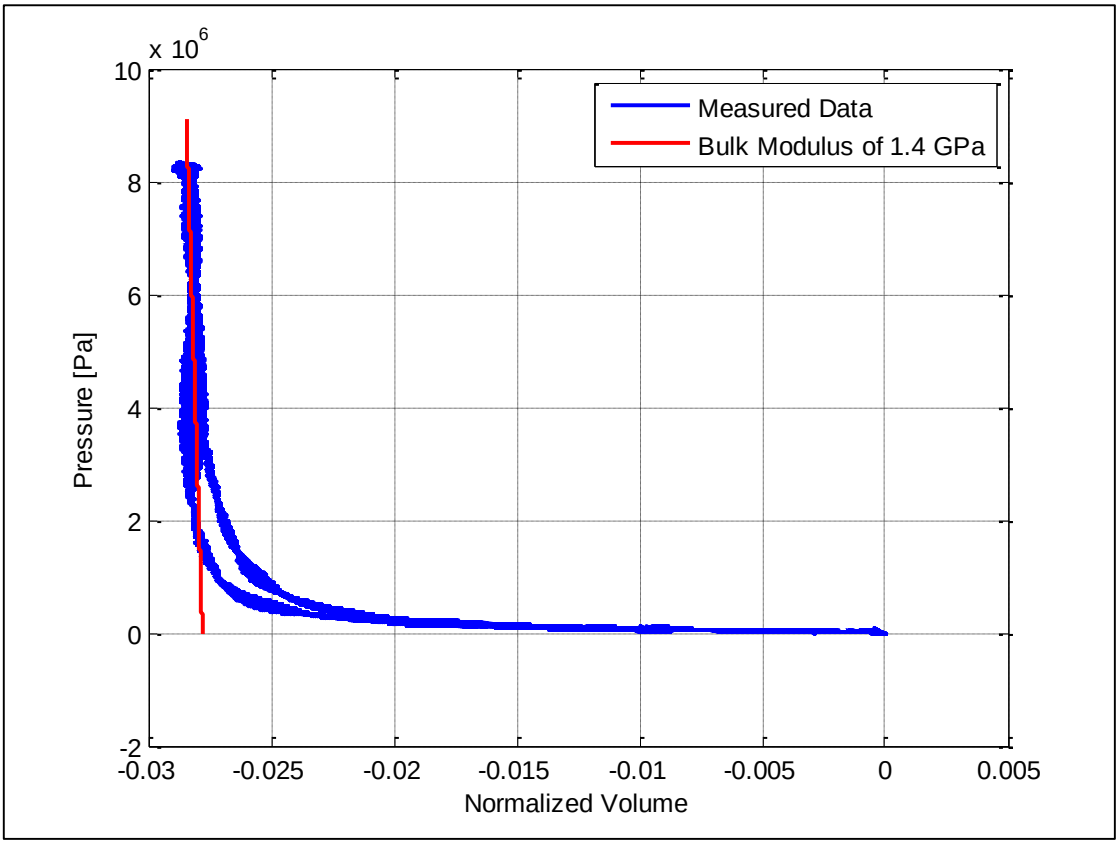

Figure 5-4. Measured Bulk Modulus for a single PHS cylinder with a Flexible Hose.

5.1.2. Force Measurement Investigation

The forces calculated from the measured pressure (i.e. using Eq. 1 on page 26) correspond very well with the forces measured with the load cell. This is shown in the Fig. 5-5, for a normal ramp input used to determine the bulk modulus. However, the difference between the two is on average approximately 1800 N. Also, it can be observed that the difference is higher when the piston is moving very slowly or standing still (i.e. on Fig 5-5 during the time interval from 10 and 20 seconds). This difference can be attributed to friction in the system and is investigated in more detail in the next chapter.

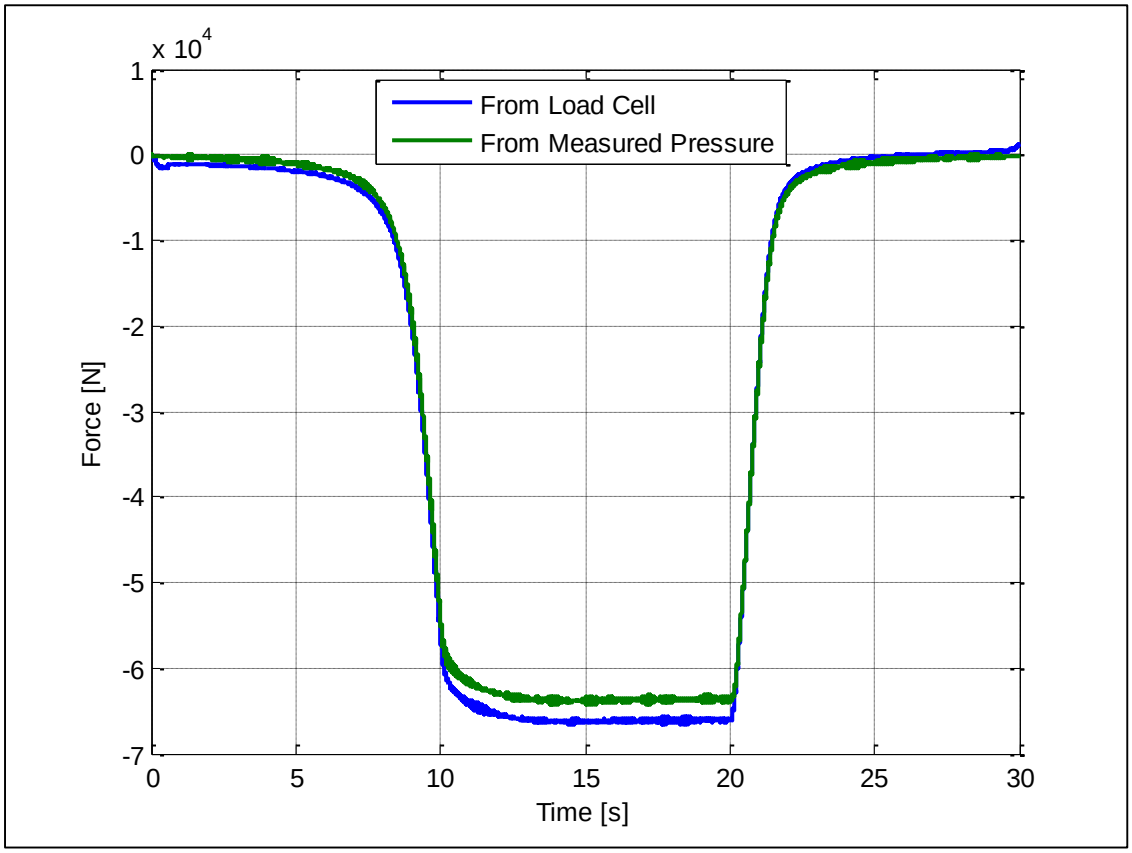

Figure 5-5. Force measurement comparison.

5.2. Model Development and Validation

From the results obtained, it was decided to model the hydraulic cylinder as discussed in section 4.1.1 and to model the oil as described in section 4.1.4. However, the oil model is refined to include the effect of the air trapped in the system. Therefore, the first section of the compression (i.e. for pressures below 2 MPa) the oil-air mixture is modelled as an accumulator. As the pressures are still low and it was proven that the ideal gas behaviour holds, the Ideal Gas (IG) accumulator model is used. This also allows one to predict the volume of air trapped in the system. A schematic, giving an overview of the model, is provided in Fig. 5-6. On the left of the diagram, the PHS component models developed are indicated and on the right the corresponding simulation procedure/logic is shown.

The model was then generated in MATLAB. To validate the model, the displacement measured (i.e. ramp input) for the bulk modulus approximation was used as an input for the model. As the volume of air trapped in the oil is not known, an iterative process was used to approximate the air volume. This was done by comparing the simulated results to the measured results. For a static air volume approximation of 3.58 ml, the results are shown in Figure 5-7.

From the graph shown in Fig. 5-7, it can be concluded that the model generated predicts the measured results fairly well. However, it must be noted that the volume of air trapped in the system is unknown and will always have to be assumed. During the tests no valuable trend could be identified to ease the prediction of the volume of air trapped, but it was observed that the air generally only had an effect on the system for pressures below 2 MPa.

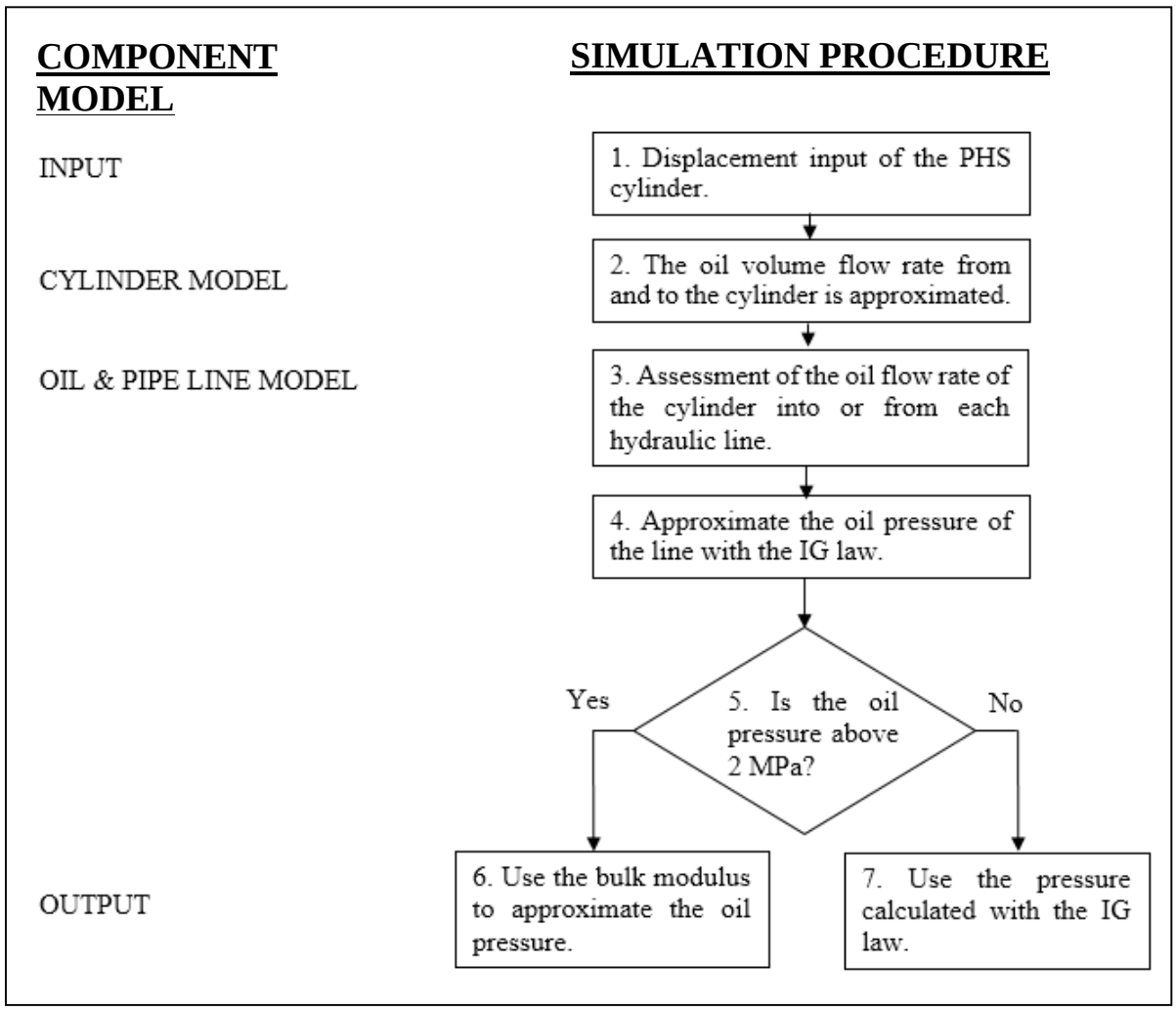

Figure 5-6. Schematic of the Cylinder and Oil Model.

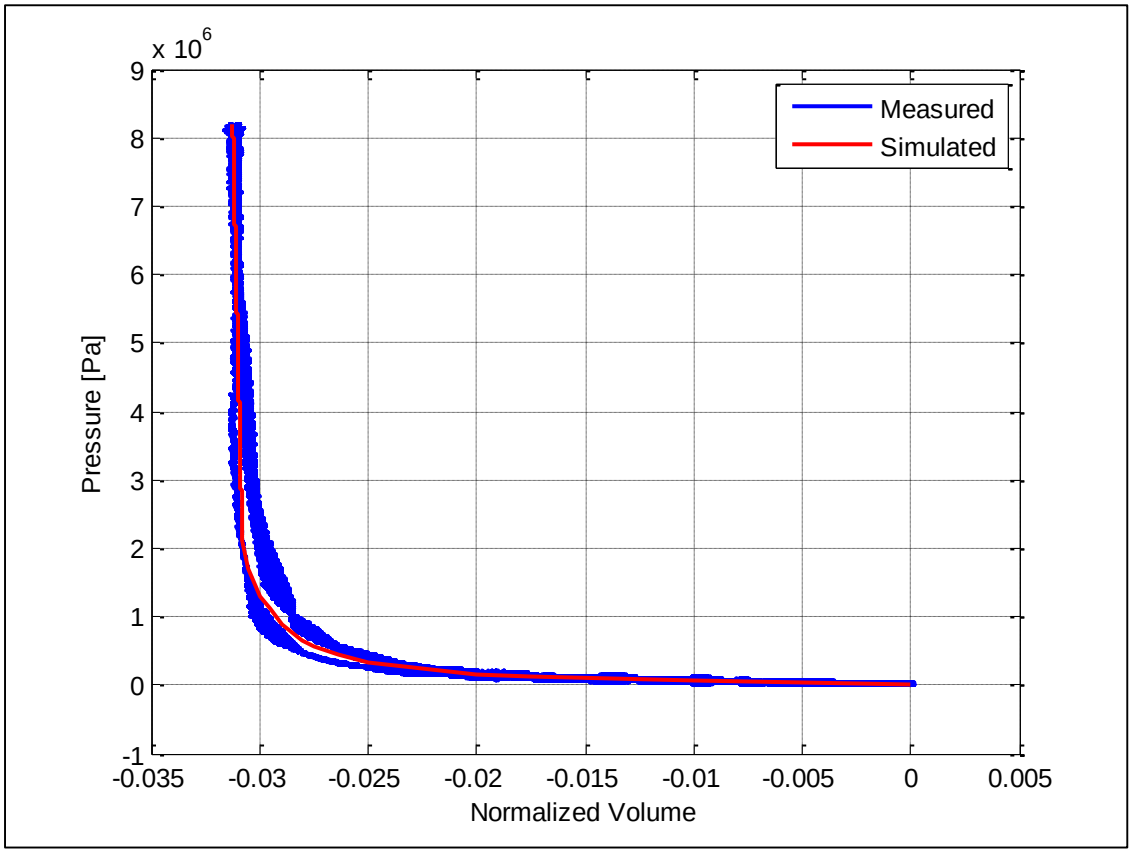

Figure 5-7. Comparing the simulated and measured results for a single PHS cylinder.

5.3. Conclusion on the PHS Cylinder Modelling and Testing

The PHS hydraulic cylinder and oil model generated were successfully validated and can now be used for further PHS model development.

Further, the high compression effect (i.e. the effect of the air in the oil) of the oil identified, can be minimised by pre-charging the fluid to 2 MPa, as originally planned for the PHS. This may be necessary to provide the necessary stiffness of the PHS system and is also explored and investigated in the following chapter.

6. Testing, Modelling and Validating of a PHS Quarter Model

In the previous chapter, the PHS hydraulic cylinder and oil were tested and modelled. Now the accumulators and reservoirs have to be characterised and modelled. One option would be to test and model each component on its own. However, it would be more valuable to characterise the accumulators and reservoirs installed as designed (i.e. installed on the PHS hydraulic lines), as this would allow one to also consider the interaction between the components. Also, the PHS is symmetric and thus allows one to perform experimental tests on a PHS quarter model, as shown in the schematic below. Testing the full setup is complex and could result in incorrect characterisation of the accumulators and reservoirs.

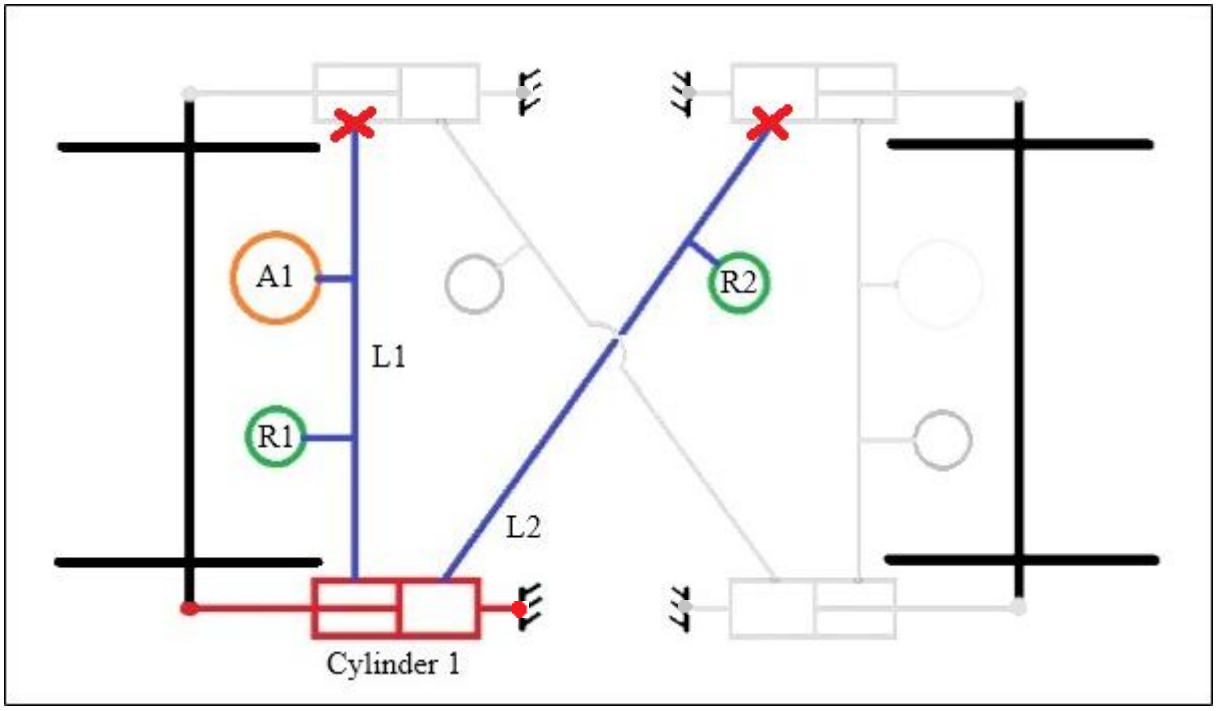

Figure 6-1. Schematic of the PHS Quarter system (A – Accumulator, R – Reservoir).

6.1. Laboratory Testing

The test setup is similar as discussed for the hydraulic cylinder tests, except that now the PHS cylinder is connected to an accumulator and two reservoirs. The laboratory test setup is shown in Figure 6-2.

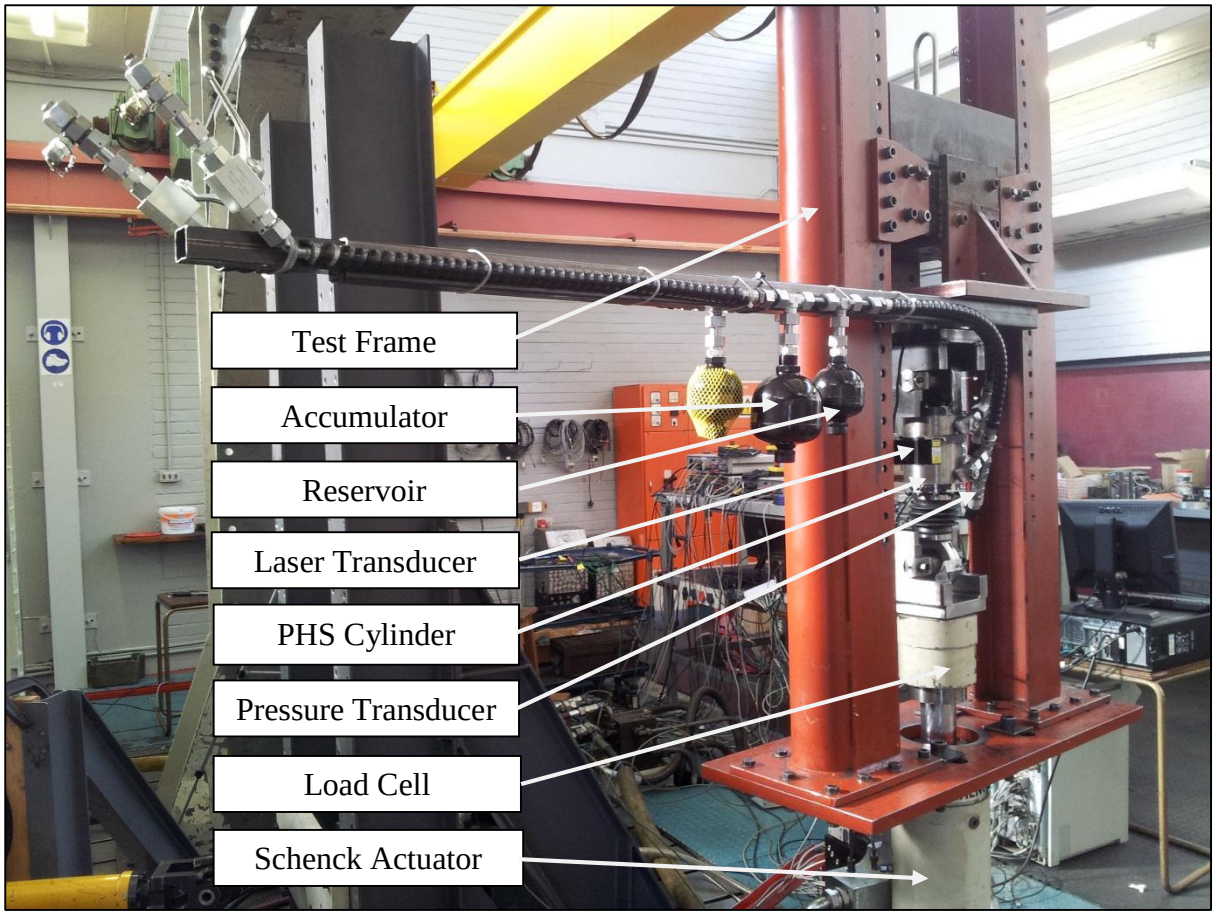

Figure 6-2. Quarter PHS System Test Setup in the Sasol Laboratory.

Further, it was unknown whether the reservoirs (initially selected for the PHS) were sufficient or optimal for their design purpose. Therefore, a more detailed investigation of their implementation was performed on four different PHS design setups, summarised in Table 6-1. The decision on an optimum design was based on properties/parameters determined and is discussed in this chapter. Please note that only the reservoir design was altered.

Table 6-1. Reservoir and Accumulator Design Options.

Setup	Design Setup Description
1	• Implemented by DCD on prototypes. • Gas side of accumulator (reservoir) is filled with oil and oil side is sealed against dust with a breather.
2	• Reservoir is connected as an accumulator. • Gas side is filled with nitrogen at atmospheric pressure, i.e. no gas pre-charge.
3	• Reservoir is connected as an accumulator. • Nitrogen gas is pre-charged to 0.5 MPa.
4	• Same as Setup 3, but with a gas pre-charge of 1 MPa.

The tests on the quarter PHS setup were aimed to approximate and evaluate the thermal time constant, spring and damper characteristic, the friction on the PHS system and to gather validation test data. In the following subsections, the methodology followed, results obtained and the discussion thereof is reported on.

6.1.1. Thermal time constant

In Chapter 4, the thermal time constant was defined and discussed. For the tests, a high speed step input was used to ensure that the system is excited adiabatically and then allowed to reach steady state. The size and direction of the step was varied to determine an average thermal time constant for the PHS system. From the measured pressure, the initial pressure (just after the step input) and the final pressure (when the system reached steady state again) was determined. These were then used to find the thermal time constant, i.e. the time needed for the pressure to reduce to the 63 % pressure point. This is illustrated in Fig. 6-3.

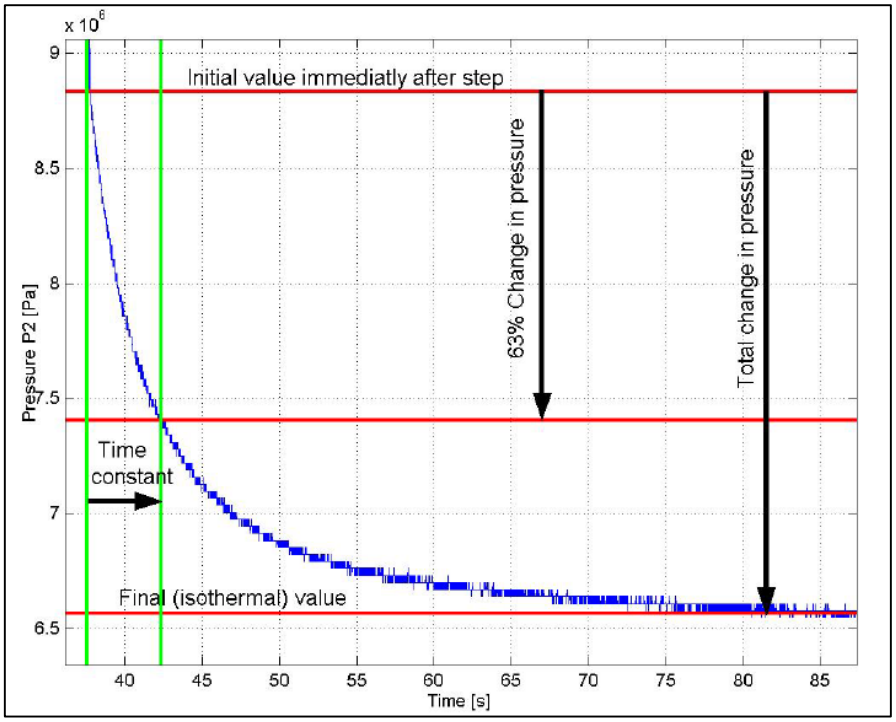

Figure 6-3. Determination of the thermal time constant (Els, 2006).

A table containing all thermal time constants, determined for the different reservoir setups and different amplitudes of the step input, is included in Annexure B. From the results, it was evident that it is very difficult to determine one single thermal time constant. The thermal time constant seems to be dependent on amplitude and pressure. It was, therefore, decided to use an average thermal time constant for each reservoir setup as tabulated in Table 6-2.

During the tests it was also observed that reservoir setup 1 is very stiff and thus only small input amplitudes could be tested. The thermal time constants obtained are overall very small.

Table 6-2. Average Thermal Time Constants Determined.

Setup	Average Thermal Time Constant [seconds]
1	0.725
2	1.73
3	0.797
4	1.376

For completeness sake, the effect of changes in the thermal time constant were investigated and are discussed in the model validation section.

6.1.2. Spring Characteristic of the PHS

The spring characteristic of the different reservoir setups was determined by exciting the quarter PHS model setup with a very slow triangular wave input (i.e. constant speed input with a frequency of 0.001Hz). The force calculated from the measured pressure, is plotted against measured displacement in Figure 6-4.

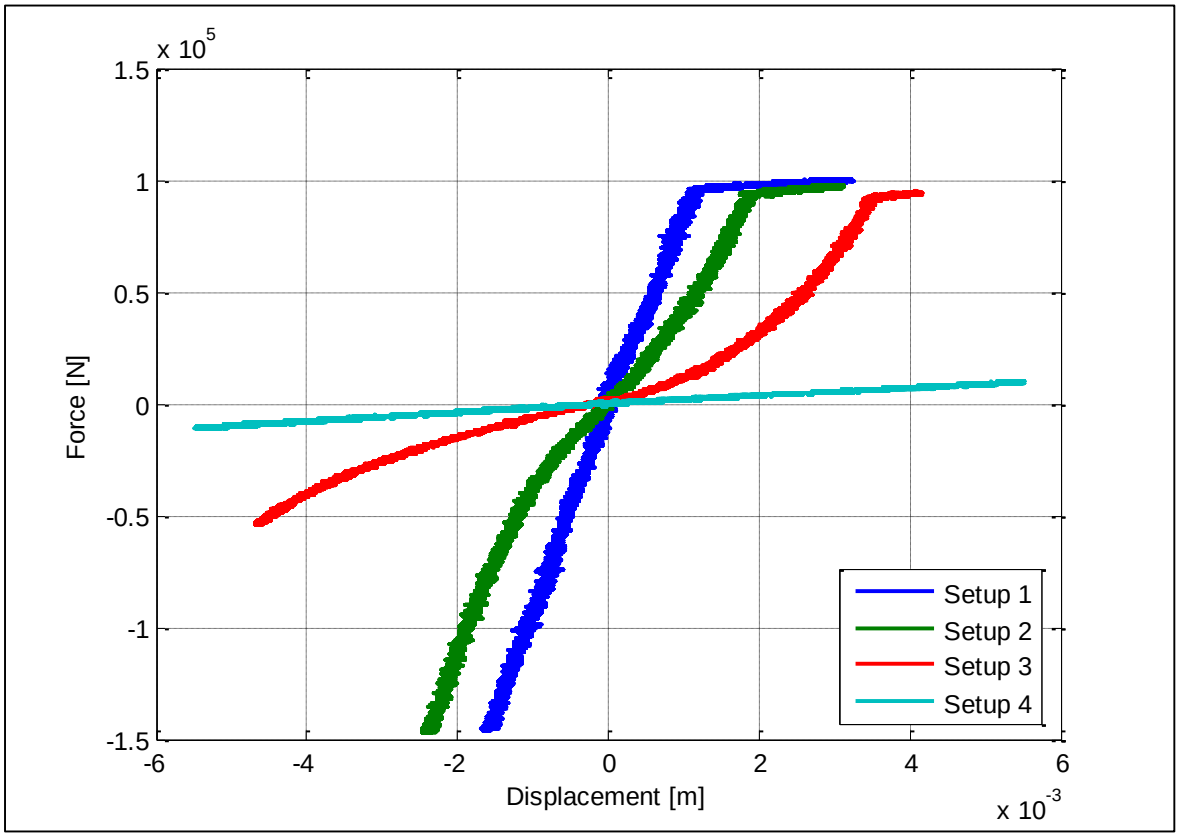

Figure 6-4. Stiffness Comparison of the different PHS Reservoir Setups (Described in Table 6-1).

In Fig 6-4, one can observe that the “blow off” accumulator works as designed and keeps the maximum force below 100 kN (15 MPa) when the hydraulic cylinder is under tension. The flattening of the graph also indicates that the volume of the accumulator is large enough to maintain a near-constant force. Please note that all force graphs go through the 0 point, as the pre-charge pressures of the two cylinder chambers were chosen to result in a zero resultant force.

Further, the stiffness in tension is different to the stiffness in compression. This is due to the difference in piston cross-sectional areas and thus oil volume displaced. For the PHS, the system stiffness is required to be as high as possible to be able to have accurate steering at small piston displacements. For setup 1 the highest stiffness was obtained. However, it was difficult to keep the oil pre-charge at 2 MPa and had to be corrected after each test run. Setup 3 and 4 have a much lower stiffness, but kept the 2 MPa oil pre-charge. This stiffness of setup 3 and 4 could be increased by increasing the oil pre-charge, but this is not ideal as the higher average oil pressure could increase the stress on the PHS system.

From the spring characteristic tests, the most ideal reservoir design was identified to be setup 2. The stiffness is similar to the one of setup 1, and the oil pre-charge did not change over the tests.

6.1.3. Damping Characteristic of the PHS

The damping characteristic was approximated by exciting the quarter PHS system with triangular waves at different frequencies. The triangular wave provides a constant speed and thus enables one to calculate the difference between the measured force (at different input speeds) and the force calculated for the spring characteristic. The calculations were performed for two different displacement amplitudes and the average damping force was calculated. The results are visualised in Figure 6-5.

It is interesting to see that the damping forces are fairly high for the stiffer reservoir designs. This can be explained by the higher friction forces due to higher oil pressures.

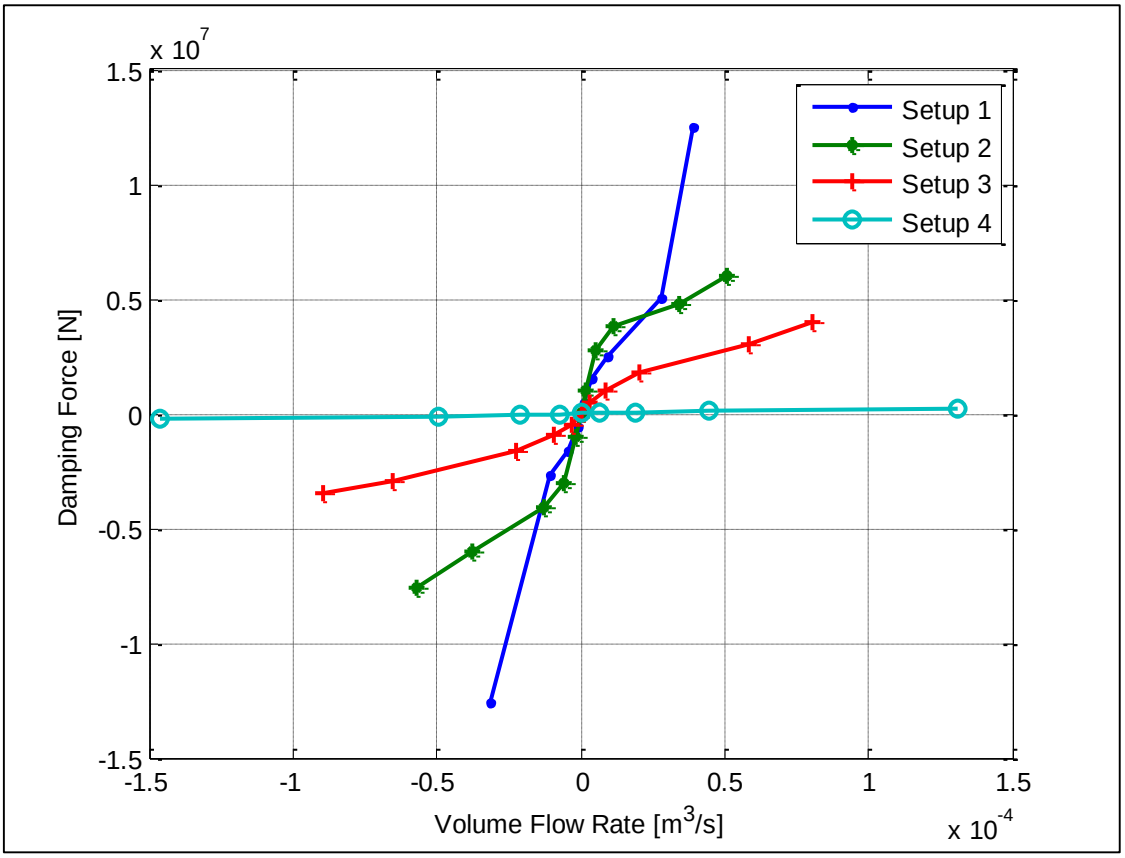

Figure 6-5. Damping Force of the different PHS Setups.

6.1.4. Friction on the PHS

Friction forces were present on all test data, as a difference between the load cell force measurements and force calculated from the measured pressures was seen. From first observation it seemed that the magnitude of the friction force is fairly similar (approximately 1.8 kN) at high and low measured forces. Unfortunately, this friction force cannot be ignored or assumed to be negligible.

It is known that friction is dependent on many factors, which include piston velocity and oil pressure. As a first approach, the velocity dependency of the friction was investigated. For this purpose, the measured force was compared to the force calculated from the measured pressure at different piston speeds. The piston speed was altered by having triangular wave inputs with different wave frequencies. In Figure 6-6, the friction forces calculated for different oil flow rates (calculated from the piston velocities), are plotted and it can be observed that a general friction pattern is present. From the graph, it is also evident that the friction is dependent on the pressure and piston design (i.e. oil seals), as the friction is higher when the piston is under tension (extending piston).

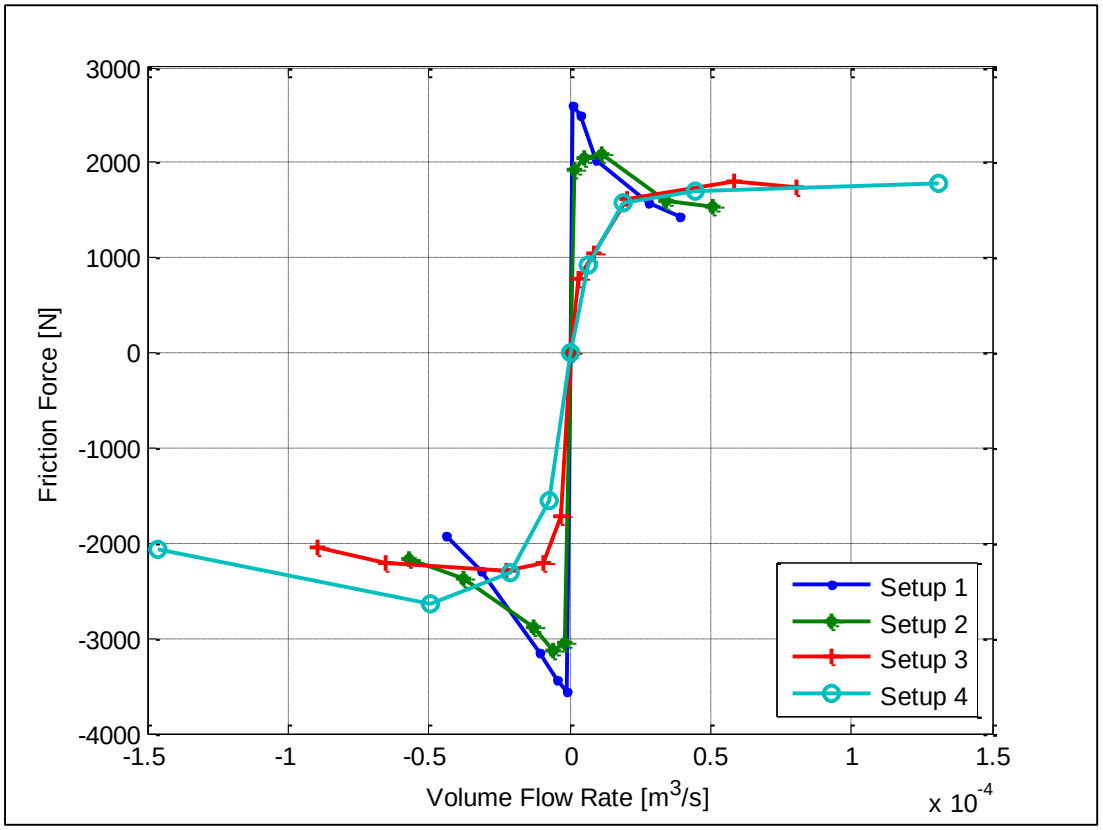

Figure 6-6. Friction Forces of the different PHS Setups.

Many articles and papers are available that discuss the friction phenomenon and suggest different friction models (for example the article by Berger (2002)). These, however, are often very complex. Therefore, it was decided to first investigate the effectiveness of a friction force versus piston speed lookup table to model the friction. The findings of this investigation are discussed in section 6.2.

6.1.5. Conclusion on Quarter Model Tests

The PHS system components were characterised successfully and all required parameters were determined. Validation data was also recorded for the validation process. It was observed that accurate measurements were very difficult as the PHS system is very sensitive to small displacements.

The results obtained for the different reservoir designs were discussed with DCD and it was decided for now that reservoir setup 2 is the most ideal (i.e. allows enough compressibility to maintain the pre-charge pressure on the oil and at the same time provide sufficient stiffness). Therefore, the mathematical model was developed for this configuration. Further investigations on the reservoir design will be done in future.

If a stiffer system is needed, one could consider exchanging the reservoir with larger volume pipes which increase the oil volume of the system. This can be explored with the mathematical model at a later stage.

6.2. Model Development

The parameters required for the accumulator and reservoir models were all determined in the previous sections. Therefore, all component models could now be generated in MATLAB, as discussed in Chapter 4, and "assembled" to represent the complete PHS system.

It was decided to divide the PHS Quarter Model into two parts. The first part approximates the hydraulic characteristic of the PHS and the output forces due to the oil pressure in the system. The second part is the friction model. The output of the friction model is the final force output approximated for the PHS cylinder.

6.2.1. PHS Hydraulic Quarter Model (Part 1)

The PHS hydraulic quarter model is made up of the component models generated in Chapter 4 and 5 and is also written in MATLAB. The general working procedure is displayed in Figure 6-7, where on the left of the diagram, the PHS component models developed are indicated and on the right the corresponding simulation procedure/logic is shown.

To aid the understanding of the model, the schematic is discussed shortly. For the following discussion, the components are named as illustrated in Fig. 6-1 and the simulation steps are numbered as indicated in Figure 6-7. The simulation process is initiated by the input of the PHS piston displacement (step 1), which in turn is used to calculate the oil volume flow rate between the chambers of hydraulic cylinder 1 (step 2) and the hydraulic lines L1 and L2.

The programme then evaluates whether more oil is needed in the lines by using the oil and pipe line model (steps 3 and 4). Each hydraulic line is evaluated separately. If more oil is needed, oil flows from the reservoir into the line (step 5) and the oil pressure of the line is approximated with the reservoir model (step 7). However, if no extra oil is needed in the pipe line, oil flows from the line into the reservoir (step 6).

The reservoir model then evaluates if the reservoir is full (step 8). If not, the oil pressure on the line is approximated with the reservoir model (step 7) and if yes, the oil model is used to approximate the line oil pressure (step 9). Further, if step 9 should be reached for hydraulic line L1 (with the large accumulators A1), step 10 is used to evaluate if the oil pressure approximated is above 15 MPa. If the pressure is above 15 MPa, the hydraulic oil pressure is predicted by using the accumulator model (step 11) and if the pressure is below 15 MPa, the approximated pressure is not changed. Step 10 and 11 are framed in red as they are only used for line L1. For line L2 these two steps are not necessary.

As a final step (step 12 and 13), the approximated hydraulic oil pressure in each line is used to calculate the force exerted by the oil on the piston.

The effect of the air trapped in the system (i.e. which was first included in the PHS cylinder model) was included by increasing the gas volume of the reservoirs. This reduces the complexity of the model and thus improves the computational efficiency.

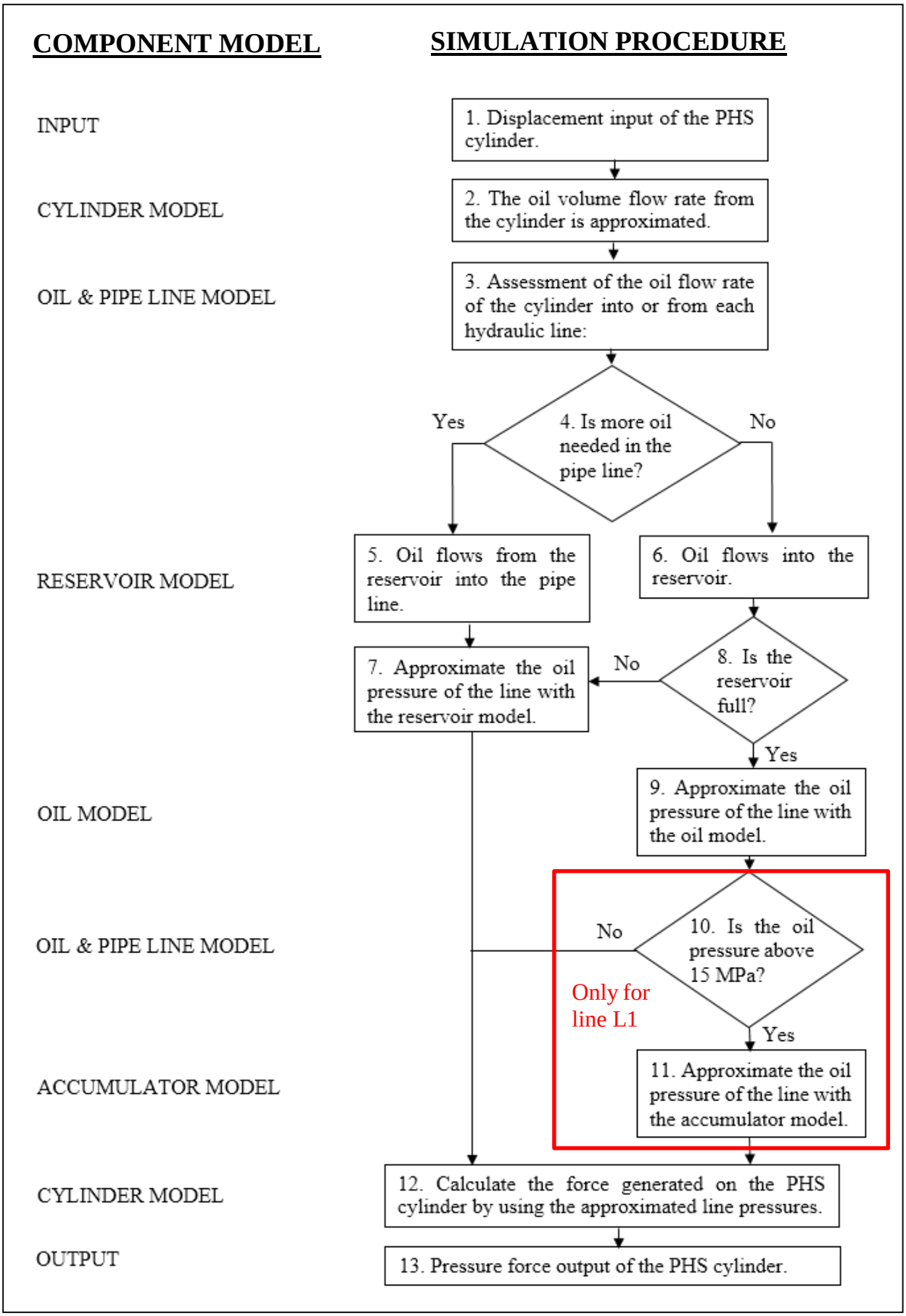

Figure 6-7. General Working Procedure of the PHS Quarter Assembly Model.

6.2.2. Friction Model (PHS Model Part 2)

During the laboratory tests, it was evident that the friction acting on the PHS is not negligible. Therefore, a friction model had to be generated. As stated before, different friction models are available, but it was decided to first evaluate the effectiveness of a friction look-up table.

The friction was calculated as discussed in section 6.1.4 for different piston velocities. The tests were repeated and the average friction for the different velocities was recorded in the look-up table. The friction results obtained are plotted in Figure 6-8.

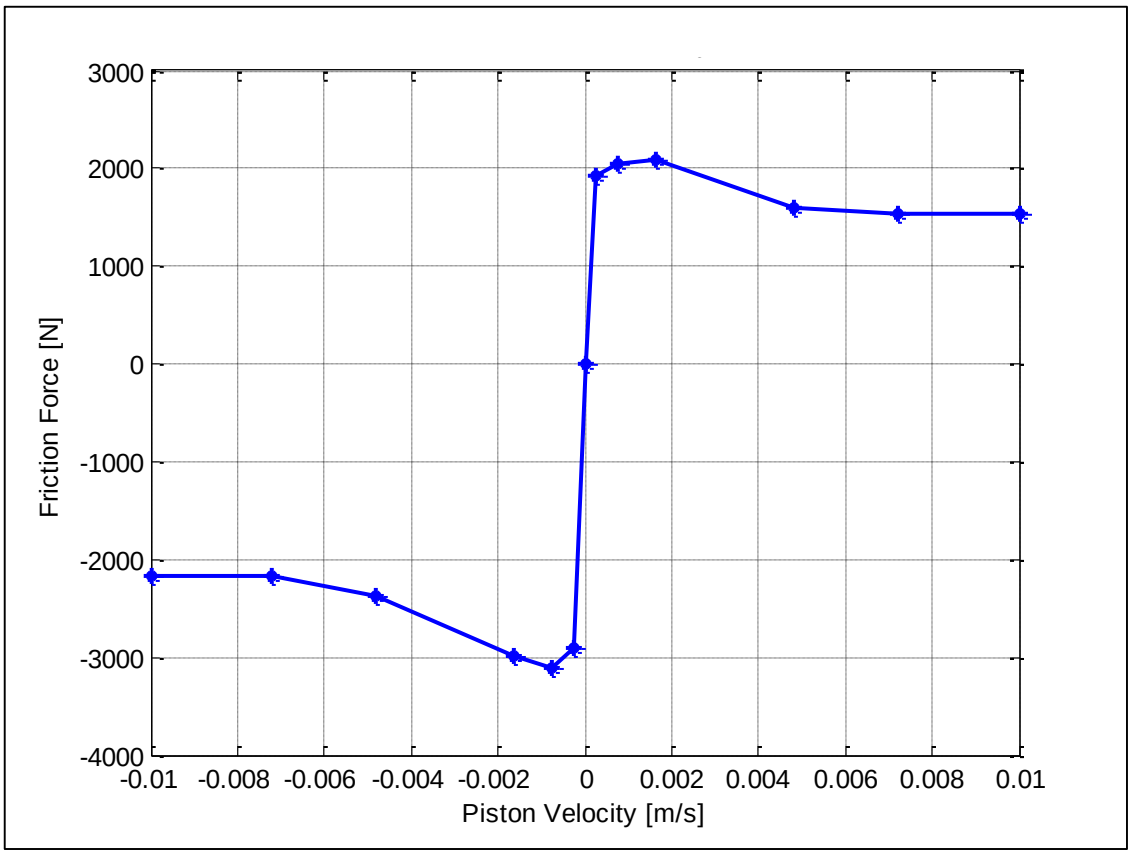

Figure 6-8. Friction Force on a PHS Cylinder.

A friction model was then generated in MATLAB using the look-up table. The model calculates the velocity of the piston from the displacement inputs and then approximates the friction force by means of interpolation. The working procedure is shown in Fig. 6-9. Again, the model used is indicated on the left and the modelling process on the right of the figure.

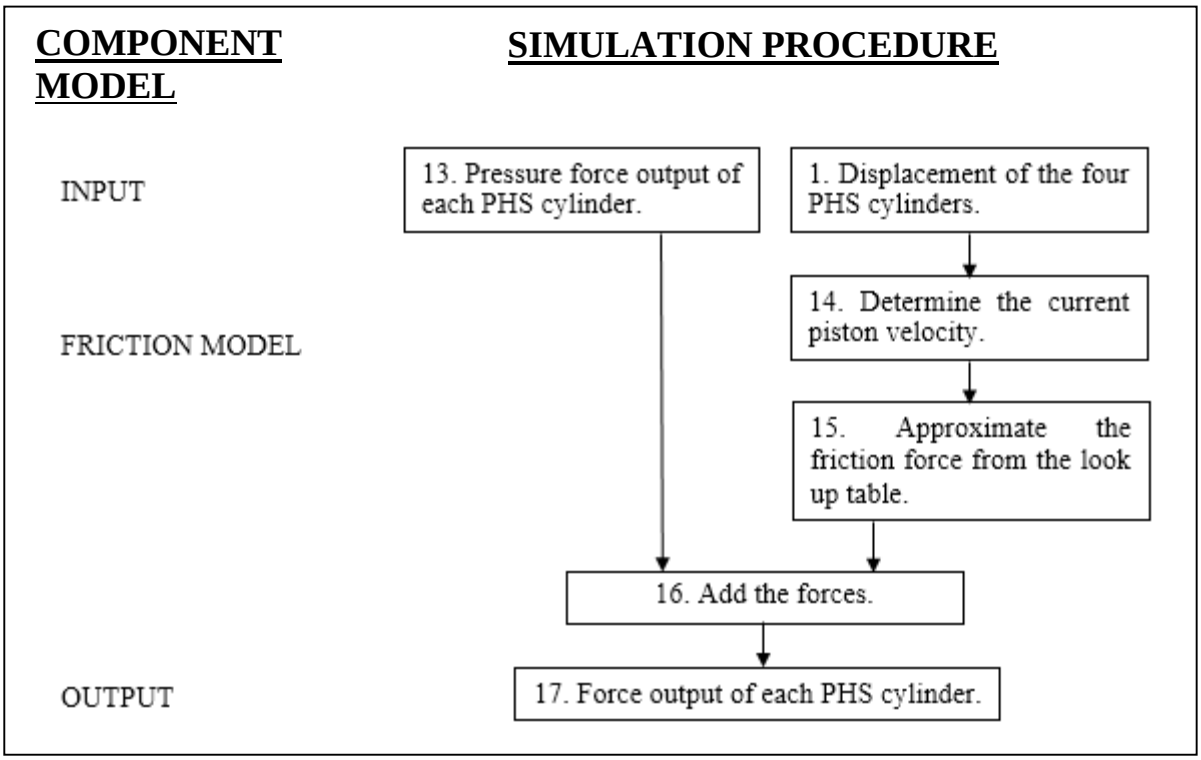

Figure 6-9. General Working Process of the PHS Friction Model.

6.3. PHS Quarter Model Validation

Different validation options exist and it was decided to compare time histories of measured and simulated data and as a first approach qualitative validation was used. This was done by superimposing the simulated data on the measured data. For discussion purposes, an example of measured and simulated results is shown in Figures 6-11 to 6-13, where the system was excited by a sinusoidal displacement input (Fig. 6-10). Additional results (for a triangular wave input) are included in Annexure C.

On Fig 6-10, the small difference in the maximum and minimum amplitude is due to play on the cylinder and elastic deformation of the test equipment under the resulting load. It must also be noted that the displacement is very small, i.e. the maximum is 1.5 mm.

Now, when comparing the results shown on Figure 6-11, which indicate the measured and simulated forces acting on cylinder 1 (i.e. only part 1 of the model, i.e. no friction included), one can conclude that the simulation results correspond very well with the force calculated from the measured oil pressures (indicated on the graph as measured pressure force). It can also be concluded that the simulations using the different gas laws give similar results.

The same conclusion can be made on the results shown on Figure 6-12, where the measured and simulated forces of cylinder 1 are plotted against piston displacement without friction taken into account. The force measured with the load cell shows a small hysteresis loop, which indicates the friction acting on the system.

To approximate the measured load cell force correctly, the second part of the PHS (friction model) is used. The improved simulated cylinder 1 forces are superimposed on Figure 6-13. From Fig. 6-13, it can be seen that the simulated forces now correspond very well with the measured load cell forces acting on cylinder 1. However, small differences are still visible at points where the piston movement changes direction. This is due to difficulties of approximating the friction force in the vicinity of zero piston velocity, i.e. around the zero point the measured piston velocity can easily alternate between positive and negative values.

For different input scenarios, similar results were obtained and thus it can be concluded that the PHS model is qualitatively validated successfully with measurement results from a quarter test setup.

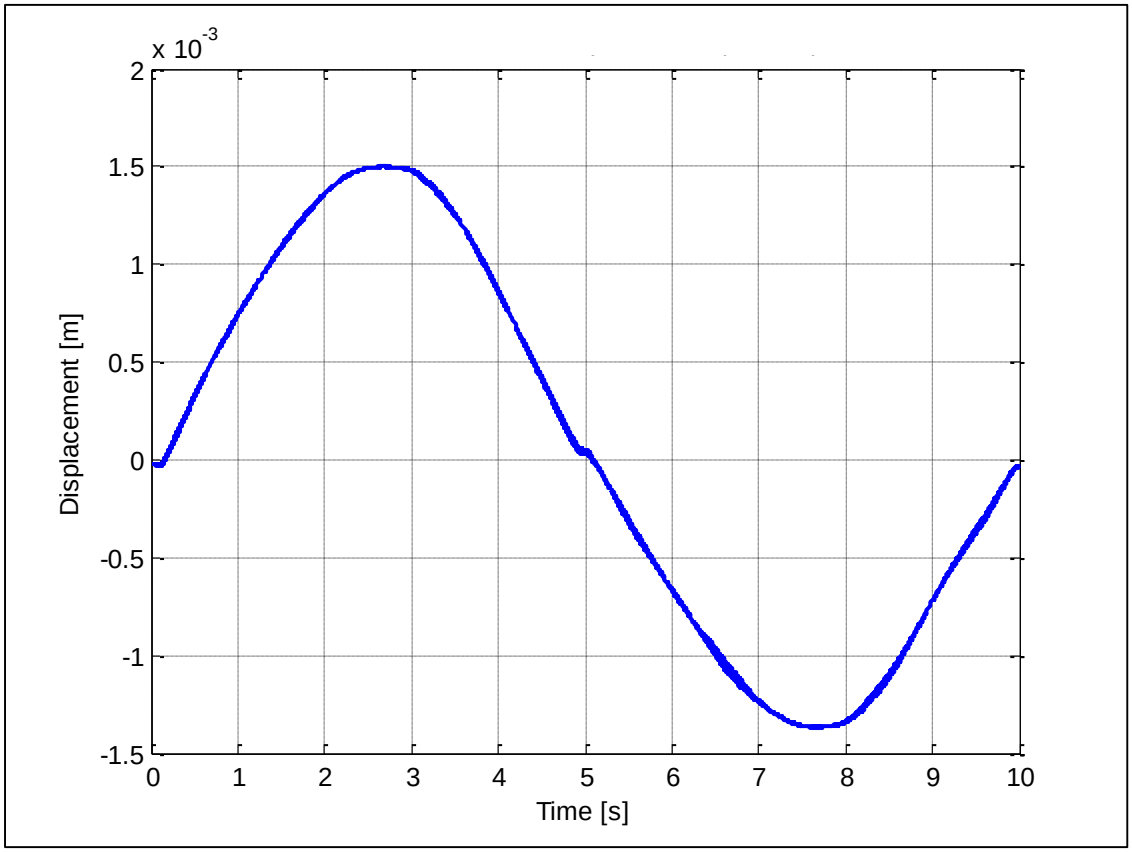

Figure 6-10. Quarter PHS Test Setup: Measured piston displacement.

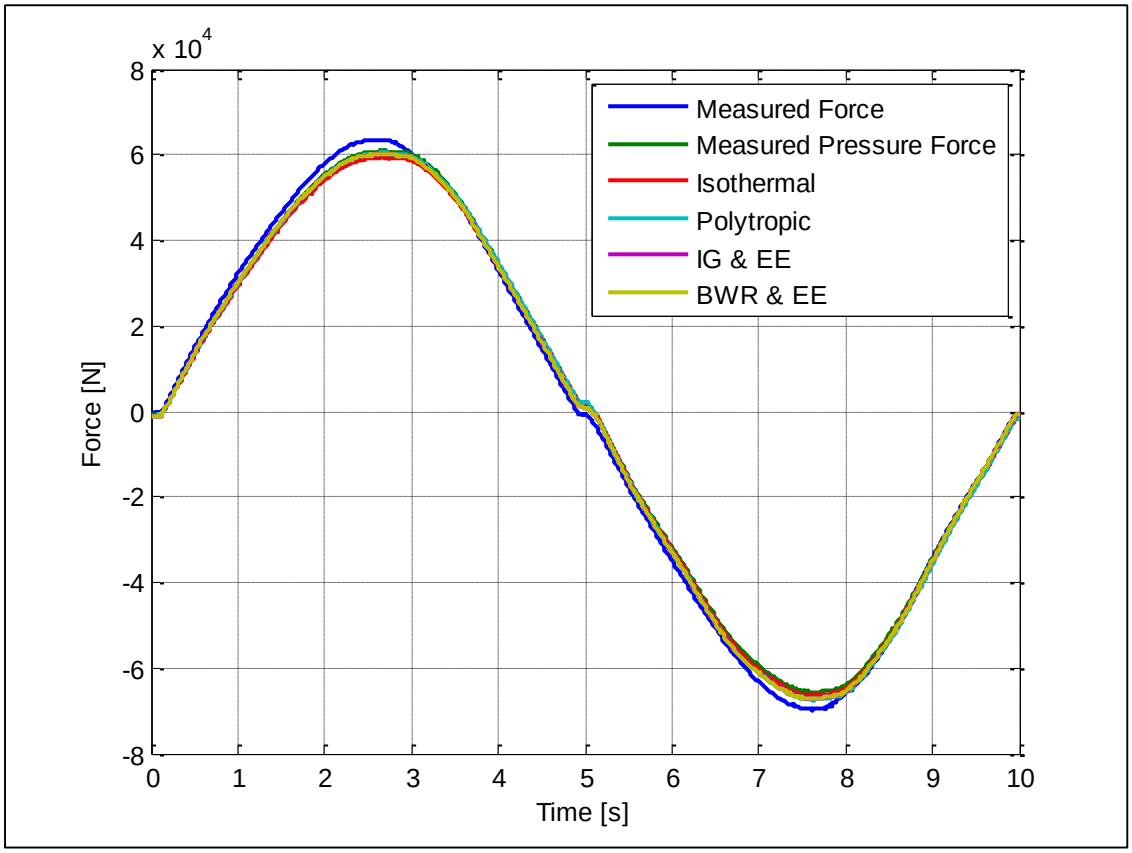

Figure 6-11. Quarter PHS Test Setup: Force on Cylinder 1 vs. Time (results of PHS model part 1).

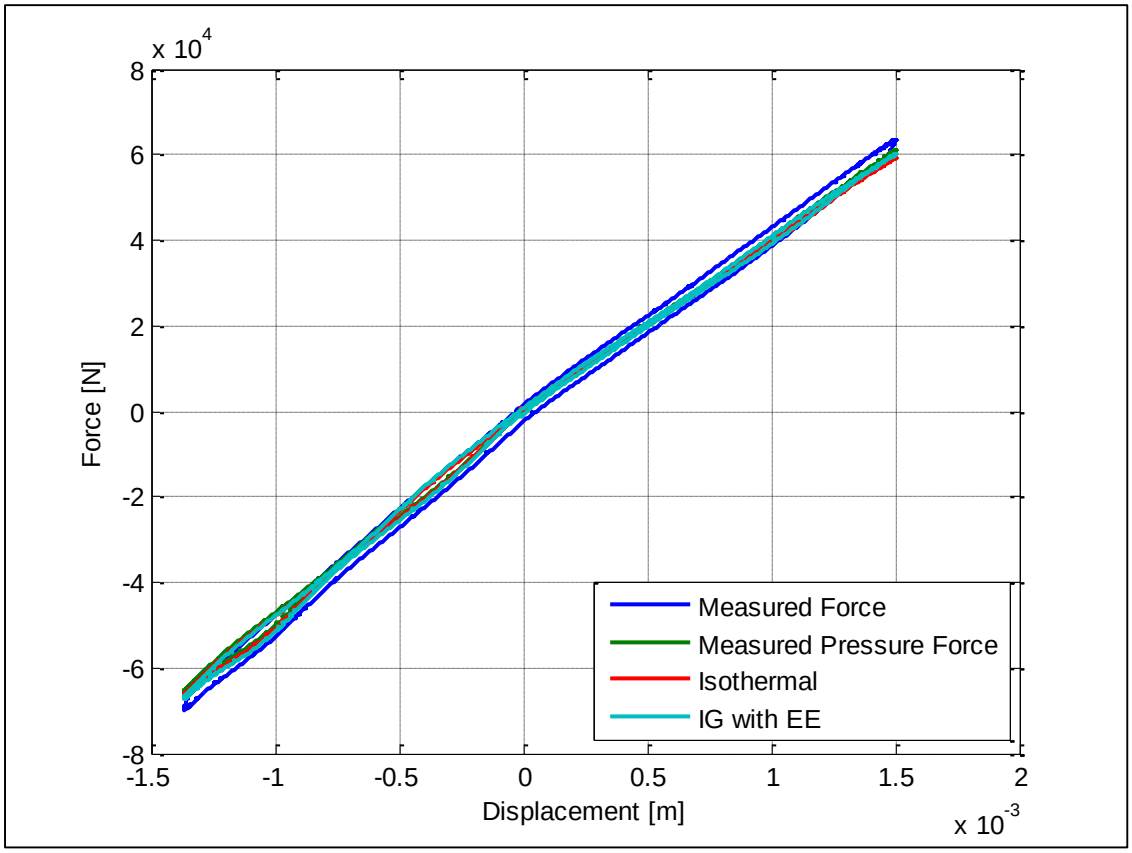

Figure 6-12. Quarter PHS Test Setup: Force on Cylinder 1 vs. Displacement (results of PHS model part 1).

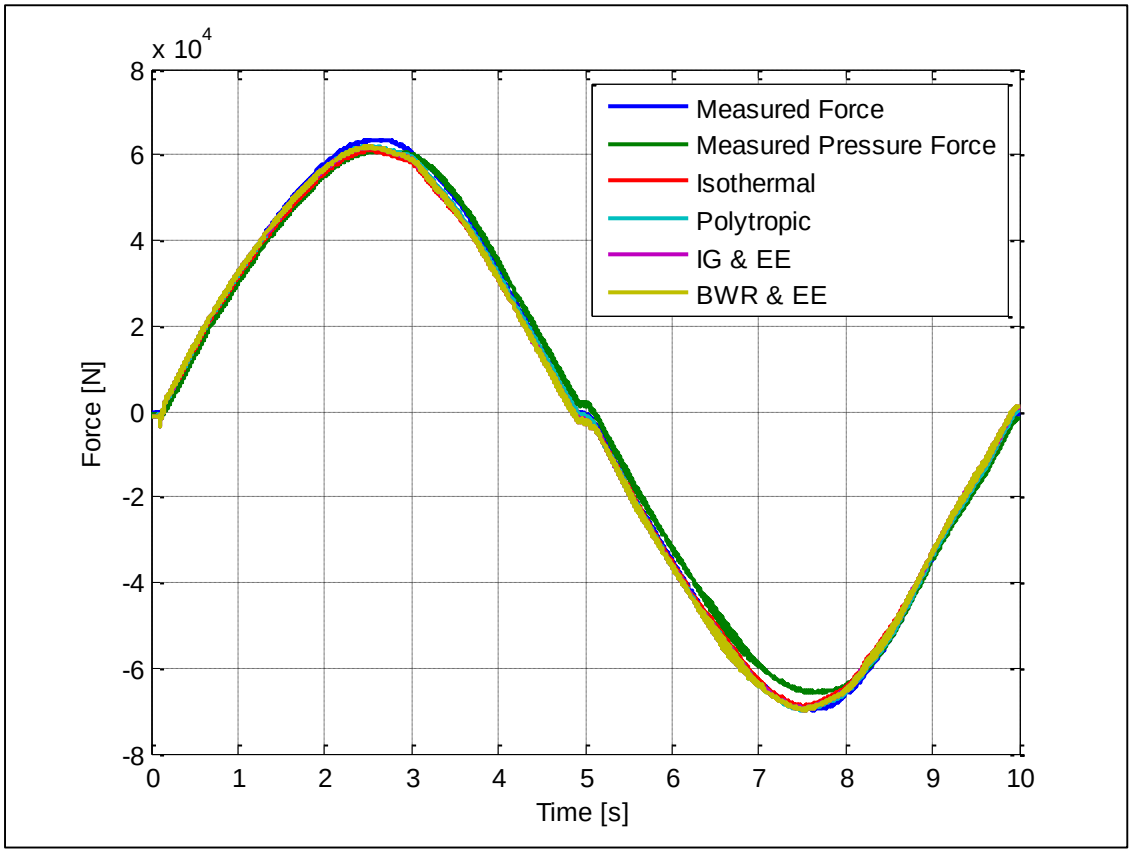

Figure 6-13. Quarter PHS Test Setup: Force on Cylinder 1 vs. Time (results of PHS model part 2).

To objectively quantify the results, a validation metric based on relative error, developed by Kat and Els (2012), was also used. The validation metric was developed to be able to quantify agreement or disagreement between measured and predicted system responses by evaluating the relative error. The results obtained for the mean percentage relative error ($m\%RE^m$) and the mean percentage relative error below a specified percentage relative error ($m\%RE^s$) of 12 % are tabulated in Table 6-3. For the $m\%RE^m$ the percentage relative error is automatically limited to 100 %, i.e. if a percentage relative error higher than 100 % is obtained, the percentage relative error is taken as 100 %.

Three comparisons were made. The first was the comparison of the force calculated from the measured pressure with the force predicted by the first part of the PHS model, the second was the comparison of the load cell force measured with the force predicted by the first part of the PHS model and thirdly the comparison of the load cell force measured with the predicted force of the full PHS model.

From the error approximations, it can be observed that the simulation results of all the different nitrogen gas approximations correlate very well with the measured data. It is interesting to see that with the isothermal ideal gas assumption, the hydraulic PHS model performs best (highlighted in yellow in table 6-3). However, when including the friction model, the best correlation is obtained with the polytropic assumption (highlighted in green in table 6-3). This is due to the nature of the friction model (i.e. look-up table).

Table 6-3. Quarter PHS Test Setup: Quantitative Validation. (Explanation of notation example: $m\%RE^m$ = 2.5% P(91.0%) means that 91.0% of the %REs are at or below the mean %RE of 2.5%).

Displacement Input	Accumulator & Reservoir Gas Law	Quantitative Validation					
		Simulated Pressure Force Compared to Force from Measured Pressure		Simulated Pressure Force Compared to Force Measured (Load cell Measurements)		Simulated Force (i.e. Including Friction) Compared to Force Measured (Load Cell Measurements)	
		$m\%RE^m$	$m\%RE^s$	$m\%RE^m$	$m\%RE^s$	$m\%RE^m$	$m\%RE^s$
Sinusoidal Wave (0.1 Hz) Dataset 1 Approx. 1.5 mm Amplitude	IG (Isothermal)	2.4696% P(91.0%)	12% P(97.9%)	12.9148% P(81.9%)	12% P(80.8%)	8.3187% P(86.2%)	12% P(89.8%)
	Polytropic	2.6818% P(62.0%)	12% P(97.8%)	12.5033% P(81.4%)	12% P(80.8%)	7.4038% P(85.3%)	12% P(90.4%)
	IG with EE	4.8614% P(85.0%)	12% P(92.7%)	10.245% P(83.7%)	12% P(85.8%)	10.1862% P(83.6%)	12% P(85.8%)
	BWR with EE	5.102% P(84.9%)	12% P(92.4%)	10.0505% P(84.0%)	12% P(86.2%)	10.2818% P(83.4%)	12% P(85.5%)
Triangular Wave (0.25 Hz) Dataset 2 Approx. 1.5 mm Amplitude	IG (Isothermal)	1.9655% P(76.1%)	12% P(99.0%)	18.0356% P(79.0%)	12% P(69.8%)	8.9741% P(85.9%)	12% P(88.9%)
	Polytropic	2.315% P(46.2%)	12% P(99.1%)	17.8873% P(78.8%)	12% P(70.0%)	8.0765% P(86.7%)	12% P(89.4%)
	IG with EE	4.8968% P(82.4%)	12% P(91.1%)	15.7175% P(79.7%)	12% P(75.7%)	9.8479% P(81.0%)	12% P(84.8%)
	BWR with EE	5.1857% P(82.3%)	12% P(90.7%)	15.5465% P(79.8%)	12% P(76.0%)	9.914% P(80.9%)	12% P(84.7%)

Further, a short sensitivity analysis was performed. For this analysis the qualitative comparison approach was followed. Parameters that were investigated were the accumulator and reservoir gas volumes, oil volumes, thermal time constant and bulk modulus. It was immediately realised that this is a very difficult task as all these parameters affect the results and different combinations thereof can give similar results.

The oil and gas volumes for the simulations at the static position were approximated to be 0.04848 litre and 1.85 litre respectively on each hydraulic line. These approximations gave the most accurate correlation. The gas volume was approximated by assuming the nitrogen to be an ideal gas and knowing the approx. nitrogen volume at atmospheric pressure and then doubling it. The oil volume measured when the test setup was done, was approximately 1.1 litres, which is lower than the approximated value. This difference is quite high and thus needs to be investigated further.

Changes in the bulk modulus influence the simulation results severely. It was also evident that the bulk modulus had a noticeable effect on the oil volume used in the simulation. This was then used to determine a bulk modulus resulting in a more accurate oil volume approximation. When using an oil volume of 1.1 litres (as measured), the best correlations were obtained for a bulk modulus of 1.17 GPa. This is a difference of about 16 % compared to the experimentally determined bulk modulus of 1.4 GPa and should be acceptable, as it is very difficult to accurately determine the bulk modulus of the complete system. This is further investigated and discussed in the following chapter.

When considering the thermal time constant, one can observe that the correlations to the measured data improve as the thermal time constant is reduced. This indicates that the PHS is best described by the isothermal ideal gas approximation.

6.4. Conclusion on the PHS Quarter Model Development and Testing

A mathematical PHS quarter model was successfully generated in MATLAB that predicts the hydraulic effects of the PHS and the friction on the system very accurately. All required physical parameters were determined and it was also decided to use the reservoir design, where the reservoir is connected as an accumulator and the gas side is filled with nitrogen at atmospheric pressure, i.e. no gas pre-charge. Further, the model was validated with measured data from the laboratory tests.

7. Testing, Modelling and Validating of a PHS Full Model

The final step is to model the complete PHS system and validate it with measured data. A schematic of the full PHS system is given below. This is the same as shown in chapter 4.

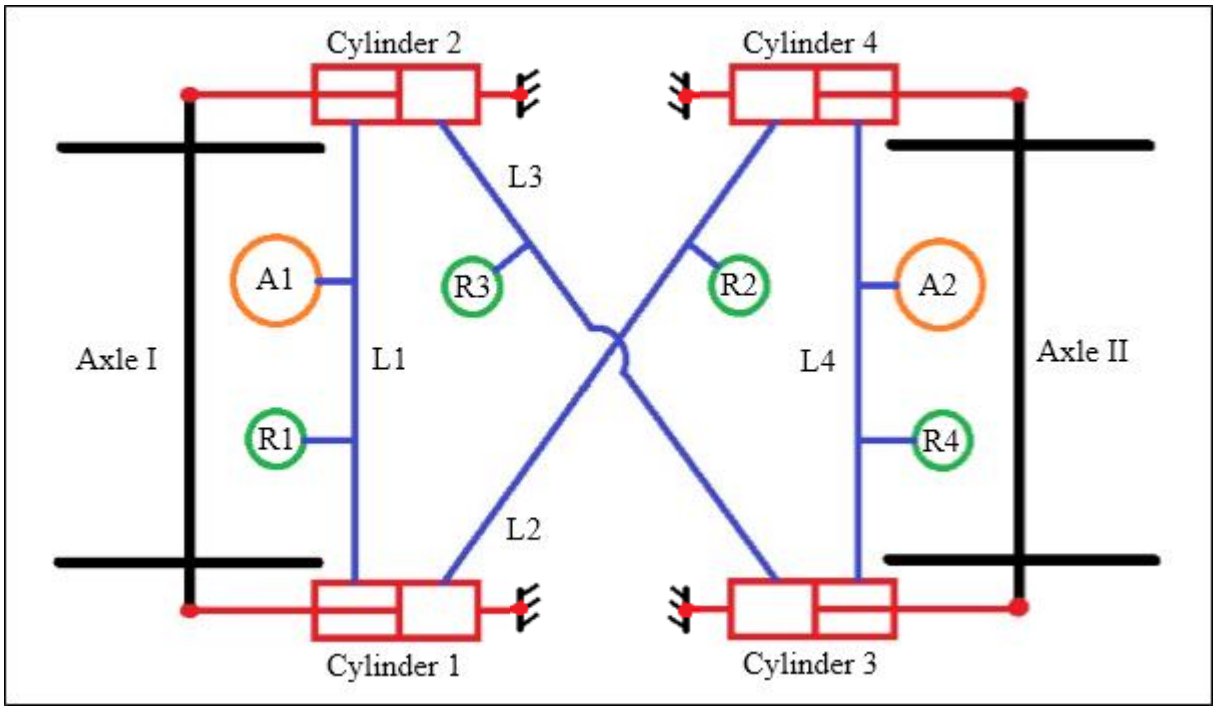

Figure 7-1. Schematic of the PHS system (A – Accumulator, R – Reservoir).

7.1. Laboratory Testing

For the full PHS test setup, it was initially planned to actuate all four PHS cylinders with Schenk actuators. Unfortunately, not enough actuators were available when the tests were performed and thus two cylinders (active, cylinder 1 and 2) were actuated and two cylinders (passive, cylinder 3 and 4) were mounted to a hinged beam (simulating the train axle). The two hinged cylinders would only react to the input of the other two actuators and are guided by the beam to move only in one plane. Please refer to Figures 7-2 and 7-3 for the test setup.

On each cylinder, either a laser transducer or a wire displacement transducer was mounted to measure the piston displacement and a load cell to measure the force. The oil pressure on the different hydraulic pipe lines was measured with 4 Wika pressure transducers.

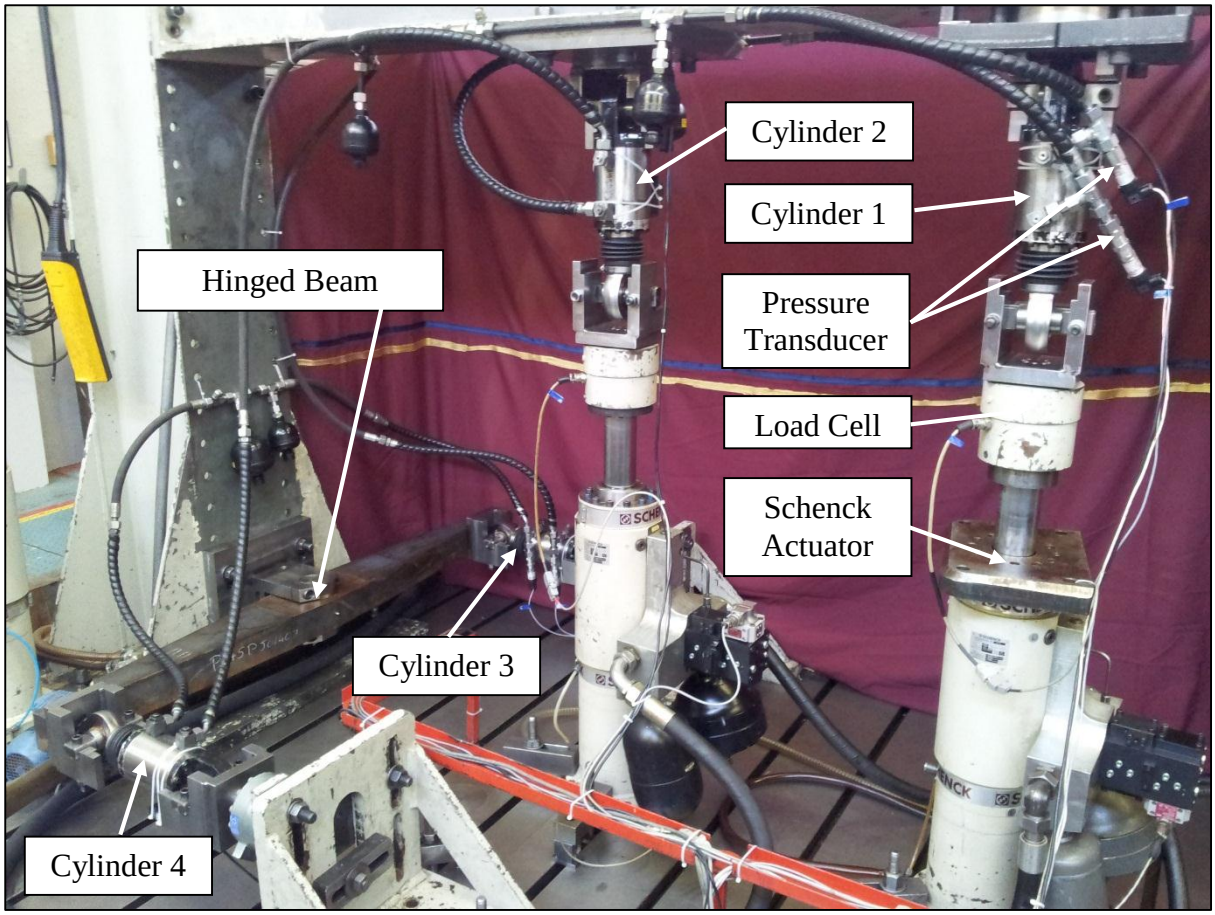

Figure 7-2. Full PHS Test Setup in the Sasol Laboratory.

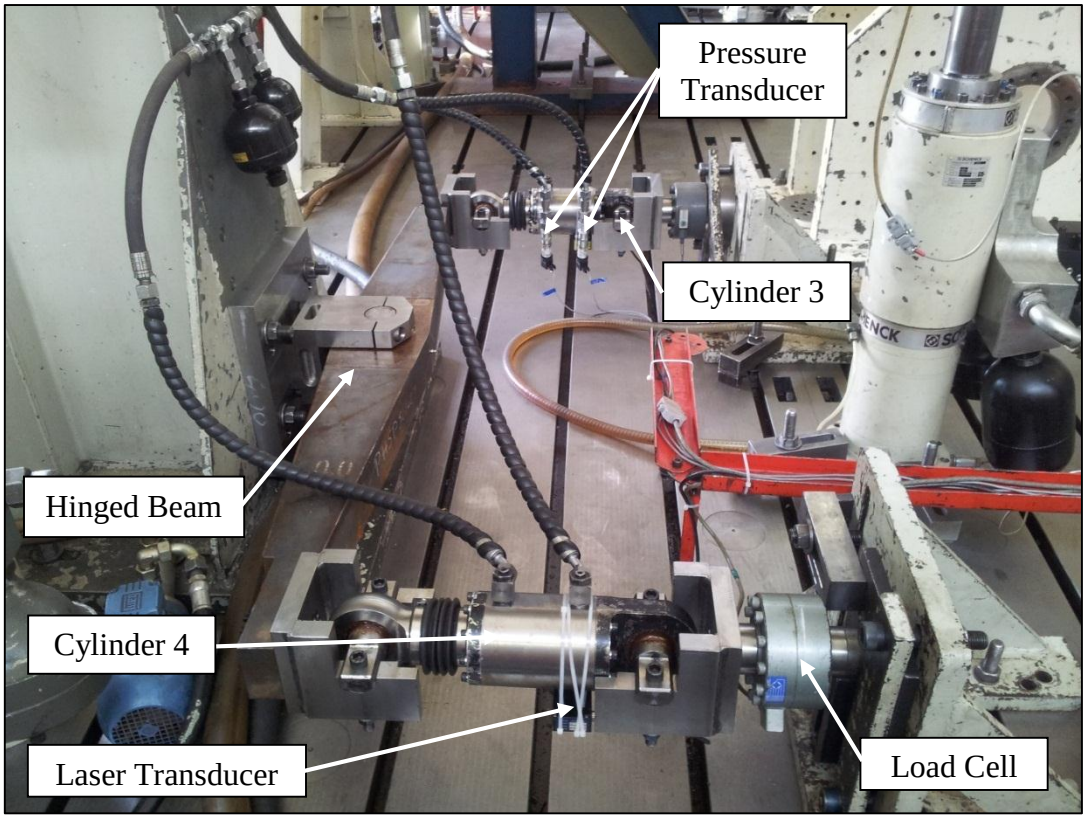

Figure 7-3. Hinged Beam linking the two passive PHS Cylinders.

The full PHS setup laboratory test was aimed at gathering validation data for the full system. Different test scenarios (as discussed in Chapter 5) were used as input. A variety of test data was obtained and is discussed in the validation section of this chapter.

7.2. Model Development

The full PHS model is also divided into two parts. Again, the first part approximates the hydraulic characteristic of the complete PHS and the output forces due to the oil pressure in the system and the second part the friction on the system and predicts the final force output for each of the four PHS cylinders acting on the locomotive wheels and bogie.

For the full PHS hydraulic model (ignoring friction), the quarter hydraulic model (ignoring friction) was expanded to include all PHS components for a complete system. The working procedure schematic shown in Fig. 6-7 was changed accordingly and the resulting full model procedure is shown in Fig. 7-4.

Again, the simulation process is initiated by the input of the PHS piston displacements, which is used to calculate the oil volume flow rate into or from the hydraulic pipe, reservoir and accumulator systems. Decisions on which component model to use are based on the change in oil volume in the reservoirs and the prevailing oil pressure. The hydraulic model approximates the pressure in the individual PHS cylinder chambers, and thus the force exerted by the oil onto the pistons.

The friction model (part 2) is the same as discussed for the quarter model and is expanded to include the four cylinders. For a working procedure please refer to Fig 6-9, on page 57.

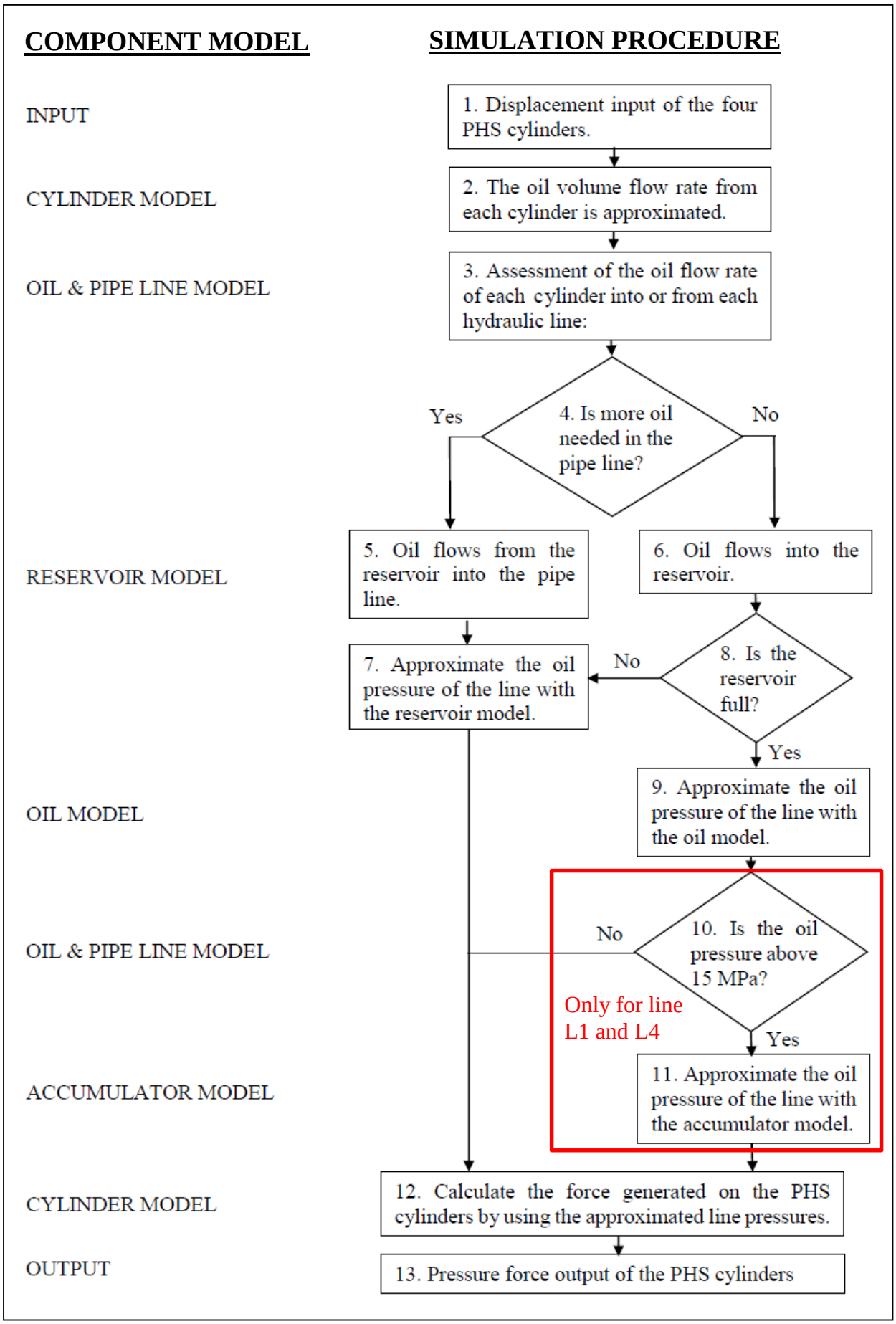

Figure 7-4. General Working Procedure of the PHS Assembly Model.

7.3. PHS System Validation

As a final validation, the PHS model was compared to the measured data from the laboratory tests. Again, different input scenarios were investigated which resulted in similar trends. For discussion purposes, only one set of the full PHS test setup validation data is discussed in this report. A second set of data (for a triangular wave input) is included in Annexure C.

The results discussed in this section where obtained when exciting cylinder 1 and 2 individually with a sinusoidal wave input (180° out of phase) as shown on Figure 7-5. This input simulates the bending mode shown in Fig. 2-12 (on page 17) and is used to simulate steering of the wheels when driving over a curved rail track. Also in Figure 7-5, the displacement measured for the reacting cylinders 3 and 4 and the displacement measurements from the Schenck actuators are indicated. From the difference between the Schenck displacements and piston displacements, it is evident that there is play or elasticity in the system. The resulting forces of the cylinders (measured and simulated) are plotted on the Figures 7-6 to 7-10. It must be noted, that only the results of the IG (isothermal) approximation were plotted. The other gas models all predicted similar results.

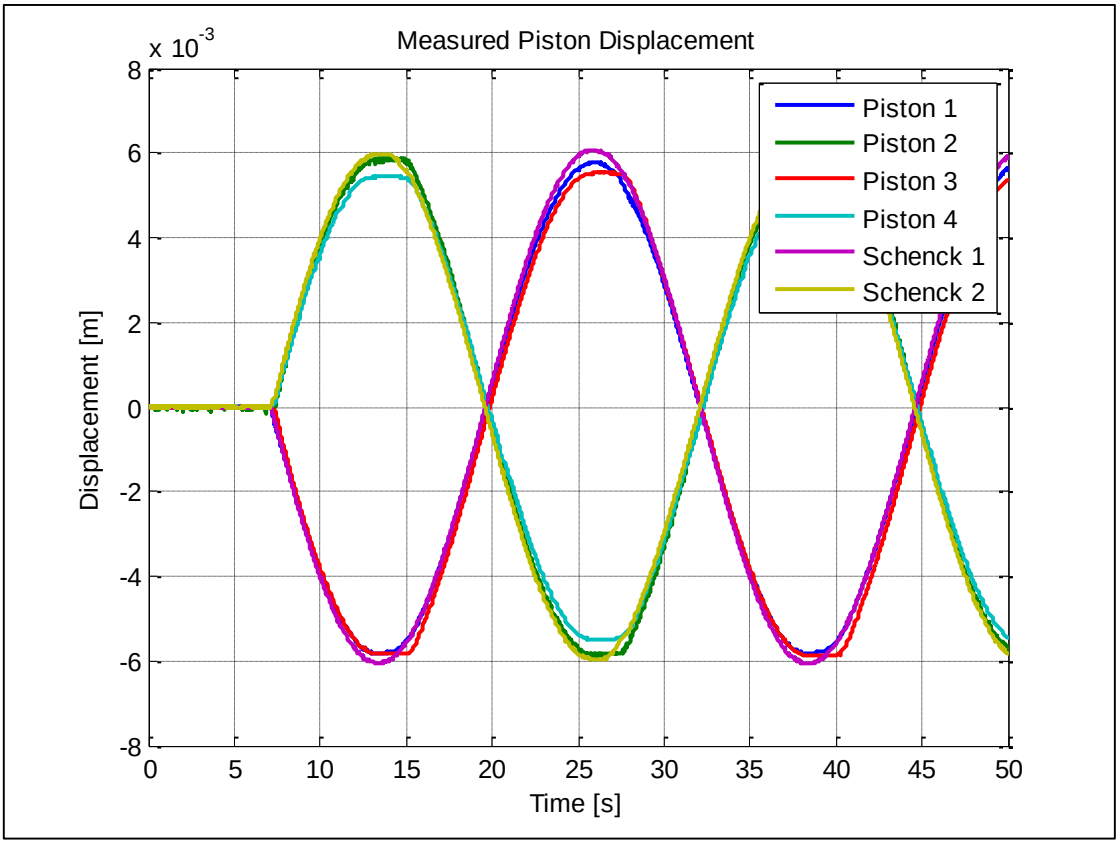

Figure 7-5. Full PHS Test Setup: Measured piston displacements (Sin Input).

In Fig. 7-6, the force measured with the load cells and the force calculated from the measured pressures are shown. These graphs show that for a steering scenario, the forces acting on the PHS system are low and that friction dominates the prevailing forces.

From Fig. 7-7, one can compare the forces obtained from the measured pressure to the forces predicted from the pressure simulated using the IG isothermal model and one can conclude that the PHS model predicts the forces due to the hydraulics (PHS model part 1) fairly well. The correlation is, however, not as good as obtained with the quarter PHS test results. Further, on Figure 7-8, the same conclusion can be made as the predicted values follow the measured data. Also, the hysteresis loops seen on the graphs on Fig. 7-8 are predicted fairly well. The hysteresis is a result of the interconnections of the cylinders.

Looking at Fig. 7-9, one can observe that the prediction of the force measured with the load cells is fairly accurate. However, it can be seen that cylinders 1 and 2 compare well, but 3 and 4 not. This is again due to difficulties of approximating the friction force in the vicinity of zero piston velocity, i.e. around the zero point the measured piston velocity can easily alternate between positive and negative values. Also, the forces measured are very small compared to the friction forces and are prone to measurement errors. The play on the hinged beam connecting cylinders 3 and 4 also contributes to the error. These errors are discussed in more detail in section 7.5.

To ease final comparison, the measured and simulated forces on cylinder 2 have been superimposed on Figure 7-10.

An attempt was also made to evaluate the correlation of the simulated data with the measured data in a quantitative manner. Unfortunately, due to the small forces and prediction differences of about 1000 N, the mean percentage relative errors ($m\%RE^m$) do not give a fair representation of the correlation. The $m\%RE^m$ values obtained when comparing the hydraulic simulation results with the force calculated from the measured pressures, ranged from 5 % to 45 % and when comparing the full PHS model predicted force with the force measured at the load cells, ranged from 15 % to 100 %. Therefore, the validation with the full test setup is only based on a qualitative approach (i.e. graphical comparison).

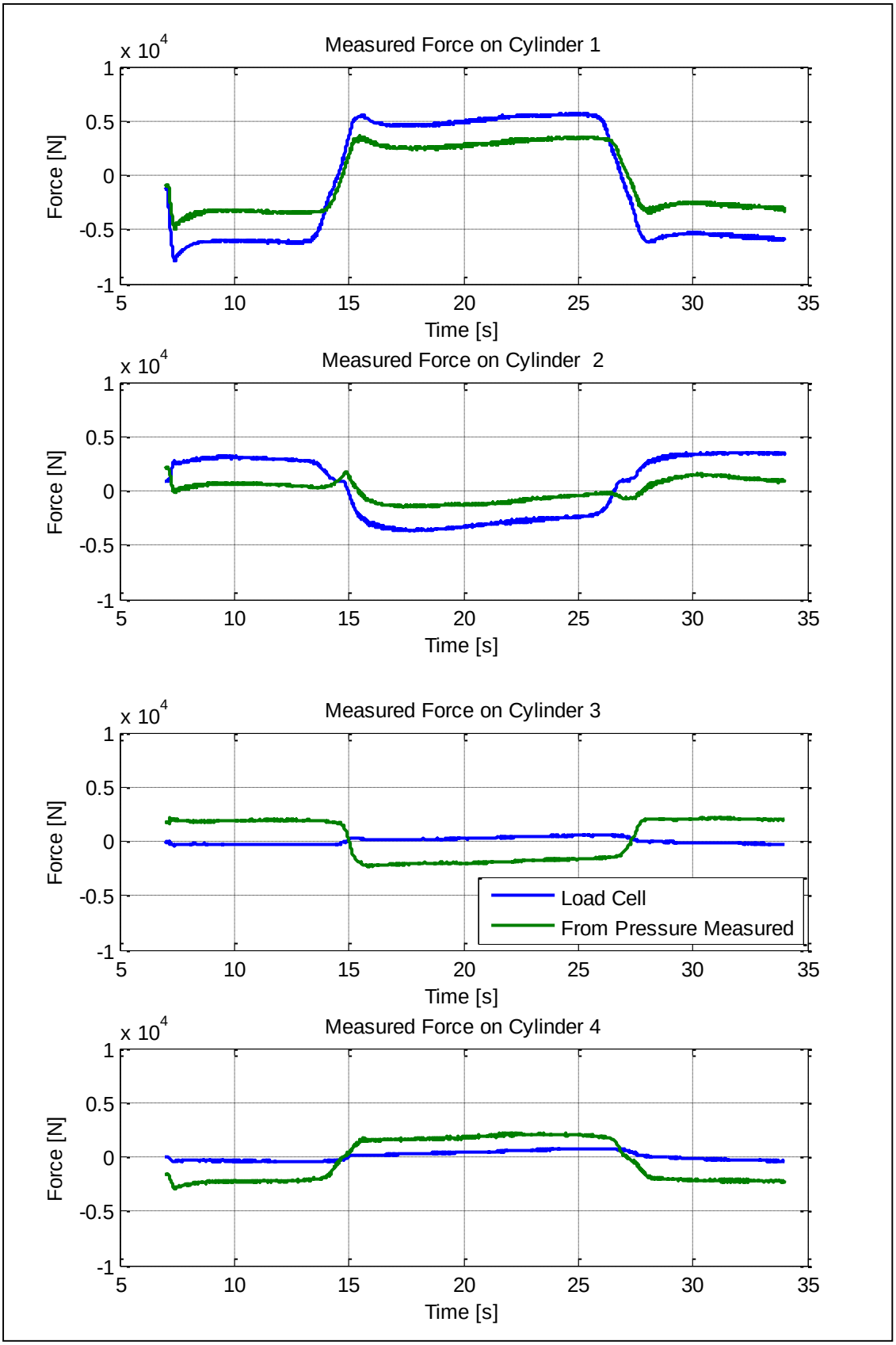

Figure 7-6. Full PHS Test Setup: Measured Forces on the PHS cylinders.

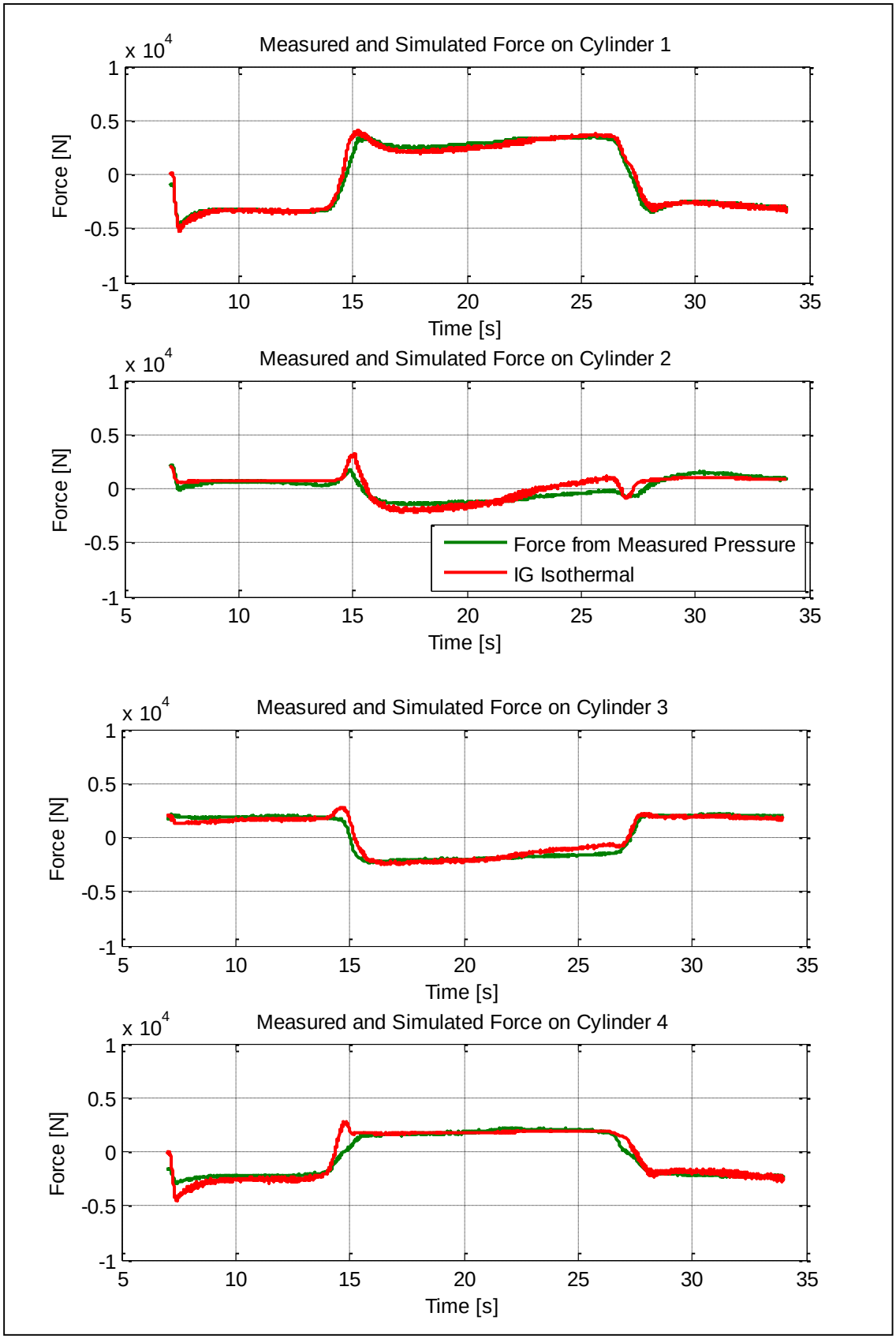

Figure 7-7. Full PHS Test Setup: Measured & Simulated (ignoring friction) Forces on the PHS cylinders.

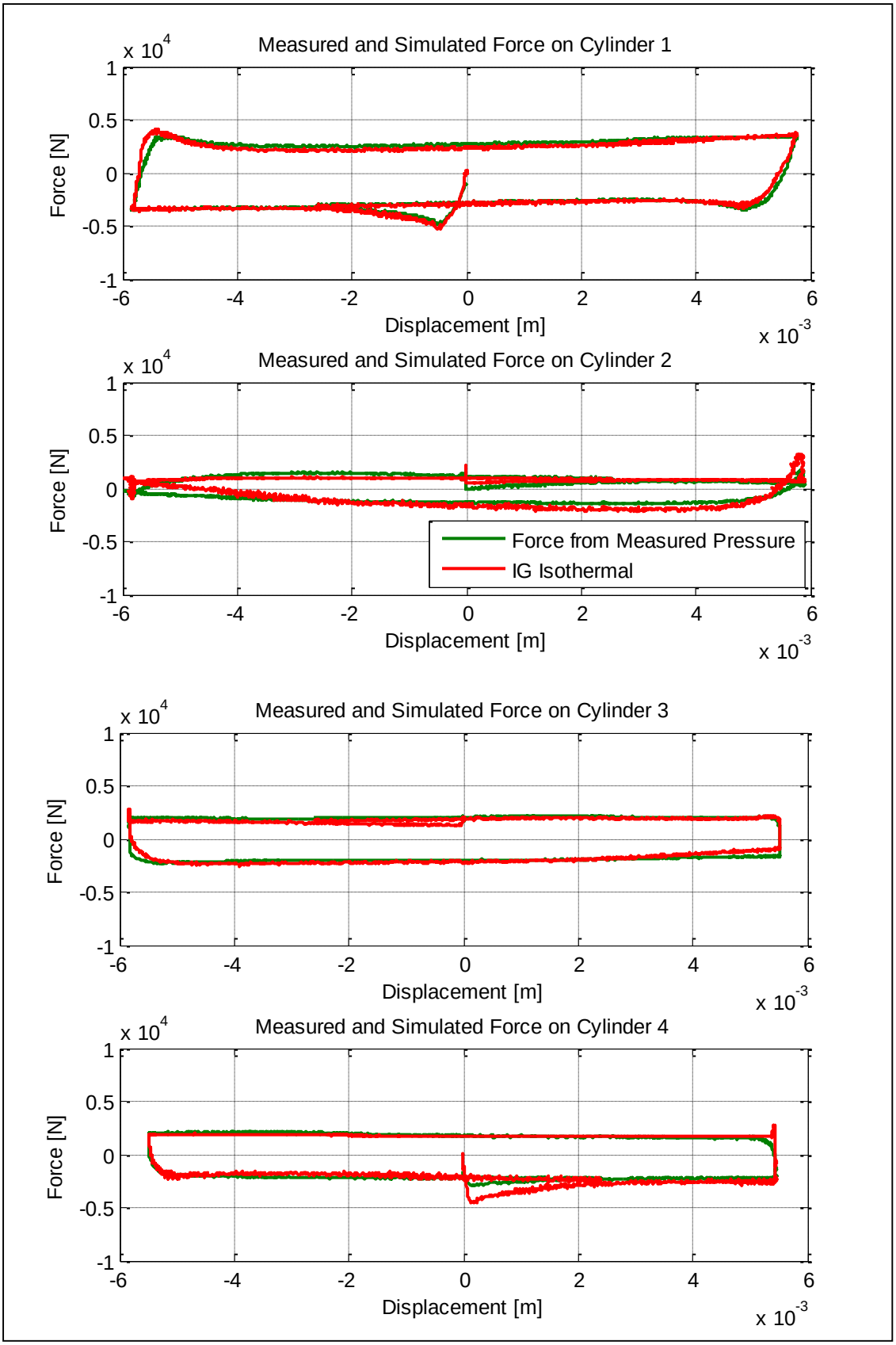

Figure 7-8. Full PHS Test Setup: Measured & Simulated (ignoring friction) Forces on the PHS cylinders.

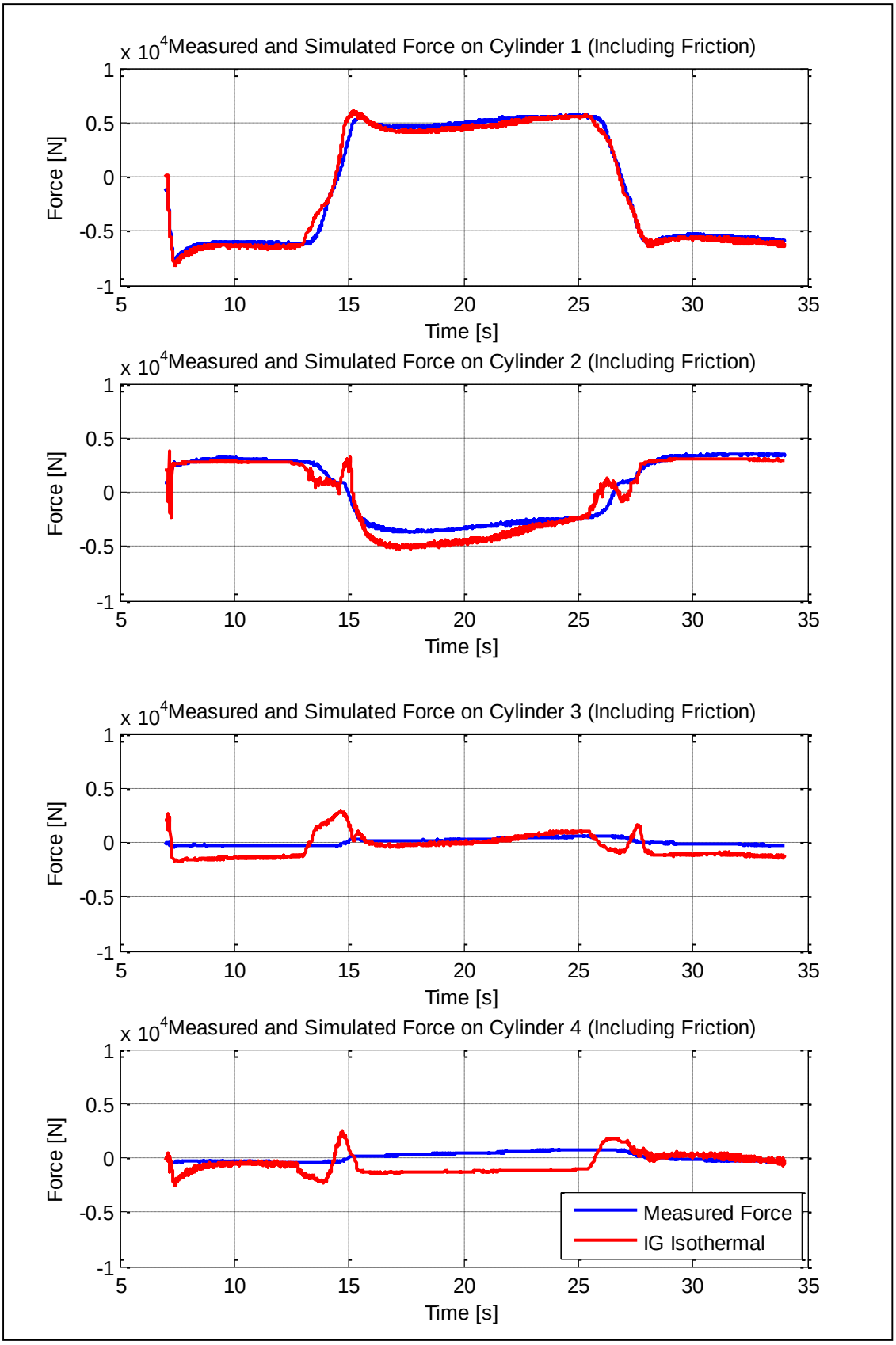

Figure 7-9. Full PHS Test Setup: Measured & Simulated (including friction) Forces on the PHS cylinders.

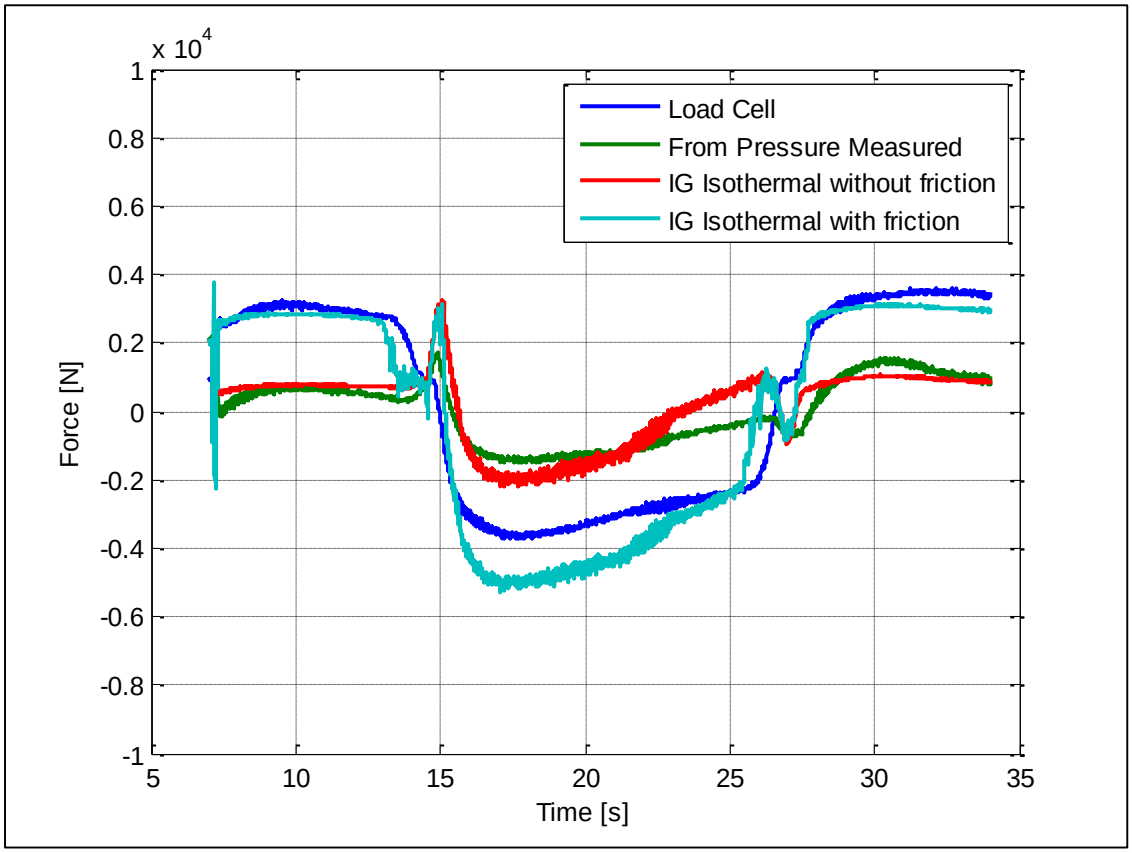

Figure 7-10. Comparison: Measured and simulated forces on Cylinder 2.

From the different validations, it can be concluded that the PHS model predictions correlate fairly well with the measured data, especially at larger movements and high forces, where the friction plays a secondary role.

Finally, for the full test setup, the nitrogen gas volume was assumed to be 0.04848 litre (as approximated for the quarter model) and the oil volume in the hydraulic lines 1 to 4 (Line 1- connection between cylinder 1 & 2, Line 2- connection between cylinder 1 & 3, Line3- connection between cylinder 2 & 4, Line 4- connection between cylinder 3 & 4) was approximated to be about 1.9, 2.5, 2.5 and 1.9 litres respectively. This is again more than the measured volume and could indicate that the bulk modulus and the nitrogen gas volume approximations may not be fully correct.

The effect of the bulk modulus was again investigated. When using the measured oil volumes, optimum results were obtained for a bulk modulus of 1.16 GPa. This is very similar to the one obtained for the quarter PHS model.

Further, during the tests it was observed that under the high pressures seen, the system components deformed and expanded slightly. This could explain the difference in the experimentally determined bulk modulus. Therefore, it was decided to adjust the experimentally determined bulk modulus (in chapter 5) to 1.16 GPa.

7.4. Investigation of the Effect of Pipe Failure

For completeness, the effect of pipe failures on the system operation was also investigated during the laboratory tests. Due to the oil pre-charge, the system does not retain its steady state position. Failures of the cross connection, i.e. the connections between cylinder 1 and 2 and cylinders 3 and 4, only cause lateral shifting of the axis. However, failure of one of the diagonal connections, i.e. the connection between cylinder 1 and 2 or cylinder 2 and 3, result in the axis pulling skew in the bending mode. This is not ideal and DCD is currently busy to implement a possible warning/safety feature to the PHS design.

7.5. Conclusion on the Full PHS System Modelling and Testing

A PHS system model was developed in Matlab. The mathematical model was validated with measured data from a quarter and full PHS laboratory test setup. It is recommended that the model should also still be validated with data from field tests. This could be done by implementing the PHS on a multi-body dynamic locomotive model. Field tests and the multi-body dynamic locomotive modelling have been planned for the near future.

From the validation process, it was observed that the correlation of the predicted forces compared to the measured data of the full test setup still show some errors. For this reason possible causes of these uncertainties/errors were identified and investigated.

During calibration and initial testing, it was noticed that the PHS system is very sensitive to small changes and that one of the main contributions to erratic results was possibly due to measurement errors. Further, the system cannot be assumed to be fully rigid. Under the high pressures seen, the system components deformed and expanded slightly and thus affected results.

On the simulation side, the bulk of the errors come from assumptions made and numerical approximations. The errors coming from the numerical approximations are highly influenced on what has to be approximated and what the magnitude is. Thus, for parameters with very small magnitudes (such as the small displacements experienced by the cylinders), the errors are larger.

This explains the errors of the friction model when approximating the friction force in the vicinity of zero piston velocity. It was noticed that the numerical error was reduced when reducing the sampling frequency to about 10 Hz and also drastically reduced the sampling time. These error reductions are due to the smoother velocity projections obtained from differentiating displacements at lower sampling frequencies. This lower sampling frequency should be valid, as the system is not expected to see very fast inputs in normal operating conditions.

From the overall investigation of the PHS model, one can conclude that the PHS model does not need to be very complex and thus reduce the computational requirements. One can consider to further reduce the complexity by:

- Approximating the large accumulator as a pressure release valve and thus to assume that the oil pressure will not go above 15 MPa.
- Modelling the reservoir with the ideal gas approximation (i.e. either isothermal or polytropic). Thus not using the Ideal gas (IG) with the energy equation (EE) and the Benedict Web Rubin (BWR) with EE, which uses a 4^{th} order Runga Kutta integration (refer to section 5.1.2.).

8. Conclusion and Recommendations

The research commenced with a literature survey from which it was evident that off-flange curving designs, similar to the PHS, show great improvements in wear reduction, optimised balancing of wheel loads and several other benefits. Further, considerable cost savings result from the extended bogie overhaul cycle, general energy savings, reduced derailment damage and the reduction of wheel and rail wear. However, existing prototype PHS solutions (based on hand calculations) are not optimal yet and improvements are necessary. To be able to identify and implement potential improvements, the need exists to perform modelling of the systems to obtain a better understanding of each possible system as a whole.

Therefore, extensive laboratory tests on component basis and on the full PHS system were performed. From these tests all parameters needed for the characterisation of the PHS and the mathematical model were determined. Also, sufficient model validation data was gathered.

With this information at hand, a mathematical model of the PHS system was successfully generated and validated. Different gas models were investigated and it was observed that the isothermal and polytropic Ideal Gas approximation gave the most accurate predictions. The bulk modulus used for the modelling of the oil was experimentally determined to be 1.16 GPa. Also, the friction in the PHS system was investigated and incorporated into the PHS model. It was, however, found that the accuracy of the model decreases for very small displacements and low forces.

The PHS model can now be used in a multi-body dynamic locomotive simulation to optimise system design and to quantify actual gains and improvements and to evaluate its effectiveness. This is planned to be implemented in the near future by another Master's student.

It is further recommended that an improved PHS system should be fitted to a locomotive and the initial field tests repeated in order to quantify the actual improvements achieved in a real world application. Further investigation of the reservoir and pipeline design is also proposed to reduce the components and failure risk of the PHS system.

9. References

9.1. Literature

1. Borgnakke C. and Sonntag R.E., 2009, *Fundamentals of Thermodynamics*, SI Version, Seventh Edition, John Wiley & Sons Pte Ltd, Asia.
2. Berger E.J., 2002, *Friction modelling for dynamic system simulation*, ASME Reprint No AMR337, Applied Mechanics Reviews Volume 55 no 6.
3. DCD Rolling Stock, 2012, Technical Report: *The rationale for a Self-Steering 3-axle bogie for GF*, Doc PHS-GFB Ed.3.
4. DCD Group (Pty) Ltd, 2014, Design Drawing: *Hydraulic Piping Assembly*, Drawing No.: PHSPA01100.
5. Department of Transport, 2013, *Annual Report 2011/2012*, Republic of South Africa.
6. Els P.S., 2006, *The ride comfort vs. handling compromise for off-road vehicles*, Unpublished PhD Thesis, University of Pretoria, Pretoria. [Online] Available from: http://upetd.up.ac.za/thesis/available/etd-07152008-102911 (Accessed on 30/08/2013)
7. Els P.S. & Grobbelaar B., 1993, *Investigation of the Time- and Temperature Dependency of Hydropneumatic Suspension Systems*, SAE Technical Paper Series no. 930265, Vehicle Suspension and Steering Systems, SAE Special Publication SP-256, 1993, pp. 55-65.
8. Enblom R., 2009, *Deterioration mechanisms in the wheel–rail interface with focus on wear prediction: a literature review*, Vehicle System Dynamics: International Journal of Vehicle Mechanics and Mobility, 47:6, pages 661-700.
9. Freespirit K., 2013, *Katwise – Hitchhiking and Adventure Blog*. [Online] Available from: http://www.katwise.net/blog/?page_id=206 (Accessed on 21/08/2013).
10. General Electric Corporation, 1997, Instruction Manual: *GE Three-Axle Gen1 Steerable Truck*, MI-30001-014, GEK-76557, USA.
11. Kat C., 2009, *Suspension forces on a tri-axle air suspended semi-trailer*, Master's Thesis, University of Pretoria, Pretoria. [Online] Available from: http://upetd.up.ac.za/thesis/available/etd-06242009-153546 (Accessed on 20/03/2014)
12. Kat C. & Els P.S., 2012, *Validation metric based on relative error*, Mathematical and Computer Modelling of Dynamical Systems: Methods, Tools and Applications in Engineering and Related Sciences, 18:5, 487-520.
13. Lard W.R, 2013, William Robert Lard Illustration and Graphic design: *Train*. [Online] Available from: http://www.williamlaird.com/index.html (Accessed on 26/08/2013).

14. Liu Q.Y., Zhang B. & Zhou Z.R., 2003, *An experimental study of rail corrugation*, 14th International Conference on Wear of Materials, Volume 255, Pages 1121–1126.
15. Meier B. & Schrader S., 2001, *New Bogie Designs Reduced Life-Cycle Costs and Track Forces*, 7th International Heavy Haul Conference.
16. National Railway Safety Regulator Act (Republic of South Africa), 2002, Act No.16. [Online] Available from: http://www.info.gov.za/view/DownloadFileAction?id=6805 (Accessed on 27/09/2013)
17. Olofsson U. & Lewis R., 2006, *Tribology of the Wheel-Rail Contact*, Handbook of Railway Vehicle Dynamics, Chapter 5, Taylor& Francis Group.
18. SABS Design Institute, 2005, *Inter-design 2005 – Transport in South Africa*. [Online] Available from: http://www.interdesign2005.org.za/pages/transportSA.htm (Accessed on 22/08/2013).
19. SABS Design Institute, 2013, *ISO and SANS Code Info List*. [Online] Available from: http://www.store.sabs.co.za/catalogsearch/result/index/?limit=25&p=8&q=Rail (Accessed on 28/08/2013).
20. Smit P., 2013, Test Report: *Analysis of wheel profiles*, Summary_19E050(Ref._Loco) and_19E052_(PHS_fitted_loco)_week_41.pdf
21. Swenson C.A., 1999, *Locomotive Radial Steering Bogie Experience in Heavy Haul Services*. Presented at the International Heavy Haul Conference on Wheel-Rail Interface Moscow 1999, Russia.
22. Swenson C.A. & Scott R.T., 1996, *The Effect of Locomotive Radial Steering Bogies on Wheel and Rail Wear*, Prepared for ASME/IEEE Joint Railroad Conference May 1996, Oak Brook, Illinois, USA.
23. Swenson, C.A. & Wagner, R., 1994, *A New Class of High Power Diesel Electric Locomotives*, The Dalian International Symposium of Locomotives and Motor Cars October 1994, Dalian.
24. Transnet Freight Rail (TFR), 2012, *Transnet Freight Rail Annual Report 2012*. [Online] Available from: http://www.transnet.co.za:9999/InvestorRelations/Transnet Reports/Transnet Annual Report 2012.mht (Accessed on 22/08/2013).
25. Transnet Freight Rail (TFR) Technology Management, 2010, Research and Development Report: *Experimental Passive Hydraulic Steering system for the 19E locomotive (Phase 1).* Document: BBD 7644 Revision 1.
26. Turolla (Danfoss Group), 2013, *Hydraulic Fluids and Lubricants Technical Information*, Document l021414 Rev C.

27. Van der Westhuizen S.F. and Els P.S., 2014, *Comparison of different gas models to calculate the spring force of a hydropneumatic suspension*, Unpublished Article, University of Pretoria, Pretoria.

9.2. Persons Referenced

1. Mr Pat Smit, Product engineer at DCD Rolling Stock
   Tel.: 011 914 1400
   E-mail: pat@dcd.co.za

2. Prof P.S Els, Professor at the University of Pretoria
   Tel.: 012 420 2045
   Email: schalk.els@up.ac.za

3. Mr Sarel Maartens, Transnet Freight Rail
   Tel.: 083 297 9233
   E-mail: Sarel.Maartens@transnet.net

Annexure A (Nitrogen Gas Constants and Properties)

Information from Borgnakke and Sonntag (2009)

Nitrogen Critical Pressure = 3.39 MPa
Nitrogen Critical Temperature = 126.2 K

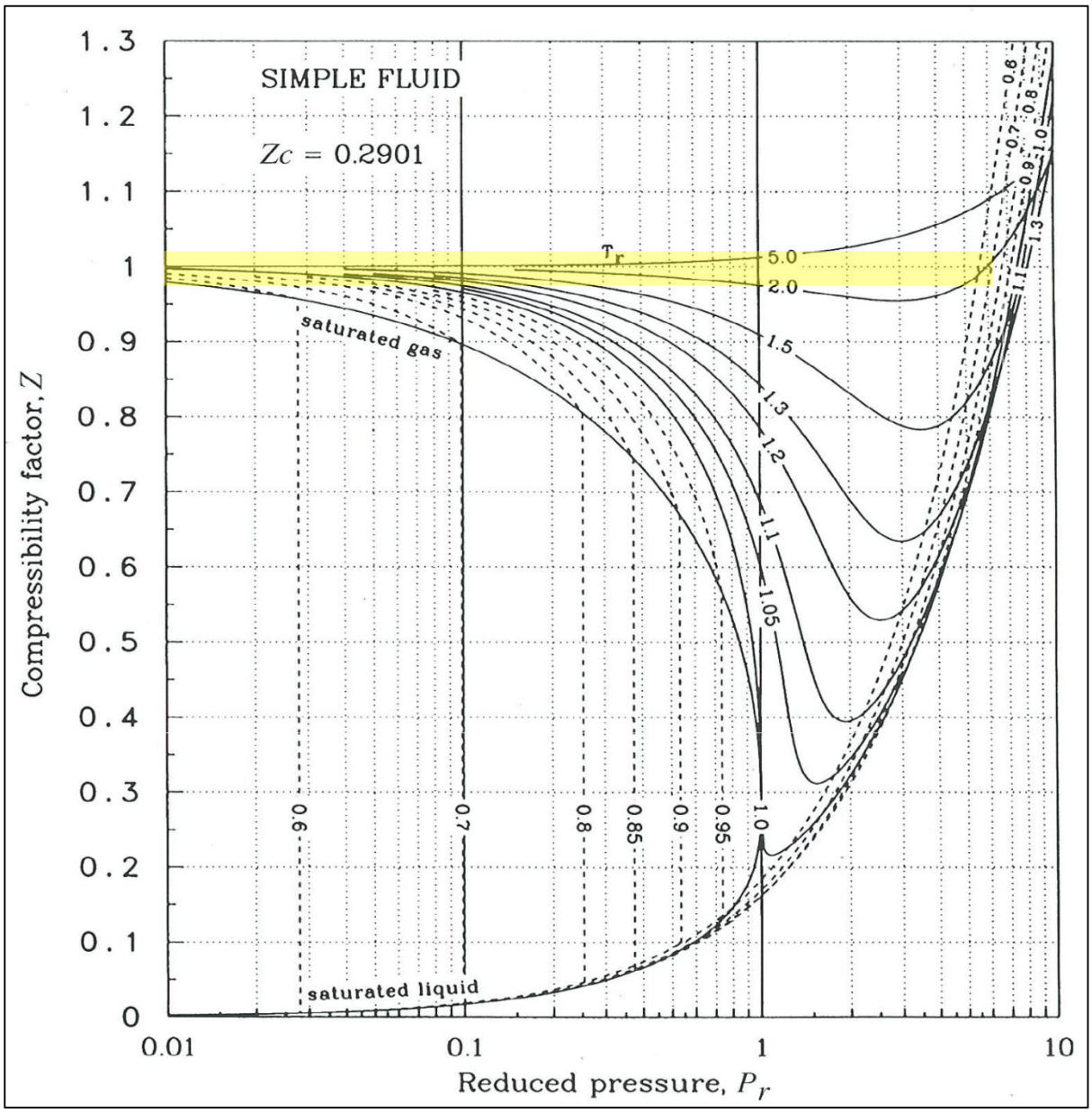

Figure A-1. Lee-Kessler simple fluid compressibility chart (Borgnakke and Sonntag, 2009).

Information from Els & Grobbelaar (1993)

Constants for the BWR equation:

a = 0.115703387 $[(m^3/kg)^3.(N/m^2)]$

A_0 = 136.0474619 $[(m^3/kg)^3.(N/m^2)]$

b	= 2.96625 x 10^{-6}	[$(m^3/kg)^3$]
B_0	= 0.001454417	[m^3/kg]
c	= 7.3806143 x 10^{-5}	[$(m^3/kg)^3.K^2.(N/m^2)$]
C_0	= 1.0405873 x 10^{-6}	[$(m^3/kg)^3.K^2.(N/m^2)$]
α	= 5.7863972 x 10^{-9}	[$(m^3/kg)^3$]
γ	= 6.7539311 x 10^{-6}	[$(m^3/kg)^2$]
R	= 296.797	[J/(kg.K)]

Constants for the IG specific heat capacity calculation:

N_1	= - 735.21
N_2	= 34.224
N_3	= - 0.557648
N_4	= 3.504
N_5	= - 1.7330 x 10^{-5}
N_6	= 1.7465 x 10^{-8}
N_7	= - 3.5689 x 10^{-12}
N_8	= 1.0054
N_9	= 3353.4061

Annexure B (Thermal Time Constants)

Table B-1. Thermal Time Constants Determined.

Test Situation (C-Compression, R - Rebound)		Reservoir Setup	Step Input Magnitude [mm]		P_{begin} [MPa]	P_{end} [Mpa]	Delta P [MPa]	63 % Pressure point [Mpa]	Thermal Time Constant (Tau) [s]
Chamber 1	Chamber 2		Schenk	Laser					
	C	1	3	1.2	9.6	8.935	0.665	9.35395	1.5
R			3	1.2	0.99	1.053	-0.063	1.01331	0.7
	C	1	6	3	14.14	13.96	0.18	14.0734	0.7
R			6	3	0	0	0	0	0
C		2	-6	-2.6	19.36	19.36	0	19.36	0
	R		-6	-2.6	0.764	0.764	0	0.764	0
C		2	-3	-1.5	9.14	8.99	0.15	9.0845	4.9
	R		-3	-1.5	1.127	1.127	0	1.127	0
	C	2	3	1.43	9.34	9.055	0.285	9.23455	3.1
R			3	1.43	0.88	0.89	-0.01	0.8837	0.5
	C	2	6	3.05	14.28	14.165	0.115	14.23745	2.8
R			6	3.05	0.505	0.514	-0.009	0.50833	2
	C	2	12	8.73	15.7	15.2	0.5	15.515	3
R			12	8.73	0.01	0.066	-0.056	0.03072	1
C		3	-6	-4.65	8.518	7.474	1.044	8.13172	0.8
	R		-6	-4.65	0.885	1.08	-0.195	0.95715	0.7
C		3	-3	-2.45	3.98	3.56	0.42	3.8246	0.64
	R		-3	-2.45	1.41	1.582	-0.172	1.47364	0.63
	C	3	3	2.45	6.56	6.023	0.537	6.36131	0.53
R			3	2.45	1.42	1.579	-0.159	1.47883	0.59
	C	3	6	4.15	14.33	13.733	0.597	14.10911	0.28
R			6	4.15	1.06	1.283	-0.223	1.14251	0.5
	C	3	12	9.73	15.28	14.655	0.625	15.04875	2.1
R			12	9.73	0.45	0.735	-0.285	0.55545	1.2
C		4	-6	-5.37	3.17	2.787	0.383	3.02829	1.15
	R		-6	-5.37	1.6	1.841	-0.241	1.68917	1.3
C		4	-3	-2.63	2.55	2.34	0.21	2.4723	0.4
	R		-3	-2.63	2.03	2.168	-0.138	2.08106	0.81
	C	4	3	2.85	3.4	3.118	0.282	3.29566	1
R			3	2.85	1.68	1.785	-0.105	1.71885	1.3
	C	4	6	5.61	4.64	3.976	0.664	4.39432	1.9
R			6	5.61	1.42	1.575	-0.155	1.47735	2.3
	C	4	12	11	10.21	7.658	2.552	9.26576	1.4
R			12	11	1.06	1.285	-0.225	1.14325	2.2

Annexure C (Additional Validation Figures)

In this Annexure more validation figures are provided for other PHS displacement inputs. These figures were also used to validate the PHS model qualitatively (i.e. visually).

Quarter PHS Test Setup Validation

The following figure shows the input to Cylinder 1. The input of the other cylinders was assumed to be 0. It must be noted that the test data was gather for a quarter PHS model, but the full PHS model was used. The measured and simulated results are provided in Figures C-2 to C-4. From these results it can be observed that the simulation results obtained are a very good approximation of the measured results.

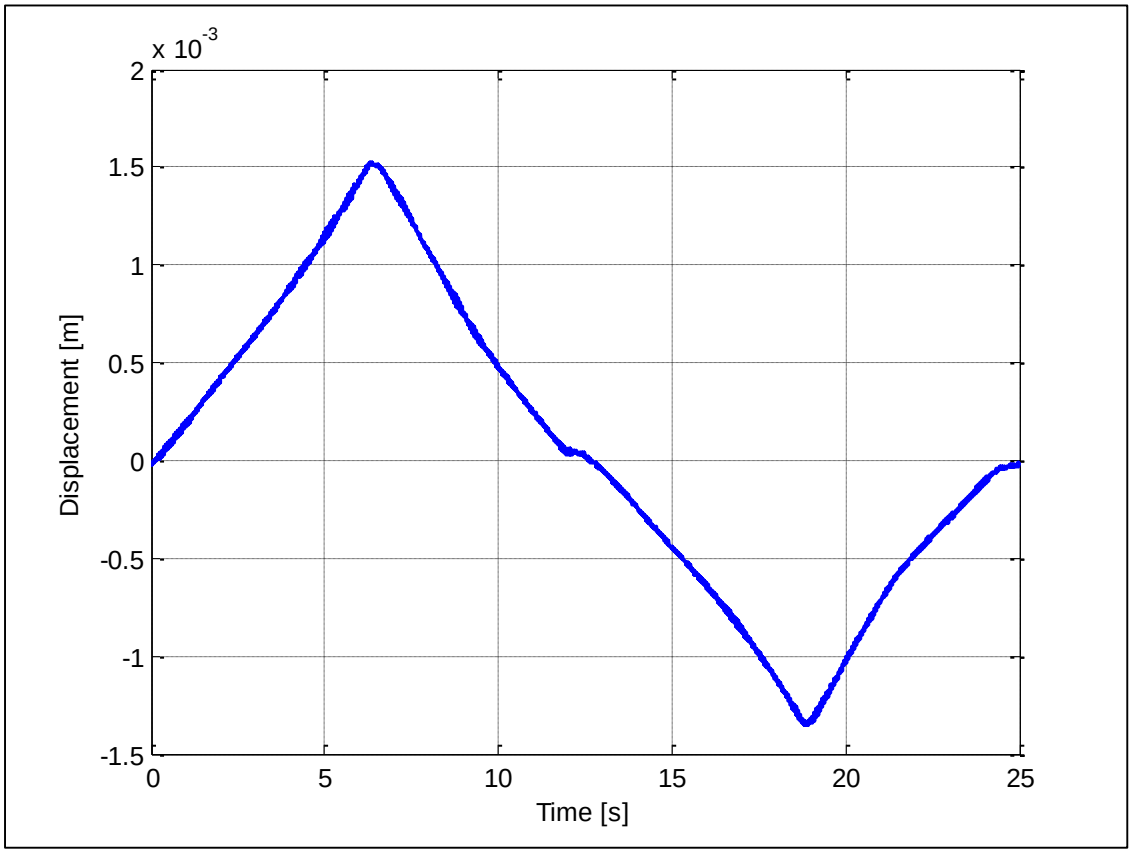

Figure C-1. Quarter PHS Test Setup: Measured Piston Displacement (Triangular-wave input).

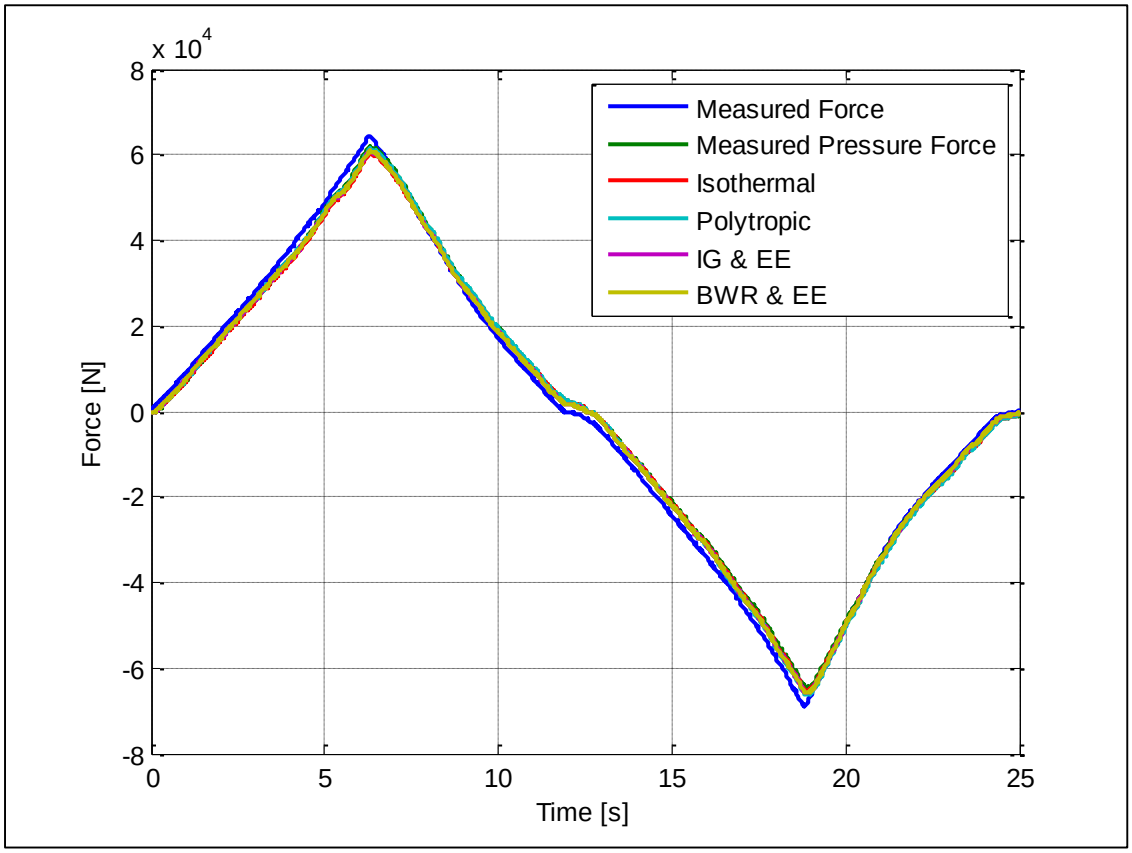

Figure C-2. Quarter PHS Test Setup: Measured & Simulated (ignoring friction) Forces on the PHS cylinders.

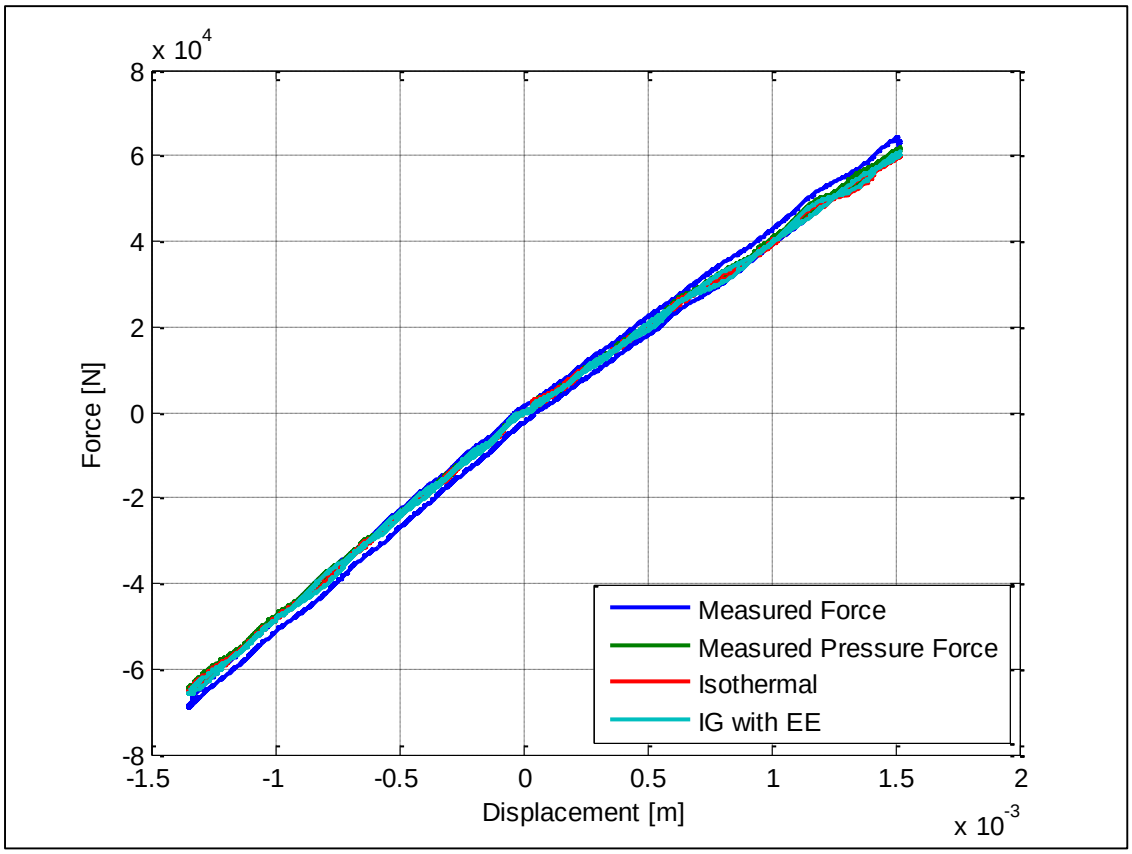

Figure C-3. Quarter PHS Test Setup: Measured & Simulated (ignoring friction) Forces on the PHS cylinders.

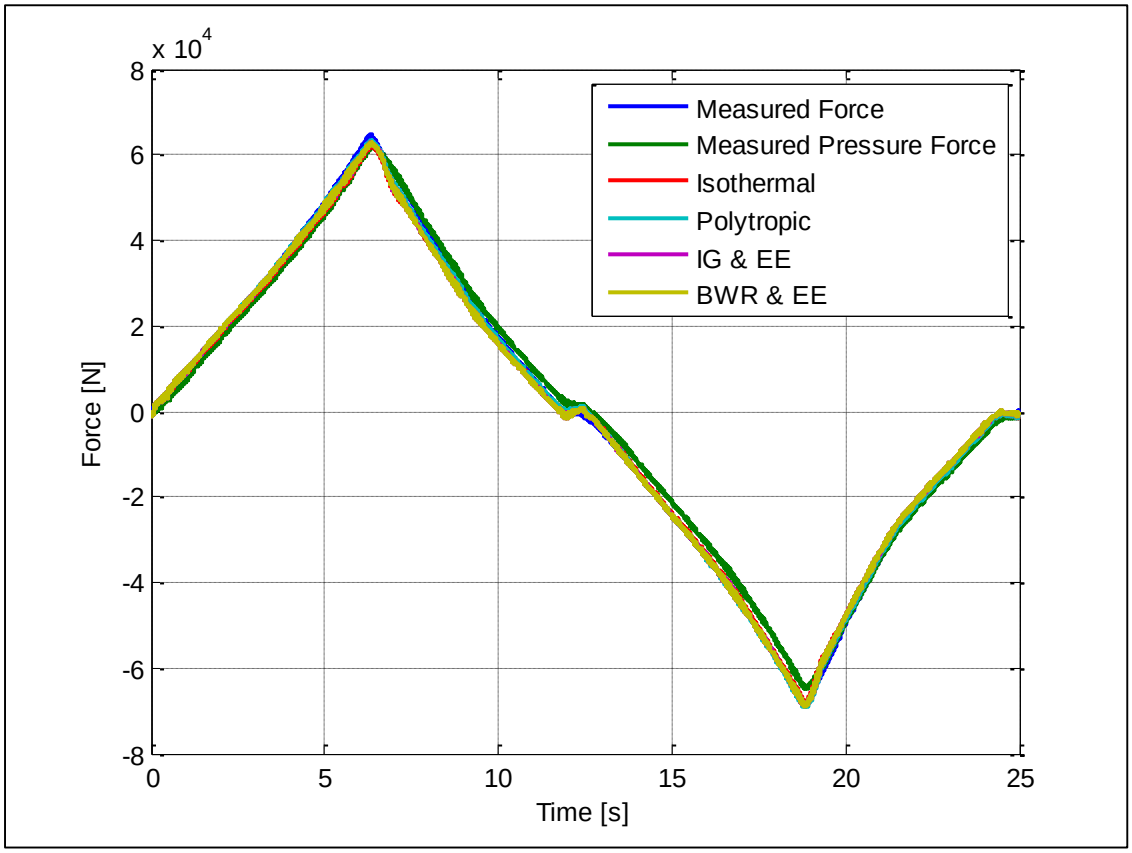

Figure C-4. Quarter PHS Test Setup: Measured & Simulated (including friction) Forces on the PHS cylinders.

Full PHS Test Setup Validation

The triangular wave simulation displacement inputs, gathered from the full PHS test setup, are shown in Figure C-5. The displacement measurements from the Schenck actuators are also indicated on the figure. From these it is evident that there is play on the system, as the difference between Schenck displacement and measured piston displacement is quite high. The resulting forces of the cylinders (measured and simulated) are plotted on the Figures C-6 to C-8.

From the results it can be observed that the simulation results obtained are a good approximation of the measured results.

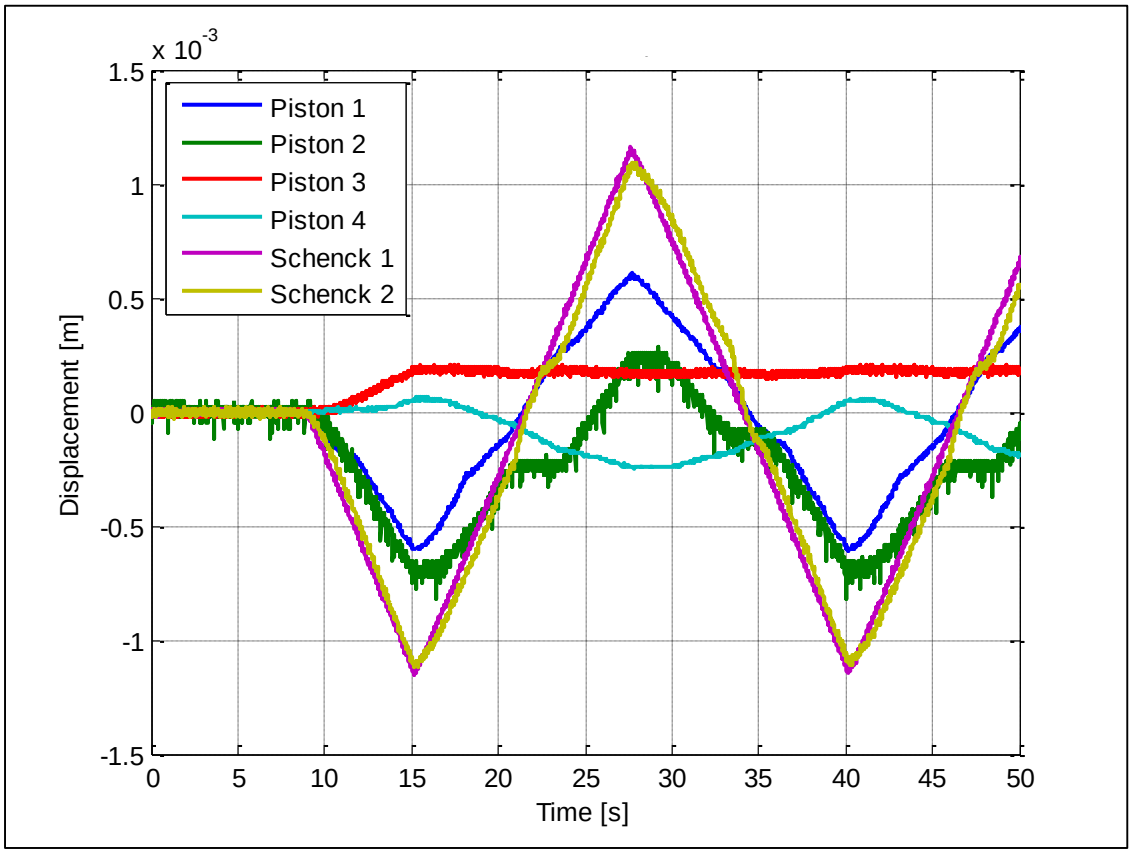

Figure C-5. Full PHS Test Setup: Measured Piston Displacement (Triangular-wave input).

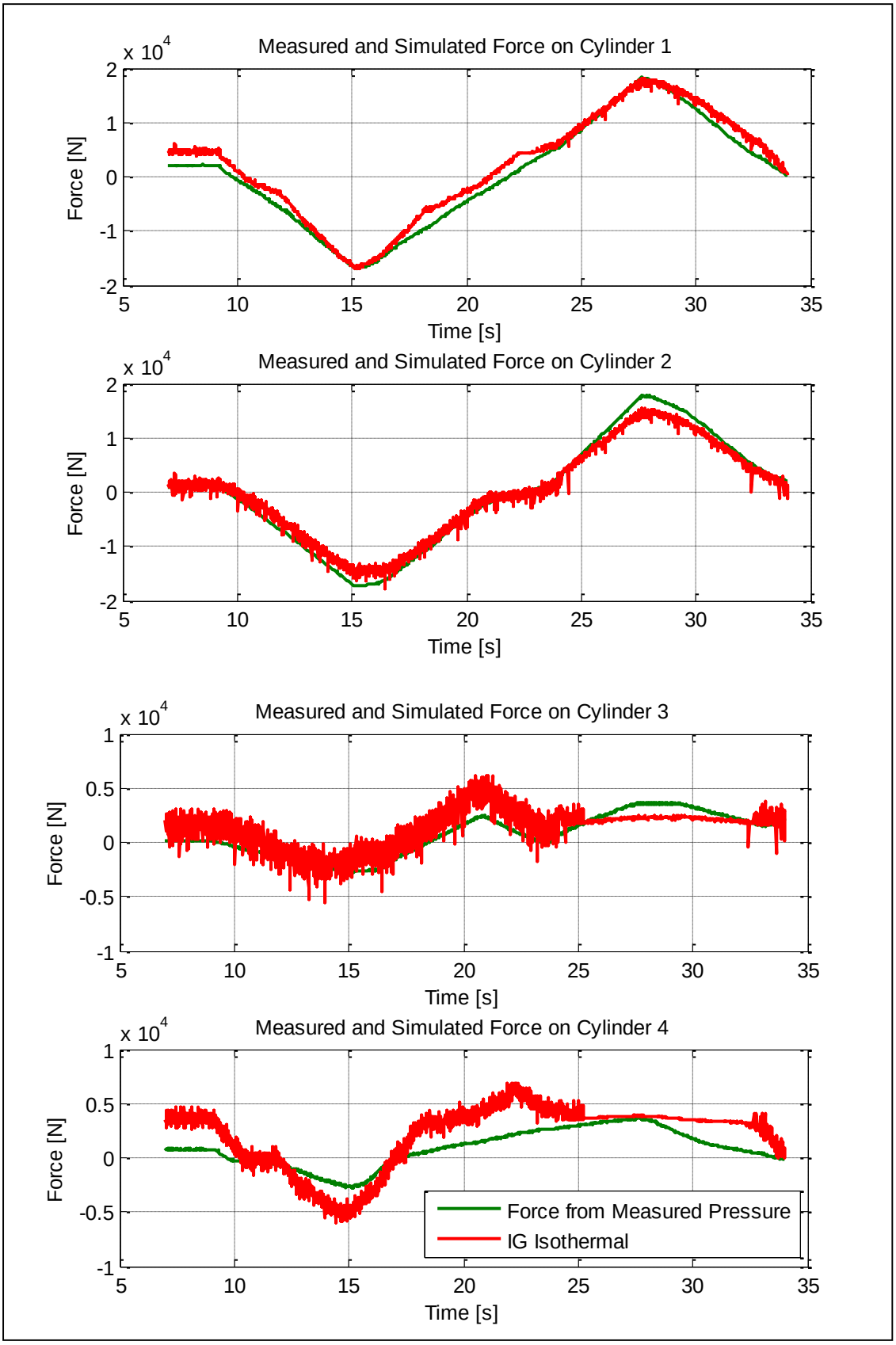

Figure C-6. Full PHS Test Setup: Measured & Simulated (ignoring friction) Forces on the PHS cylinders.

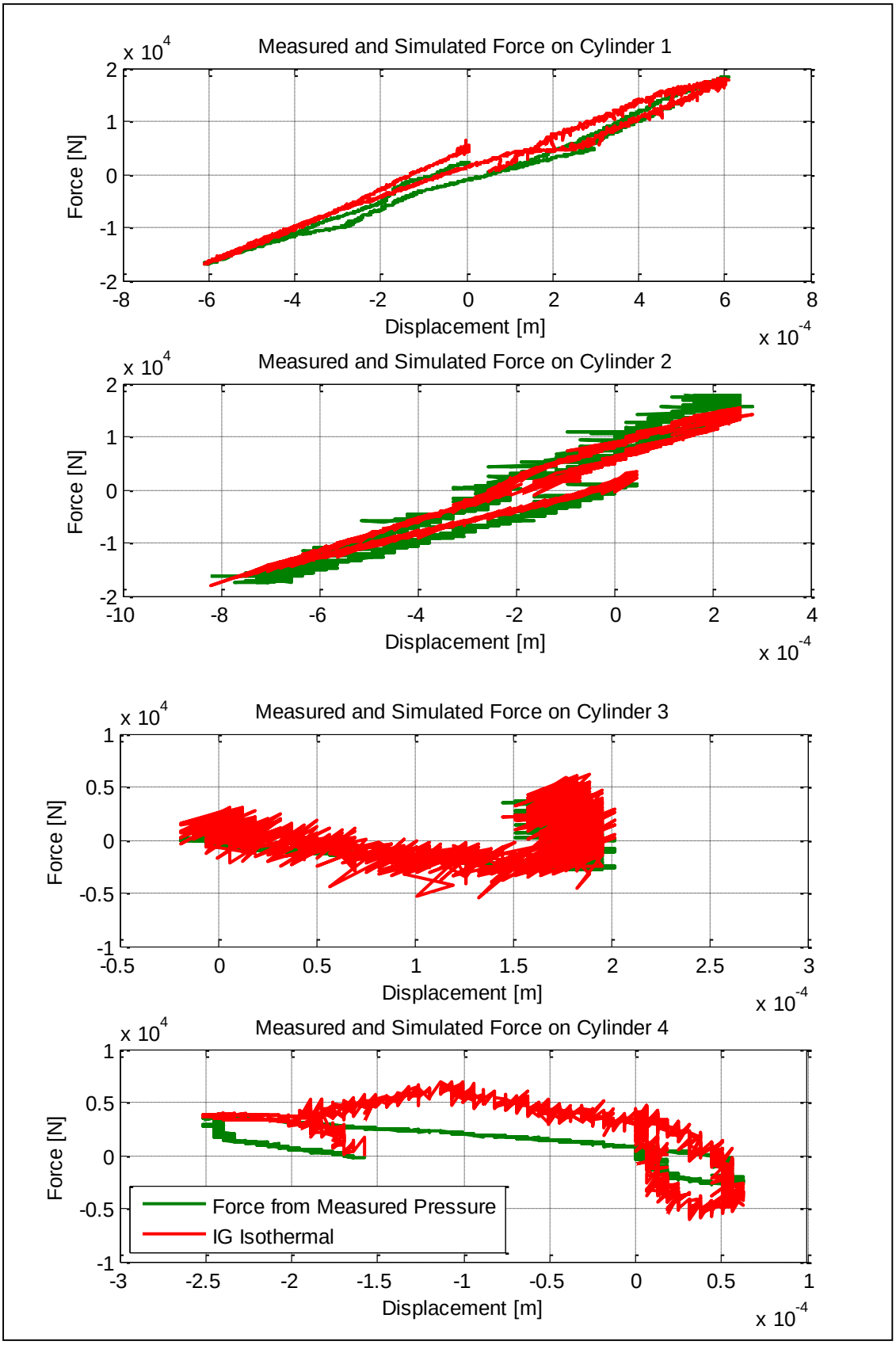

Figure C-7. Full PHS Test Setup: Measured & Simulated (ignoring friction) Forces on the PHS cylinders.

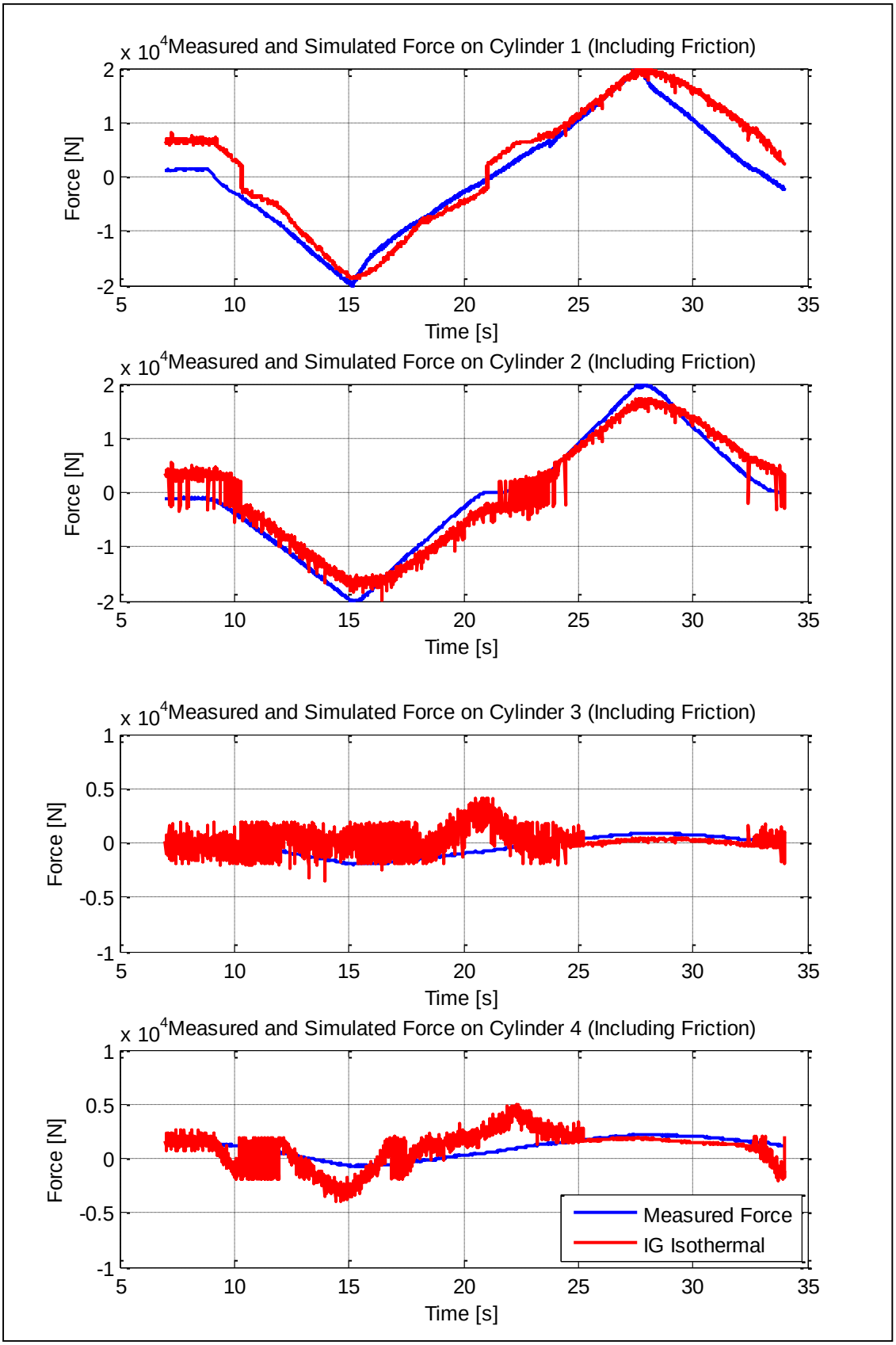

Figure C-8. Full PHS Test Setup: Measured & Simulated (including friction) Forces on the PHS cylinders.